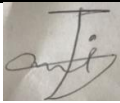




Universitetet
i Stavanger

FACULTY OF SCIENCE AND TECHNOLOGY

MASTER'S THESIS

Study program/specialization: Master of Science in Petroleum Engineering/ Drilling Engineering	Spring semester, 2020. Open access
Author: Alireza Nasiri	 _____ (Author's signature)
Supervisor(s): Dmitry Shogin	
Title of master's thesis: "Rheological characterization of HPAM solutions in steady and transient shear flows using single-mode physical models of polymeric liquids"	
Credits: 30 ECTS	
Keywords: Polymer Material function Shear stress start-up Shear stress relaxation FENE-P C-FENE-P	Number of pages: + supplemental material/other: Stavanger, 15th June 2019

"Rheological characterization of HPAM solutions in steady and transient shear flows using single-mode physical models of polymeric liquids"

By

Alireza Nasiri

Master's Thesis

Presented to the Faculty of Science and Technology

The University of Stavanger

THE UNIVERSITY OF STAVANGER

JULY 2020

Acknowledgment

I want to express my high level of gratitude to my dedicated supervisor Dmitry Shogin who first accepted me in his research group and then kindly supervised me throughout whole period of this research, even if when he was so busy due to born of his lovely daughter. In fact, he taught me the basics about polymer, how to write thesis, and how to produce beautiful graph with the help of Mathematica Wolfram software. Also, I want to express my appreciation to Kim Andre Nesse Vorland who helped me a lot in conducting experimental part, even if during COVID-19 disease time. At the end I want to donate this research to my devoted parents who support me in whole my life with their high level of kindness.

Abstract

The material function of Partially Hydrolyzed Polyacrylamide (HPAM) in three concentration of $C_c=3.10^4$ ppm, $C_c=2.10^4$ ppm and $C_c=1.5.10^4$ ppm both for steady and transient flow was studied in this research. Then data was fitted to proposed physical in literature such as Modified Finitely Elongated Nonlinear Elastic Dumbbell model (FENE-P), Charged Modified Finitely Elongated Nonlinear Elastic Dumbbell model (C-FENE-P), and different version of Phan-Thien-Tanner model (PTT) to recognize the best representative model for describing material function description of Partially Hydrolyzed Polyacrylamide polymer (HPAM) both for steady and transient flow. Although the concentration is not focus of this work, it was observed that the slope of power-law region of first normal stress coefficient (Ψ_1) versus applied shear rate ($\dot{\gamma}$) is almost independent of concentration at least for three tested concentration tested in this research ($C_c=3.10^4$ ppm, 2.10^4 ppm, $1.5.10^4$ ppm). On the other hand, the slope of power-law region of viscosity (η) versus shear rate ($\dot{\gamma}$) is relatively dependent on concentration again at least for three tested concentration in this research. Moreover, monotonous relation between concentration and material function of both startup and cessation of steady shear flow was observed for these three tested concentrations of HPAM polymer. Finally, the importance of adopting correct approach of data fitting was shown in modeling part of this research, where one should not be rely on slope of exponential decay of cessation of steady shear rate test for modeling part anymore. Furthermore, for almost first time in literature the most recent proposed physical model by Dmitry Shogin and Amundsen (Shogin and Amundsen 2020) called C-FENE-P was evaluated in this research and it was recognized as the best model for describing the material function of both steady and transient flow of HPAM polymer specially regarding more dilute concentrations ($C_c=2.10^4$ ppm and $C_c=1.5.10^4$ ppm). Finally, it was observed that both single-mode affine LPPT and single-mode FENE-P model had relatively good performance for describing material function of HPAM polymer for more concentrated sample ($C_c=3.10^4$ ppm), though they both relatively failed in prediction of size of overshoot in stress growth of start-up of steady shear rate flow test.

Nomenclature

Scalars

a Yasuda exponent [-,first used in Eq.2.28]

b nonlinearity parameter [-,defined by equation 2.42]

C desired concentration of dilute polymer [ppm, defined by Eq.3.5]

C_c concentration of polymer [ppm, first used in Eq.3.1]

$C_{convert}$ converting factor [s,defined by Eq.2.43]

C_0 true concentration of concentrated polymer [ppm, first used in Eq.3.5]

C_{rel} true concentration of resulted solution [ppm,defined by Eq.3.2]

dS Surface element [m^2 , first used Eq.2.3]

ΔT time interval [s]

dV volume element [m^3 , first used Eq.2.4]

E electric-to-elastic energy ratio [-,defined by Eq.2.46]

ε relative permittivity of the solvent [-,first used in Eq.2.44,2.45]

ε_0 permittivity of vacuum [$F m^{-1}$, first used in Eq.2.44]

ϵ extensional parameter [-,first used in Eq.2.48]

ξ affinity parameter [-,first used in Eq.2.48]

η non-Newtonian viscosity [Pa s, first used in Eq. 2.20]

η_∞ infinite -shear- rate Non-Newtonian viscosity [Pa s, first used in Eq.2.29 2.28]

η_0 zero- shear- rate Non-Newtonian viscosity [Pa s, first used in Eq. 2.28]

η^+ Shear stress growth function [Pa s, first used in Eq.2.21]

η^- Shear stress relaxation function [Pa s, first used in Eq.2.22]

H Warner spring coefficient [$N m^{-1}$, first used in Eq.2.29]

k Boltzmann's constant [$J.K^{-1}$, first used in Eq.2.32]

k coefficient of additional transport quantity related to dilatational viscosity [Pa s, first used in Eq.2.13]

k_o permeability of formation relative to oil [md, first used in Eq. 2.1]

k_w permeability of formation relative to water [md, first used in Eq. 2.1]

L_0 initial state length [m]
 L_S steady state expanded length [m]
 λ time constant [s, first used in Eq. 2.28]
 λ_e experimental time constant [s, defined by Eq.2.41]
 λ_H time constant of FENE-P model [t, defined by Eq.2.412.40]
 λ_Q time constant of rigid dumbbell model [s, first used in Eq.2.41]
 m model parameter called consistency index [Pa sⁿ, first used in Eq.2.27]
 M relative mobility ratio of water in comparison with oil [-, defined by Eq. 2.1]
 M_c theoretical mass of concentrated polymer [g,first used in Eq.3.4]
 M_{cp} mass of concentrated solution taken in practice [g,first used in Eq.3.5]
 m_d desired mass of dilute solution [g,first used in Eq.3.3]
 M_L local mass flow rate [Kg, defined by Eq.2.3]
 m_o mobility ratio of oil [md (Pa s)⁻¹, first used in Eq. 2.1]
 $m_{overshoot}$ magnitude of overshoot [-]
 M_P required mass of polymer [g,defined by Eq.3.13.13.13.1]
 M_{Pa} practical mass of polymer taken in practice [g,first used in Eq.3.2]
 m_{relax} slope of exponential decay of cessation of steady shear rate test [-, defined by Eq.2.57]
 M_S measured mass of solvent [g, first used in 3.2]
 m_t total mass of dilute solution required [g, defined by Eq.3.4]
 M_w molecular weight [g mole⁻¹]
 m_w mobility ratio of water [md (Pa s)⁻¹, first used in Eq. 2.1]
 μ Newtonian viscosity [Pa s, first used in Eq.2.13]
 μ_o oil viscosity [Pa s, first used in Eq. 2.1]
 μ_w water viscosity [Pa s, first used in Eq. 2.1]
 n power-law region exponent [-,first used in Eq. 2.282.29]
 n model parameter, called the power -law index[-,first used in Eq.2.27]
 n number concentration of dumbbells [m⁻³, first used in Eq.2.32]
 \mathbf{n} normal force vector of
 P thermodynamic pressure [Pa, first used in Eq.2.12]

Q length of dumbbell extension (or the absolute value of connector force) [m, first used in Eq.2.31 2.30]

Q_0 maximum length of dumbbell extension [m, first used in Eq. 2.30]

q effective charge [C, first used in Eq.2.442.45]

ρ fluid density [Kg.m³, first used Eq.2.3]

Ψ_1 first normal stress differences coefficient [Pa s², first used in Eq. 2.20]

Ψ_1^+ First normal stress difference growth coefficient [Pa s², first used in Eq. 2.21]

Ψ_1^- First normal stress difference growth coefficient [Pa s², first used in Eq. 2.22]

Ψ_2 second normal stress differences coefficient [Pa s², first used in Eq. 2.20]

T thermodynamic temperature [K, first used in Eq.2.32]

$\tau_{xx} - \tau_{yy}$ first normal stress differences [Pa, defined by Eq.2.21 2.20]

τ_{xy} shear stress [Pa, defined by Eq.2.24]

$\tau_{yy} - \tau_{zz}$ second normal stress differences [Pa, defined by Eq. 2.20]

V_L local volume rate [m³. S⁻¹, defined by Eq.2.2]

w_i Weissenberge number [-]

x mean-square relative dumbbell extension[-,first used in Eq.2.36 2.35]

Z Z-factor [-, defined by Eq.2.37]

$\dot{\gamma}$ shear rate [Pa]

$\dot{\gamma}_D$ dimensionless shear rate [-, defined by Eq.2.44]

ζ hydrodynamic drag coefficient [Kg s⁻¹, first used in Eq.2.32]

Vectors

F_c connector force [N, defined by Eq.2.29]

g gravitational acceleration [ms⁻² first used in Eq.2.9]

n normal force vector [N, first used in Eq.2.2]

Q connector vector [m,first used in Eq. 2.29]

v velocity vector [m.s⁻¹, first used in Eq.2.2]

$\frac{dv_x}{dy}$ Velocity gradient [m.s⁻¹, first used in Eq.2.23]

Tensors

$\boldsymbol{\pi}$ total flux momentum displaced during flow or total stress tensor [Pa, first used in Eq.2.12]

$\boldsymbol{\delta}$ unit tensor [Pa, first used in Eq.2.12]

$\boldsymbol{\tau}$ deviatoric, commonly called "extra stress tensor" [Pa, defined by Eq.2.132.12]

$(\nabla \boldsymbol{v})$ nabla velocity tensor [ms^{-1} , first used in Eq.2.13]

$(\nabla \boldsymbol{v})^T$ transpose of nabla velocity tensor [m.s^{-1} , first used in Eq.2.13]

$\dot{\boldsymbol{\gamma}}$ rate- of - strain tensor [s^{-1} , first used in Eq.2.16]

Special

∇ del operator [m^{-1} , first used in Eq.2.5]

\mathbf{D} the material derivative [s^{-1} , first used in Eq.2.38]

$\langle \ \rangle$ configuration-space average [-, first used in Eq.2.322.312.30]

List of Contents

Acknowledgment	iii
Abstract	iv
Nomenclature	v
List of Contents	ix
List of Figures	xiii
List of Tables.....	xviii
1 Introduction	19
1.1 Objective	20
1.2 Research structure	21
2 Literature review	22
2.1 Quick introduction on polymer flooding process.....	22
2.2 Introduction on polymer basics	24
2.2.1 Polymer categorization.....	24
2.3 Introduction on fluid dynamic.....	26
2.3.1 Introduction on equation of fluid dynamic (“Generalized Navier-Stokes equations”)	26
2.3.2 Conservation of Mass.....	27
2.3.3 Conservation of momentum	28
2.3.4 Solving the equation of fluid dynamic (“Generalized Navier-Stokes equations”)	31
2.3.5 Definition of Newtonian and non-Newtonian fluid	32
2.4 Non-Newtonian phenomena in polymeric solution	33
2.4.1 shear-dependent viscosity	33
2.4.1.1 Tube flow.....	34
2.4.2 Normal stress and their differences	35
2.4.2.1 Rod climbing	35

2.4.2.2	Extrude swell (die swell)	36
2.4.3	Time-dependent phenomena	37
2.4.3.1	Cutting an Aluminum soap solution	37
2.4.3.2	Filament of low-density Polyethylene	38
2.4.3.3	The tubeless siphon	38
2.5	Material function	39
2.5.1	Shear flow	39
2.5.1.1	Shear flow Characteristic	39
2.5.1.2	Shear flow stress tensor	40
2.5.2	Steady shear flow	41
2.5.2.1	Steady shear rate material function	41
2.5.3	start-up of steady shear flow	44
2.5.3.1	start-up of steady shear flow characteristic	44
2.5.3.2	Material function of startup of steady shear flow	44
2.5.4	Cessation of steady shear flow	47
2.5.4.1	Cessation of steady flow characteristic	47
2.5.4.2	cessation of steady shear rate flow material function	48
2.6	Modeling part	50
2.6.1	Mathematical modeling	51
2.6.1.1	“The generalized Newtonian fluid model”	51
2.6.1.2	“The Power- law model” of Ostwald and de Waele (with m and n parameters)	52
2.6.1.3	The Bird-Carreau-Yasuda Model (with η^∞ , η^0 , λ , a , n parameters)	54
2.6.2	Physical modeling	55
2.6.2.1	Hookean Dumbbells model	56
2.6.2.2	Finitely Elongated Nonlinear Elastic (FENE) Dumbbell	57
2.6.2.3	FENE-P dumbbell model (with (nkT), b, λH model parameters)	58

2.6.2.4	C-FENE-P Dumbbell Model (with (nkT) , b , λH and E model parameters)	63
2.6.2.5	Phan-Thien-Tanner model (PTT) (<i>with ϵ, ξ, λ and η_0</i> model parameters)	68
3	Experimental workflow	73
3.1	Quick introduction on experimental workflow	73
3.1.1	First step: Preparation of mother solution	74
3.1.2	Dilution of mother solution	76
3.1.3	Conducting tests	79
3.1.3.1	Introduction on Rheometer	79
3.1.3.2	shear ramping test	80
3.1.3.3	startup of steady shear rate experiment	81
3.1.3.4	Cessation of steady shear rate test	82
4	Data analysis	82
4.1	Data analysis without considering physical models.....	82
4.1.1	Shear ramping experiments.....	82
4.1.1.1	Viscosity analysis (η)	82
4.1.1.2	First normal stress differences coefficient (Ψ_1) analysis	86
4.1.2	Startup of steady shear flow experiment	89
4.1.3	cessation of steady shear flow experiment.....	95
4.2	Data analysis with considering physical model	100
4.2.1.1	Viscosity data fitting using full LPPT	101
4.2.1.2	Viscosity data fitting using affine LPPT	103
4.2.1.3	Viscosity data fitting using affine exponential PPT(EPPT)	106
4.2.1.4	Viscosity data fitting using affine C-FENE-P model	108
4.2.2	Startup and relaxation of steady shear flow experiment	110
4.2.2.1	Startup and relaxation of steady shear flow data fitting with affine LPPT model	110

4.2.2.2	Startup of and relaxation of steady shear flow data fitting with FENE-P model	114
4.2.2.3	Startup and cessation of steady shear flow data fitting with C-FENE-P model	118
5	Discussion and conclusions.....	126
5.1	Discussion and conclusion regarding data analysis without considering physical models	126
5.2	Discussion and conclusion regarding data analysis with considering physical models	127

List of Figures

FIGURE 2.1. BASIC DEFINITION OF POLYMER FLOODING (RELLEGADLA ET AL., 2017)	23
FIGURE 2.2. NORMALIZED OIL RECOVERY FOR DIFFERENT MOBILITY RATIO BASED ON MOBILITY RATIO (STAVLAND, JONSBRÅTEN, & STRAND, 2013).....	23
FIGURE 2.3. CHEMICAL STRUCTURE OF PARTIALLY HYDROLYZED POLYACRYLAMIDES (HPAM) POLYMER (BIRD, CURTISS ET AL. 1987).....	24
FIGURE 2.4. ARBITRARY VOLUME OVER SPACE (BIRD ET AL., 1987).....	28
FIGURE 2.5. ELEMENT OF ds ACROSS WHICH A FORCE πnds IS TRANSMITTED (BIRD ET AL., 1987).....	30
FIGURE 2.6. SKECH SHOWING THE SIGN CONVECTION AND INDEX CONVECTION FOR COMPONENTS OF STRESS TENSOR π (BIRD, DOTSON ET AL. 1980).....	30
FIGURE 2.7. DIFFERENT BEHAVIOR OF DIFFERENT TYPES OF FLUID REGARDING APPLIED SHEAR RATE (RESEARCHGATE.COM).....	34
FIGURE 2.8. FLOW OF NEWTONIAN AND NON-NEWTONIAN FLOW IN A) IN PRIMARY STATE (BOTTOM COVERED) AND B) IN SECONDARY STATE (REMOVED BOTTOM COVERED) (BIRD ET AL., 1987)(ISLAM 2019)	34
FIGURE 2.9. ROD CLIMBING PHENOMENA (YOUTUBE.COM).....	36
FIGURE 2.10. DIE SWELLING PHENOMENA IN RIGHT (NEWTONIAN) AND LEFT (POLYMERIC) SOLUTION(YOUTUBE.COM)	37
FIGURE 2.11. CUTTING AN ALUMINUM SOAP SOLUTION PHENOMENA FIRST CONDUCTED BY LODGE (LODGE 1964) TAKEN FROM (BIRD ET AL., 1987).....	38
FIGURE 2.12. TUBELESS SIPHON PHENOMENON IN (A) NEWTONIAN AND(B) POLYMERIC SOLUTION (ISLAM 2019)...	39
FIGURE 2.13. REPRESENTED SHAPE OF SHEAR FLOW (CHEGG.COM).....	40
FIGURE 2.14. NON-NEWTONIAN VISCOSITY(η) OF LOW-DENSITY MELTED POLYETHYLENE VERSUS SHEAR RATE(γ) IN DIFFERENT TEMPERATURE IN LOG-LOG SCALE AXIS(DUNSTAN 2019).....	42
FIGURE 2.15. THE TYPICAL CHANGING TREND OF FIRST NORMAL STRESS COEFFICIENT(Ψ) VERSUS REDUCED APPLIED SHEAR RATE (γ) for a low density polyethylene melt (RIBAU, FERRÁS ET AL. 2019).....	43
FIGURE 2.16. SIMPLE SCHEMATIC OF STARTUP FLOW (BIRD ET AL., 1987).....	44
FIGURE 2.17. SHEAR STRESS GROWTH ($\eta + (t, \gamma_0)$) VERSUS OF TIME (t) FOR MELTED LOW-DENSITY POLYETHYLENE WITH RESPECTED TO DIFFERENT INITIAL SHEAR RATE (BIRD ET AL., 1987).....	45
FIGURE 2.18. NORMALIZED SHEAR STRESS GROWTH ($\eta + (t, \gamma_0)\eta(\gamma_0)$) VERSUS TIME(t) FOR 1.5% POLYACRYLAMIDE IN 50/50 MIXTURE BY WEIGHT OF WATER AND GLYCERIN (BIRD, CURTISS ET AL. 1987).....	46
FIGURE 2.19. SHOWS FIRST NORMAL STRESS COEFFICIENT GROWTH ($\Psi_1 + (t, \gamma_0)$) OF MELTED LOW-DENSITY POLYETHYLENE OVER ELAPSED TIME (BIRD ET AL., 1987)	47
FIGURE 2.20. SIMPLE SCHEMATIC OF RELAXATION FLOW (BIRD ET AL., 1987).....	47
FIGURE 2.21. NORMALIZED LOGARITHMIC SHEAR STRESS RELAXATION ($\log \eta - (t, \gamma_0)\eta(\gamma_0)$)) VERSUS TIME(t) OF LOW DENSITY POLYETHYLENE IMPLEMENTATION OF DIFFERENT INITIAL SHEAR RATE TAKEN FROM (BIRD ET AL., 1987).....	49
FIGURE 2.22. SYSTEMATIC COMPARISON FOR RELAXATION MOOD BETWEEN SHEAR STRESS (SHOWN WITH) FIRST NORMAL STRESS DIFFERENCES COEFFICIENT(SHOWN WITH) (BIRD, CURTISS ET AL. 1987).....	50

FIGURE 2.23. VISCOSITY CURVE (SOLID LINE) AND APPROXIMATION BY THE POWER LAW MODEL (DASHED LINE) IN EQ. 41 (RUDOLPH AND OSSWALD 2014) (DE WAELE 1923, OSTWALD 1923, OSTWALD 1929).....	52
FIGURE 2.24. CONCEPT OF GENERALIZED FLUID MODEL FOR ALL DIFFERENT KIND OF FLOW ("WHAT ARE THE PROPERTIES OF NON-NEWTONIAN FLUIDS,").....	53
FIGURE 2.25. THE BIRD-CARREAU-YASUDA MODEL SCHEMATIC (RUDOLPH AND OSSWALD 2014)	54
FIGURE 2.26. DUMBBELLS MODEL SCHEMATIC	56
FIGURE 2.27. DIMENSIONLESS VISCOSITY($\eta - \eta^\infty \eta_0 - \eta^\infty$)VERSUS DIMENSIONLESS SHEAR RATE ($\lambda e \dot{\gamma}$) FOR DILUTE SOLUTION OF FENE-P DUMBBELLS BASED ON EQUATION(21) IN (BIRD, DOTSON ET AL. 1980).....	61
FIGURE 2.28. MASTER CURVE OF DIMENSIONLESS VISCOSITY ($\eta \eta_0$) (SHOWN WITH BLUE CURVE) AND NORMALIZED FIRST NORMAL STRESS COEFFICIENT (SHOWN WITH RED CURVE) VERSUS DIMENSIONLESS SHEAR RATE ($\dot{\gamma} D = C \text{Convert. } \dot{\gamma}$)	62
FIGURE 2.29. DIMENSIONLESS SHEAR STRESS RELAXATION($\eta - \eta^\infty \eta_0 - \eta^\infty -$) AS A FUNCTION OF DIMENSIONLESS TIME($t \lambda e$) AFTER CESSATION OF STEADY SHEAR FLOW FOR FENE-P DUMBBELLS, FROM EQUATION(49) OF (BIRD, DOTSON ET AL. 1980)	63
FIGURE 2.30. NON-NEWTONIAN VISCOSITY (B) OF C-FENE-P DUMBBELLS, PLOTTED AS A FUNCTION OF DIMENSIONLESS SHEAR RATE ($\lambda \dot{\gamma}$), , FOR DIFFERENT VALUES OF E . THE LIMITING CASES $E = 0$ (UNCHARGED FENE-P DUMBBELLS) AND $E \rightarrow \infty$ (RIGID DUMBBELLS) ARE MARKED. THE NONLINEARITY PARAMETER, B, IS SET TO A MODERATE VALUE OF 50.(SHOGIN AND AMUNDSEN 2020)	65
FIGURE 2.31. NORMALIZED POLYMER CONTRIBUTION TO SHEAR STRESS [(A), (C), AND (E)] AND FIRST NORMAL STRESS DIFFERENCE [(B), (D), AND (F)] GROWTH FUNCTIONS OF C-FENE-P DUMBBELLS, PLOTTED AGAINST DIMENSIONLESS TIME, T/A, FOR DIFFERENT VALUES OF PARAMETER AT E AT $\lambda \dot{\gamma} = 0.5$ [(A) AND (B)], $\lambda \dot{\gamma} = 5$ [(C) AND (D)], AND $\lambda \dot{\gamma} = 50$ [(E) AND (F)]. THE LIMITING CASES $E = 0$ (FENE-P DUMBBELLS) AND $E \rightarrow \infty$ (RIGID DUMBBELLS) ARE SHOWN. ALL CURVES ARE PLOTTED AT $B = 50$ (SHOGIN AND AMUNDSEN 2020).....	66
FIGURE 2.32. NORMALIZED POLYMER CONTRIBUTION TO SHEAR STRESS AND FIRST NORMAL STRESS DIFFERENCE RELAXATION FUNCTIONS OF C-FENE-P DUMBBELLS, PLOTTED AGAINST DIMENSIONLESS TIME T/A AT $\lambda \dot{\gamma} = 5$ (A) AND $\lambda \dot{\gamma} = 50$ (B) FOR DIFFERENT VALUES OF E. THE FENE-P LIMIT, $E = 0$, AND THE RDB LIMIT, $E \rightarrow \infty$, ARE ALSO SHOWN. THE VALUE OF B IS SET TO 50 (SHOGIN AND AMUNDSEN 2020)	67
FIGURE 2.33. SIMPLE REPRESENTATIVE OF PHAN-THIEN-TANNER MODEL (PTT) (THIEN AND TANNER 1977).....	69
FIGURE 2.34. DIMENSIONLESS VISCOSITY. $B = \lambda_0 \dot{\gamma}$, DIMENSIONLESS SHEAR RATE. FOR $\epsilon = 0.01$, FOR $\epsilon = 0.2$..	70
FIGURE 2.35. MASTER CURVE OF DIMENSIONLESS VISCOSITY ($\eta \eta_0$) (SHOWN WITH BLUE CURVE) AND NORMALIZED FIRST NORMAL STRESS COEFFICIENT (SHOWN WITH RED CURVE) VERSUS DIMENSIONLESS SHEAR RATE ($\dot{\gamma} D = C \text{Convert. } \dot{\gamma}$) FOR AFFINE LPPT MODEL	71
FIGURE 3.1. FROM LEFT; GRADUATED CYLINDER, MEASURING SPOON, SCALE NUMBER 1 AND SCALE NUMBER 2.....	75
FIGURE 3.2 FROM LEFT; HPAM POLYMER POWDER ,MOTHER SOLUTION $C_c=3.10^4$ PPM, MIXER FOR MIXING POLYMER POWDER AND WATER AND MAGNETIC MIXER.....	75
FIGURE 3.3. HPAM POLYMER WITH CONCENTRATION FROM LEFT; $C_c = 1.5.10^4$ ppm, $C_c = 2.10^4$ ppm	77
FIGURE 3.4. FROM LEFT; ANTON PAAR RHEOMETER, CONE-AND-PLATE ATTACHMENT, GRADUATED PIPETTE FOR PORING POLYMER INTO RHEOMETER.....	79
FIGURE 3.5. SETTING PARAMETER OF SHEAR RAMPING TEST	80
FIGURE 3.6. SETTING PARAMETER OF STARTUP OF STEADY SHEAR RATE EXPERIMENT	81

FIGURE 4.1. PRODUCED GRAPH OF VISCOSITY (η) VERSUS SHEAR RATE (γ) FOR $CC=3.10^4$ PPM, $CC=2.10^4$ PPM AND $CC=1.5.10^4$ PPM HPAM POLYMER SOLUTION IN LOG-LOG AXIS SCALE	83
FIGURE 4.2. NORMALIZED VISCOSITY (η/η_0) VERSUS APPLIED SHEAR RATE (γ) FOR $CC=3.10^4$ PPM HPAM POLYMER SOLUTION IN LOG-LOG AXIS.....	84
FIGURE 4.3. NORMALIZED VISCOSITY (η/η_0) VERSUS APPLIED SHEAR RATE (γ) FOR $CC=2.10^4$ PPM HPAM POLYMER SOLUTION IN LOG-LOG AXIS.....	84
FIGURE 4.4. NORMALIZED VISCOSITY (η/η_0) VERSUS APPLIED SHEAR RATE (γ) FOR $CC=1.5.10^4$ PPM HPAM POLYMER SOLUTION IN LOG-LOG AXIS.....	85
FIGURE 4.5. CUMULATIVE RESULT OF FIGURE 4.2 TO FIGURE 4.4	85
FIGURE 4.6. FIRST NORMAL STRESS DIFFERENCES COEFFICIENT (Ψ_1) VERSUS SHEAR RATE (γ) OF $CC=3.10^4$ PPM HPAM POLYMER SOLUTION IN LOG-LOG AXIS.....	86
FIGURE 4.7. FIRST NORMAL STRESS DIFFERENCES COEFFICIENT (Ψ_1) VERSUS SHEAR RATE (γ) OF $CC=2.10^4$ PPM HPAM POLYMER SOLUTION IN LOG-LOG AXIS.....	87
FIGURE 4.8. FIRST NORMAL STRESS DIFFERENCES COEFFICIENT (Ψ_1) VERSUS SHEAR RATE (γ) OF $CC=1.5.10^4$ PPM HPAM POLYMER SOLUTION IN LOG-LOG AXIS.....	88
FIGURE 4.9. NORMALIZED START UP GROWTH($\eta + (t, \gamma_0)\eta(\gamma_0)$) VERSUS TIME (t) FOR SHEAR RATE $\gamma = 0.01$...	89
FIGURE 4.10. NORMALIZED START UP GROWTH($\eta + (t, \gamma_0)\eta(\gamma_0)$) VERSUS TIME (t) FOR SHEAR RATE $\gamma = 0.1$...	90
FIGURE 4.11. NORMALIZED START UP GROWTH($\eta + (t, \gamma_0)\eta(\gamma_0)$) VERSUS TIME (t) FOR SHEAR RATE $\gamma = 1$	90
FIGURE 4.12. NORMALIZED START UP GROWTH($\eta + (t, \gamma_0)\eta(\gamma_0)$) VERSUS TIME (t) FOR SHEAR RATE $\gamma = 10$	91
FIGURE 4.13. NORMALIZED START UP GROWTH($\eta + (t, \gamma_0)\eta(\gamma_0)$) VERSUS TIME (t) FOR SHEAR RATE $\gamma = 20$	91
FIGURE 4.14. NORMALIZED START UP GROWTH($\eta + (t, \gamma_0)\eta(\gamma_0)$) VERSUS TIME (t) FOR SHEAR RATE $\gamma = 60$	92
FIGURE 4.15. NORMALIZED START UP GROWTH($\eta + (t, \gamma_0)\eta(\gamma_0)$) VERSUS TIME (t) FOR SHEAR RATE $\gamma = 100$	92
FIGURE 4.16. CUMULATIVE COMPARISON ON SIZE OF OVERSHOOT REGARDING DIFFERENT INITIAL SHEAR RATES AND CONCENTRATIONS.....	94
FIGURE 4.17. CUMULATIVE COMPARISON ON DEVIATION TIME REGARDING DIFFERENT INITIAL SHEAR RATES AND CONCENTRATIONS.	94
FIGURE 4.18. NORMALIZED STRESS RELAXATION ($\eta - (t, \gamma_0)\eta(\gamma_0)$) OF HPAM POLYMER $CC=3.10^4$ PPM VERSUS TIME(t) REGARDING DIFFERENT INITIAL SHEAR RATE BEFORE CESSION IN LOG-LINEAR SCALE AXIS.	95
FIGURE 4.19. NORMALIZED STRESS RELAXATION ($\eta - (t, \gamma_0)\eta(\gamma_0)$) OF HPAM POLYMER $CC=2.10^4$ PPM TIME(t) REGARDING DIFFERENT INITIAL SHEAR RATE BEFORE CESSION IN LOG-LINEAR SCALE AXIS	96
FIGURE 4.20. NORMALIZED STRESS RELAXATION ($\eta - (t, \gamma_0)\eta(\gamma_0)$) OF HPAM POLYMER $CC=1.5.10^4$ PPM VERSUS TIME(t) REGARDING DIFFERENT INITIAL SHEAR RATE BEFORE CESSION IN LOG-LINEAR SCALE AXIS	96
FIGURE 4.21. NORMALIZED STRESS RELAXATION ($\eta - (t, \gamma_0)\eta(\gamma_0)$) VERSUS TIME (t) OF DIFFERENT CONCENTRATION REGARDING INITIAL SHEAR RATE ($\gamma = 0.1$)	97
FIGURE 4.22. NORMALIZED STRESS RELAXATION $\eta - (t, \gamma_0)\eta(\gamma_0)$ VERSUS TIME(T) OF DIFFERENT CONCENTRATION REGARDING INITIAL SHEAR RATE ($\gamma = 1$).....	98
FIGURE 4.23. NORMALIZED STRESS RELAXATION $\eta - (t, \gamma_0)\eta(\gamma_0)$ VERSUS TIME (T) OF DIFFERENT CONCENTRATION REGARDING INITIAL SHEAR RATE ($\gamma=10$)	98
FIGURE 4.24. CUMULATIVE RESULT OF SLOPE OF REDUCTION IN EXPONENTIAL REGION.....	99

FIGURE 4.25. DIMENSIONLESS VISCOSITY ($\eta\eta_0$) VERSUS DIMENSIONLESS SHEAR RATE ($\lambda\gamma$) IS FITTED TO FULL LPPT MODEL (SHOWN WITH BLUE CURVE) FOR $Cc=3 \cdot 10^4$ PPM HPAM POLYMER SOLUTION	102
FIGURE 4.26. DIMENSIONLESS VISCOSITY ($\eta\eta_0$) VERSUS DIMENSIONLESS SHEAR RATE ($\lambda\gamma$) IS FITTED TO FULL LPPT MODEL (SHOWN WITH BLUE CURVE) FOR $Cc=2 \cdot 10^4$ PPM HPAM POLYMER SOLUTION	102
FIGURE 4.27. DIMENSIONLESS VISCOSITY ($\eta\eta_0$) VERSUS DIMENSIONLESS SHEAR RATE ($\lambda\gamma$) IS FITTED TO FULL LPPT MODEL (SHOWN WITH BLUE CURVE) FOR $Cc=1.5 \cdot 10^4$ PPM HPAM POLYMER SOLUTION.....	103
FIGURE 4.28. DIMENSIONLESS VISCOSITY ($\eta\eta_0$) VERSUS DIMENSIONLESS SHEAR RATE ($3\varepsilon_2 \lambda\gamma$) IS FITTED TO AFFINE LPPT MODE(SHOWN WITH BLUE CURVE) FOR HPAM POLYMER $Cc=3 \cdot 10^4$ PPM	104
FIGURE 4.29. DIMENSIONLESS VISCOSITY ($\eta\eta_0$) VERSUS DIMENSIONLESS SHEAR RATE ($3\varepsilon_2 \lambda\gamma$) FOR HPAM POLYMER $Cc=2 \cdot 10^4$ PPM	105
FIGURE 4.30. DIMENSIONLESS VISCOSITY ($\eta\eta_0$) VERSUS DIMENSIONLESS SHEAR RATE ($3\varepsilon_2 \lambda\gamma$) IS FITTED TO AFFINE LPPT MODE(SHOWN WITH BLUE CURVE) FOR HPAM POLYMER $Cc=1.5 \cdot 10^4$ PPM	105
FIGURE 4.31. DIMENSIONLESS VISCOSITY ($\eta\eta_0$) VERSUS DIMENSIONLESS SHEAR RATE ($2\varepsilon \lambda\gamma$) IS FITTED TO AFFINE EPPT MODE(SHOWN WITH BLUE CURVE) FOR HPAM $Cc=3 \cdot 10^4$ PPM	106
FIGURE 4.32. DIMENSIONLESS VISCOSITY ($\eta\eta_0$) VERSUS DIMENSIONLESS SHEAR RATE ($2\varepsilon \lambda\gamma$) IS FITTED TO AFFINE EPPT MODE(SHOWN WITH BLUE CURVE) FOR HPAM POLYMER $Cc=2 \cdot 10^4$ PPM	107
FIGURE 4.33. DIMENSIONLESS VISCOSITY ($\eta\eta_0$) VERSUS DIMENSIONLESS SHEAR RATE ($2\varepsilon \lambda\gamma$)) IS FITTED TO AFFINE EPPT MODE(SHOWN WITH BLUE CURVE) FOR HPAM POLYMER $Cc=1.5 \cdot 10^4$ PPM FOR HPAM	107
FIGURE 4.34. DIMENSIONLESS VISCOSITY ($\eta\eta_0$) VERSUS DIMENSIONLESS SHEAR RATE ($\lambda\gamma$) IS FITTED TO C-FENE-P MODEL (SHOWN WITH BLUE CURVE) FOR HPAM POLYMER $Cc=3 \cdot 10^4$ PPM	108
FIGURE 4.35. DIMENSIONLESS VISCOSITY ($\eta\eta_0$) VERSUS DIMENSIONLESS SHEAR RATE ($\lambda\gamma$) IS FITTED TO C-FENE-P MODEL (SHOWN WITH BLUE CURVE) FOR HPAM POLYMER $Cc=2 \cdot 10^4$ PPM	109
FIGURE 4.36. DIMENSIONLESS VISCOSITY ($\eta\eta_0$) VERSUS DIMENSIONLESS SHEAR RATE ($\lambda\gamma$) IS FITTED TO C-FENE-P MODEL (SHOWN WITH BLUE CURVE) FOR HPAM POLYMER $Cc=1.5 \cdot 10^4$ PPM).....	109
FIGURE 4.37. THE DIMENSIONLESS SHEAR STRESS GROWTH OF STARTUP OF STEADY SHEAR FLOW ($\eta + (t, \gamma_0)\eta(\gamma_0)$) VERSUS TIME (T) IS FITTED WITH FIRST APPROACH RELATIVE TO AFFINE PPT MODEL(RED, BLUE, GREEN CURVE), FOR HPAM POLYMER $Cc = 3 \cdot 10^4$ ppm, OF $w_i=0.384$, $w_i=3.84$ AND $w_i=38.4$	111
FIGURE 4.38. THE DIMENSIONLESS SHEAR STRESS RELAXATION OF CESSATION OF STEADY SHEAR FLOW $\eta - (t, \gamma_0)\eta(\gamma_0)$)VERSUS TIME (T) IS FITTED WITH FIRST APPROACH RELATIVE TO AFFINE PPT MODEL(RED, BLUE, GREEN CURVE), FOR HPAM POLYMER $Cc = 3 \cdot 10^4$ ppm, WITH OF $w_i=0.384$, $w_i=3.84$ AND $w_i=38.4$	111
FIGURE 4.39. .THE DIMENSIONLESS SHEAR STRESS GROWTH OF STARTUP OF STEADY SHEAR FLOW ($\eta + (t, \gamma_0)\eta(\gamma_0)$) VERSUS TIME (T) IS FITTED WITH SECOND APPROACH RELATIVE TO AFFINE PPT MODEL(RED, BLUE, GREEN CURVE), FOR HPAM POLYMER $Cc = 3 \cdot 10^4$ ppm, $w_i=0.132$, $w_i=1.32$ AND $w_i=13.2$	112
FIGURE 4.40. THE DIMENSIONLESS SHEAR STRESS RELAXATION OF CESSATION OF STEADY SHEAR FLOW $\eta - (t, \gamma_0)\eta(\gamma_0)$)VERSUS TIME (T)IS FITTED WITH SECOND APPROACH RELATIVE TO AFFINE PPT MODEL(RED, BLUE, GREEN CURVE), FOR HPAM POLYMER $Cc = 3 \cdot 10^4$ ppm, WITH $w_i=0.132$, $w_i=1.32$ AND $w_i=13.2$...	113
FIGURE 4.41. THE DIMENSIONLESS SHEAR STRESS GROWTH OF STARTUP OF STEADY SHEAR FLOW ($\eta + (t, \gamma_0)\eta(\gamma_0)$) VERSUS TIME(T) IS FITTED WITH FIRST APPROACH RELATIVE TO FENE-P MODEL(RED,, BLUE ,GREEN CURVE), FOR HPAM POLYMER $Cc = 3 \cdot 10^4$ ppm, $w_i=0.961$, $w_i=9.61$ AND $w_i=96.1$	115

FIGURE 4.42. THE DIMENSIONLESS SHEAR STRESS RELAXATION OF CESSATION OF STEADY SHEAR FLOW $\eta - (t, \gamma_0)\eta(\gamma_0)$ VERSUS TIME(T) IS FITTED WITH FIRST APPROACH RELATIVE TO FENE-P MODEL(RED, BLUE, GREEN CURVE), FOR HPAM POLYMER $Cc = 3 \cdot 10^4$ ppm, WITH $wi=0.961$, $wi=9.61$ AND $wi=96.1$	115
FIGURE 4.43. THE DIMENSIONLESS SHEAR STRESS GROWTH OF STARTUP OF STEADY SHEAR FLOW $(\eta + (t, \gamma_0)\eta(\gamma_0))$ VERSUS TIME(T) IS FITTED WITH SECOND APPROACH RELATIVE TO FENE-P MODEL(RED,, BLUE ,GREEN CURVE), FOR HPAM POLYMER $Cc = 3 \cdot 10^4$ ppm, WITH $wi=0.374$, $wi=3.74$ AND $wi=37.4$	116
FIGURE 4.44 THE DIMENSIONLESS SHEAR STRESS RELAXATION OF CESSATION OF STEADY SHEAR FLOW $\eta - (t, \gamma_0)\eta(\gamma_0)$ VERSUS TIME(T) IS FITTED WITH FIRST SECOND APPROACH RELATIVE TO FENE-P MODEL(RED,, BLUE ,GREEN CURVE), FOR HPAM POLYMER $Cc = 3 \cdot 10^4$ ppm, $wi=0.374$, $wi=3.74$ AND $wi=37.4$	117
FIGURE 4.45. THE DIMENSIONLESS SHEAR STRESS GROWTH OF STARTUP OF STEADY SHEAR FLOW $(\eta + (t, \gamma_0)\eta(\gamma_0))$ VERSUS DIMENSIONLESS TIME (R) IS RELATIVE TO C-FENE-P MODEL (BLUE CURVE), FOR HPAM POLYMER $Cc = 2 \cdot 10^4$ ppm, ($wi = \gamma\lambda Q$) $wi = 1$	118
FIGURE 4.46. THE DIMENSIONLESS SHEAR STRESS GROWTH OF STARTUP OF STEADY SHEAR FLOW $(\eta + (t, \gamma_0)\eta(\gamma_0))$ VERSUS DIMENSIONLESS TIME (R) IS RELATIVE TO C-FENE-P MODEL (BLUE CURVE), FOR HPAM POLYMER $Cc = 2 \cdot 10^4$ ppm, WITH ($wi = \gamma\lambda Q$) $wi = 10$	119
FIGURE 4.47. THE DIMENSIONLESS SHEAR STRESS GROWTH OF STARTUP OF STEADY SHEAR FLOW $(\eta + (t, \gamma_0)\eta(\gamma_0))$ VERSUS DIMENSIONLESS TIME (R) IS RELATIVE TO C-FENE-P MODEL (BLUE CURVE), FOR HPAM POLYMER $Cc = 2 \cdot 10^4$ ppm, WITH ($wi = \gamma\lambda Q$) $wi = 100$	119
FIGURE 4.48. THE DIMENSIONLESS SHEAR STRESS RELAXATION OF CESSATION OF STEADY SHEAR FLOW $\eta - (t, \gamma_0)\eta(\gamma_0)$ VERSUS DIMENSIONLESS TIME(R) IS FITTED WITH RELATIVE TO C -FENE-P MODEL(BLUE CURVE), FOR HPAM POLYMER $Cc = 2 \cdot 10^4$ ppm, WITH ($wi = \gamma\lambda Q$) $wi = 1$	120
FIGURE 4.49. THE DIMENSIONLESS SHEAR STRESS RELAXATION OF CESSATION OF STEADY SHEAR FLOW $\eta - (t, \gamma_0)\eta(\gamma_0)$ VERSUS DIMENSIONLESS TIME(R) IS FITTED WITH RELATIVE TO C -FENE-P MODEL(BLUE CURVE), FOR HPAM POLYMER $Cc = 2 \cdot 10^4$ ppm, WITH ($wi = \gamma\lambda Q$) $wi = 10$	121
FIGURE 4.50. THE DIMENSIONLESS SHEAR STRESS RELAXATION OF CESSATION OF STEADY SHEAR FLOW $\eta - (t, \gamma_0)\eta(\gamma_0)$ VERSUS DIMENSIONLESS TIME(R) IS FITTED WITH RELATIVE TO C -FENE-P MODEL(BLUE CURVE), FOR HPAM POLYMER $Cc = 2 \cdot 10^4$ ppm, WITH ($wi = \gamma\lambda Q$) $wi = 100$	121
FIGURE 4.51 THE DIMENSIONLESS SHEAR STRESS GROWTH OF STARTUP OF STEADY SHEAR FLOW $(\eta + (t, \gamma_0)\eta(\gamma_0))$ VERSUS DIMENSIONLESS TIME (R) IS RELATIVE TO C-FENE-P MODEL (BLUE CURVE), FOR HPAM POLYMER $Cc = 1.5 \cdot 10^4$ ppm, WITH ($wi = \gamma\lambda Q$) $wi = 0.3$	122
FIGURE 4.52. THE DIMENSIONLESS SHEAR STRESS GROWTH OF STARTUP OF STEADY SHEAR FLOW $(\eta + t, \gamma_0)\eta(\gamma_0)$ VERSUS DIMENSIONLESS TIME (R) IS RELATIVE TO C-FENE-P MODEL (BLUE CURVE), FOR HPAM POLYMER $Cc = 1.5 \cdot 10^4$ ppm, WITH ($wi = \gamma\lambda Q$) $wi = 3$	123
FIGURE 4.53. THE DIMENSIONLESS SHEAR STRESS GROWTH OF STARTUP OF STEADY SHEAR FLOW $(\eta + (t, \gamma_0)\eta(\gamma_0))$ VERSUS DIMENSIONLESS TIME (R) IS RELATIVE TO C-FENE-P MODEL (BLUE CURVE), FOR HPAM POLYMER $Cc = 1.5 \cdot 10^4$ ppm, WITH DIMENSIONLESS SHEAR RATE($wi = \gamma\lambda Q$) $wi = 30$	123
FIGURE 4.54. THE DIMENSIONLESS SHEAR STRESS RELAXATION OF CESSATION OF STEADY SHEAR FLOW $\eta - (t, \gamma_0)\eta(\gamma_0)$ VERSUS DIMENSIONLESS TIME(R) IS FITTED WITH RELATIVE TO C -FENE-P MODEL(BLUE CURVE), FOR HPAM POLYMER $Cc = 1.5 \cdot 10^4$ ppm, WITH ($wi = \gamma\lambda Q$) $wi = 0.3$	124

FIGURE 4.55. THE DIMENSIONLESS SHEAR STRESS RELAXATION OF CESSATION OF STEADY SHEAR FLOW $\eta - (t, \gamma_0)\eta(\gamma_0)$ VERSUS DIMENSIONLESS TIME(t) IS FITTED WITH RELATIVE TO C -FENE-P MODEL(BLUE CURVE), FOR HPAM POLYMER $C_c = 1.5 \cdot 10^4$ ppm, WITH ($w_i = \gamma\lambda Q$) $w_i = 3$ 124

FIGURE 4.56. THE DIMENSIONLESS SHEAR STRESS RELAXATION OF CESSATION OF STEADY SHEAR FLOW $\eta - (t, \gamma_0)\eta(\gamma_0)$ VERSUS DIMENSIONLESS TIME(t) IS FITTED WITH RELATIVE TO C -FENE-P MODEL(BLUE CURVE), FOR HPAM POLYMER $C_c = 1.5 \cdot 10^4$ ppm, WITH DIMENSIONLESS SHEAR RATE($w_i = \gamma\lambda Q$) $w_i = 30$ 125

List of Tables

TABLE 2.1. SYSTEMATIC COMPARISON BETWEEN DIFFERENT TYPES OF POLYMERS TAKEN FROM(THOMAS 2016, RELLEGADLA, PRAJAPAT ET AL. 2017, DR. R. GIRI PRASADI 2018)..... 25

TABLE 3.1:PREDEFINED CONCENTRATION VERSUS CONCENTRATION ON PRACTICE..... 78

1 Introduction

The difference in quantity is considered as a key point in generation and movement. For example, electricity moves from one point to another point due to difference in electric potential between these two points. Likewise, water moves from one point with higher height to another point with lower height due to difference in gravitational energy (the energy that is stored in material due to their height from earth). The same happens for movement of oil from its stored place (called reservoir). In fact, it moves from high pressure region of reservoir (called cap rock) to low pressure region (oil well) due to differences in pressure. This production is called primary production which can only lead to production of ten percent of original oil in place (OOIP). The more production, the more reduction in pressure differences between reservoir and wellbore and consequently the more trapped source of oil and gas in reservoir, leading to implementation of secondary recovery technology. With secondary recovery we mean production of between 15 to 60 percent of remaining OOIP by injection of external fluid, such as gas and water to maintain the reservoir pressure. Ultimately, oil industry went through Enhanced Oil Recovery (EOR) processing methods to extract even more oil and gas resources from reservoir. The EOR methods can be classified in three categories, namely chemical, thermal, and microbial treatment. But, according to Norwegian Petroleum Directorate (NPD), chemical EOR and in particular polymer flooding is predicted to be most applicable chemical approach for Enhanced oil recovery on the Norwegian Continental Shelf (NCS) (Lake 1989, Thomas 2016, Rellegadla, Prajapat et al. 2017, Dr. R. Giri Prasad 2018, NPD 2018). In fact, Injection of high viscosity polymers in to well can simply mobilize the trapped oil in reservoir, resulting in higher oil recovery (Rellegadla, Prajapat et al. 2017). So, as noted above polymers are considered as a promising way of EOR processing in oil industry.

On the other hand, there is some limitations and uncertainties which caused some serious issues in utilization of polymers in operational phase. Apart from some environmental issues, polymer loss and polymer degradation (loss of some its main properties like viscosity) during processing is considered as main drawbacks of polymer based flooding (Rellegadla, Prajapat et al. 2017). Moreover, for material to be used in the well, all its engineering properties should be predictable. In this concept rheological properties of polymers (the properties of material which relate stress to deformation empirically) and also the functions that describes these rheological properties (called material function in academia) are of great importance ((Rudolph and

Osswald 2014, Morris 2016)). But, since polymers are classified as non-Newtonian fluid (kind of fluid which does not obey classic physics rules), advanced complex models are required for prediction of their rheological properties. So, although, polymers are promising ways of EOR, there is still long way to being utilized in operation phase. This was addressed in this research and this thesis has organized accordingly to provide better understanding of not only rheology and material function properties of polymer itself, but also its behavioral proposed models.

1.1 Objective

Aline with above introduction, this master thesis has aimed primarily to study the material functions of specific kind of polymer called Partially Hydrolyzed Polyacrylamide (HPAM) polymer in three different concentration of $C_c=3.10^4$ ppm, $C_c=2.10^4$ ppm and $C_c=1.5.10^4$ ppm in steady and transient experiments: shear ramping, start-up and cessation of steady shear. Up to this point has been analyzed in Islam thesis (Islam 2019), though with different sample. But here the major key distinction is focusing on more data analysis both with considering physical models and without considering physical models via both quantitative and qualitative data analysis. In other words, performing more analysis, instead of conducting more experimental works. Hence, the secondary objective can be classified as a below.

- first experimental data related to material function of these three experiments is analyzed without considering proposed models in literature to see whether the proposed theory by Islam thesis (Islam 2019), regarding the effect of concentration on material function of steady and transient flow, can be also verified with new polymer sample (HPAM polymer) with mentioned concentrations. Though the focus of this thesis is not on concentration.
- then gained experimental data is fitted to typical physical models proposed in literature to obtain the most representative model for describing this special kind of polymer.

1.2 Research structure

The structure of this research for obtaining above defined goals, has been summarized in below.

- **Literature review:**
where some materials and references, is reviewed to acquire a basic knowledge about the topic.
- **Experimental procedure:**
where experimental procedure for running tests is introduced.
- **Data analysis:**
where resulted data from experiment part is analyzed to obtain practical outcomes in conclusion part.
- **Discussion and conclusions:**
where conclusion is made from data analysis in order to satisfy objectives listed in part 1.1.

2 Literature review

2.1 Quick introduction on polymer flooding process

The concept of polymer flooding, in which polymer is injected to the injection well to extract trapped oil is shown in Figure 2.1. From reservoir engineering point of view, all the concept arises from mobility ratio properties of fluid (the ratio between reservoir permeability relative to fluid and fluid viscosity). In fact, as it can be seen from equation 2.1 utilization of higher viscous fluids (polymers) instead of water, can lead to reduction of relative mobility ratio (the ratio between mobility of displacing fluid (water or polymer) and mobility of displaced fluid (oil)). This reduction is considered as favorable phenomenon since it can lead to more reservoir volume contacted by displacing fluid and higher degree of sweep efficiency of EOR process. Moreover, high viscous polymer solution has a plugging effect on high permeable thief zone which again is considered as a favorable effect on oil displacement (Rellegadla, Prajapat et al. 2017)

$$M = \frac{m_w}{m_o} = \frac{\frac{k_w}{\mu_w}}{\frac{k_o}{\mu_o}} \quad (2.1)$$

Where:

- M is relative mobility ratio of water in comparison with oil [–]
- m_w is mobility ratio of water [md (Pa s)⁻¹]
- m_o is mobility ratio of oil [md (Pa s)⁻¹]
- k_w is permeability of formation relative to water [md]
- μ_w is water viscosity [Pa s]
- k_o is permeability of formation relative to oil [md]
- μ_o is oil viscosity [Pa s]

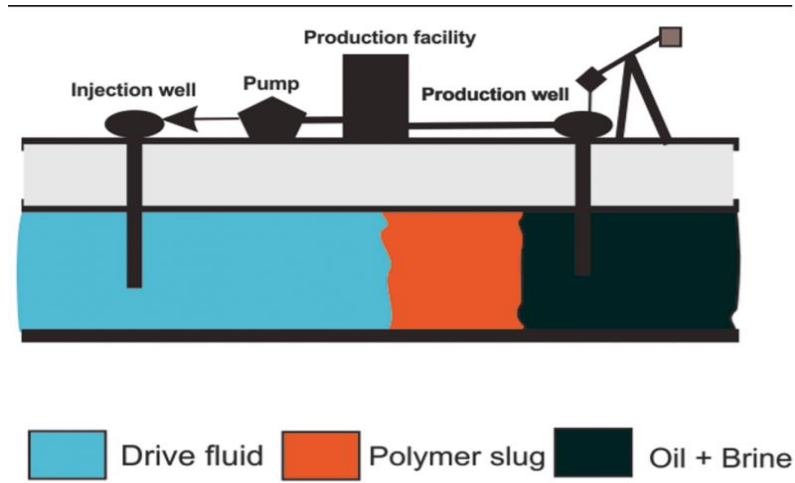


Figure 2.1. Basic definition of polymer flooding (Rellegadla et al., 2017)

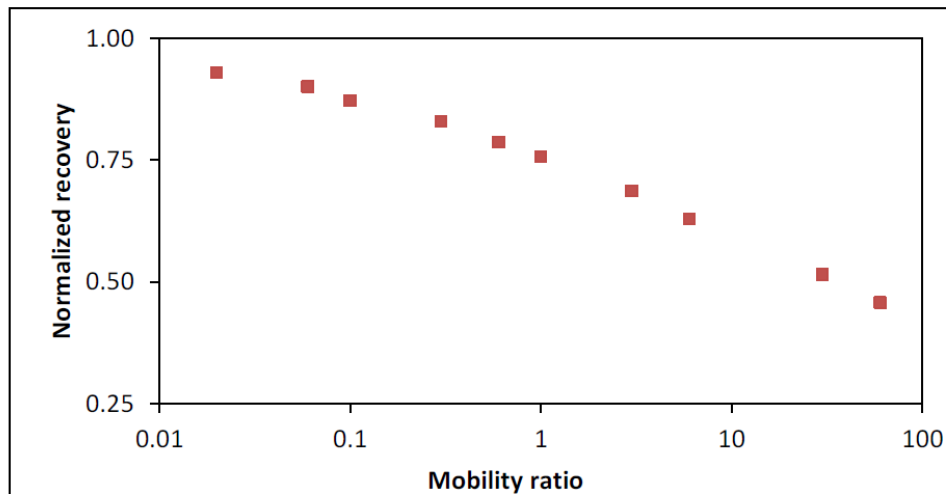


Figure 2.2. Normalized oil recovery for different mobility ratio based on mobility ratio (Stavland, Jonsbråten, & Strand, 2013)

Apart from mathematical description noted in equation 2.1 the concept of polymer flooding was addressed by practical well test in oil field (Figure 2.2). It is seen from Figure 2.2 that how this low relatively mobility ratio could increase oil recovery up to 100 percent (Stavland, Jonsbråten et al. 2013).

2.2 Introduction on polymer basics

2.2.1 Polymer categorization

Polymers are large molecules made of many small simple chemical units known as structural unit. polymers are divided in to two categories namely, synthetic (man-made) and natural (biopolymers). Synthetics are those polymers with estimated molecular weight ranging from $M_w=10^4$ g/mole until $M_w=10^6$ g/mole. Hydrolyzed polyacrylamide (HPAM), polyethylene, polyvinylchloride and polystyrene are some examples of synthetic polymers. On the other hand, natural (biopolymers) polymers are those built from two or more different type of polymers structural unit. Typical biopolymers are DNA, proteins, xanthan, and their molecular weight is of the order $M_w=10^3-10^4$ g/mole. It is also worth to note that Partially Hydrolyzed Polyacrylamides (HPAM) with molecular weight of $M_w= 5.10^5$ g/mole is used in this research. This polymer structural unit (monomer) is shown in Figure 2.3. Following Table 2.1 also summarizes fundamental differences between natural and synthetic polymers (Pearce 1978, Bird, Curtiss et al. 1987, Thomas 2016, Rellegadla, Prajapat et al. 2017, Dr. R. Giri Prasadl 2018).



Figure 2.3. Chemical structure of Partially Hydrolyzed Polyacrylamides (HPAM) polymer (Bird, Curtiss et al. 1987)

Table 2.1. Systematic comparison between different types of polymers taken from(Thomas 2016, Rellegadla, Prajapat et al. 2017, Dr. R. Giri PrasadI 2018)

Partially Hydrolyzed Polyacrylamide (HPAM),	Advantageous	Disadvantageous
	Low cost	Has low shear residence tolerance due to its high molecular weight
	Has plugging effect which ultimately results in higher EOR	Lower salt tolerance
		Degradation of synthetic polymer can cause formation damage
Biopolymers (Xanthan polymer),	Advantageous	Disadvantageous
	Good shear stability	High cost
	Good thickening power at High salinity	Difficulty in preparing
	Higher salt tolerance	
	Degradation of biopolymer ultimately cause bio-plugging which is favorable for EOR recovery	They can be consumed by bacteria and then bacteria inhibitor chemical treatments are needed which ultimately would result in environmental problems

2.3 Introduction on fluid dynamic

Before proceeding to next part, it is worth to first categorize physical quantities as a below to avoid further confusion in next parts (Fleisch 2011):

Scalars ($3^0=1$): Are described by one number like temperature (T) and density (ρ)

Vectors ($3^1=3$): assign a number to each direction like velocity (\mathbf{v}) and force (\mathbf{F})

Tensors ($3^2=9$): assign a number to each ordered pair of directions like stress tensor ($\boldsymbol{\tau}$)

One should also remember that matrixes are only one way of showing tensor. The bold font also used for **scalars** and **vectors** throughout this research.

2.3.1 Introduction on equation of fluid dynamic (“Generalized Navier-Stokes equations”)

As noted in introduction all rheological properties of material should be known for being utilized in EOR processing methods. Then, to obtain full description of polymers during flow, one should first drive the physical dynamic equation that describe polymeric properties (called “Generalized Navier-Stokes equations”), then this equation should be solved either analytically or numerically. Solving this equation for polymers either analytically or numerically is not an easy task since they do not obey classical physics rules. Though, obtaining full description of fluid motion including both scalar fields like temperature (T) and density (ρ), and vector fields like velocity (\mathbf{v}) at any point of fluid and any time of flow is considered as a great inspiration for solving this equation.

The equation of fluid dynamic is result of two equations, namely equation of continuity and equation of motion. These two equations can be obtain from conservation rules summarized below (Bird, Curtiss et al. 1987, Shogin 2020):

- Conservation of mass
- Conservation of momentum
- Conservation of energy

Conservation of energy is important for non-isothermal flows, while flows of polymers can be considered locally isothermal. So, we ignore the conservation of energy in this research.

2.3.2 Conservation of Mass

Figure 2.4 is considered as an arbitrary control volume, fixed in space. Then, if flow initiates over surface element of dS , and volume element of dV with normal force vector of \mathbf{n} , with velocity of \mathbf{v} , the local volume rate over surface of dS is defined as (Bird, Curtiss et al. 1987)

$$V_L = (\mathbf{n} \cdot \mathbf{v})dS. \quad (2.2)$$

Where:

- V_L is local volume rate over surface element of dS [$\text{m}^3 \text{S}^{-1}$]
- Inward flow is defined with negative sign (-)
- Outward flow is defined with positive sign (+)

Then local mass flow rate (M_L) is written as:

$$M_L = (\mathbf{n} \cdot \rho \mathbf{v})dS. \quad (2.3)$$

Where ρ is fluid density [Kg m^3]

Now rate of rise on mass with volume of V is only dependent on rate of addition of mass over surface of dS . This can be mathematically expressed as

$$\frac{d}{dt} \int_V \rho dV = - \int_S (\mathbf{n} \cdot \rho \mathbf{v})dS. \quad (2.4)$$

According to Gauss divergence theorem, equation 2.4 can be rewritten as

$$\frac{d}{dt} \int_V \rho dV = - \int_V (\nabla \cdot \rho \mathbf{v})dV, \quad (2.5)$$

Where ∇ is del operator.

By bringing time derivative inside integral, equation 2.5 is reformed as

$$\int_V \left[\frac{\partial \rho}{\partial t} + (\nabla \cdot \rho \mathbf{v}) \right] dV = 0. \quad (2.6)$$

In this case (integral over arbitrary volume equals to zero), the terms under integral is also equals zero. So,

$$\left[\frac{\partial \rho}{\partial t} + (\nabla \cdot \rho \mathbf{v}) \right] = 0. \quad (2.7)$$

Finally, if the fluid is assumed to be polymer which is liquid and therefore incompressible, one of the most important equations in fluid dynamic called continuity equation is driven as

$$\nabla \cdot \mathbf{v} = 0. \quad (2.8)$$

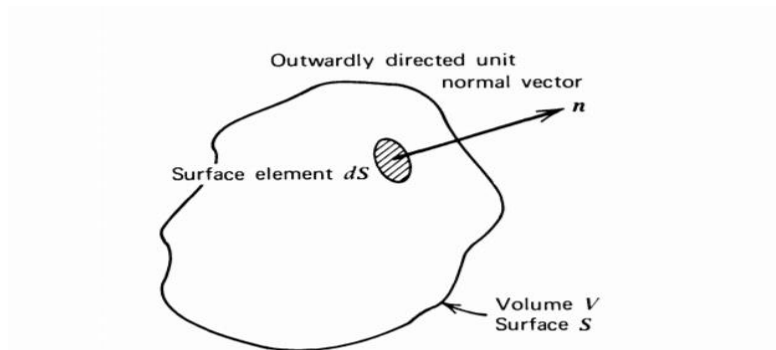


Figure 2.4. Arbitrary volume over space (Bird et al., 1987)

2.3.3 Conservation of momentum

Aline with conservation of mass discussed at pervious section, the transport of momentum equation plays crucial role in driving dynamic of fluid equation. This conservation rule can be interpreted in two different ways which are identical mathematically. In fact, the interpretation of macroscopic (flow) and microscopic contributions to momentum transfer is key distinction between these two approaches. According to first approach; the transportation of momentum

of fluid across surface element of dS (see Figure 2.5) can be done internally via both contribution due to bulk flow ($[\mathbf{n} \cdot \rho \mathbf{v} \mathbf{v}]dS$) and contribution due to macroscopic flow ($[\mathbf{n} \cdot \boldsymbol{\pi}]dS$), and externally via external applied force like gravity ($\rho \mathbf{g} dV$). This can be expressed mathematically as (Bird, Curtiss et al. 1987)

$$\frac{d}{dt} \int_V \rho \mathbf{v} dV = - \int_S [\mathbf{n} \cdot \rho \mathbf{v} \mathbf{v}] dS - \int_S [\mathbf{n} \cdot \boldsymbol{\pi}] dS + \int_V \rho \mathbf{g} dV. \quad (2.9)$$

Where:

- \mathbf{g} is gravitational acceleration [m s^{-2}]
- $\boldsymbol{\pi}$ is tensor associated with contribution due to microscopic flow [Pa]
- \mathbf{v} is velocity of fluid, dependent on position and time [m s^{-1}]
- ρ is fluid density assumed to be constant in case of incompressible fluid [Kg m^3]

Again, using Gauss divergence theorem and convert surface element dS to volume element dV , to obtain consistent equation one can arrive at

$$\int_V \frac{\partial}{\partial t} \rho \mathbf{v} dV = - \int_V [\nabla \cdot \rho \mathbf{v} \mathbf{v}] dV - \int_V [\nabla \cdot \boldsymbol{\pi}] dV + \int_V \rho \mathbf{g} dV. \quad (2.10)$$

Integral can be eliminated from both side of equation 2.10, resulting in

$$\frac{\partial}{\partial t} \rho \mathbf{v} = -[\nabla \cdot \rho \mathbf{v} \mathbf{v}] - [\nabla \cdot \boldsymbol{\pi}] + \rho \mathbf{g}. \quad (2.11)$$

Equation 2.11 is called equation of motion.

So, as it is seen in equation 2.9, the total microscopic transport of momentum across surface element of dS , has been described as a $\boldsymbol{\pi}_n = [\mathbf{n} \cdot \boldsymbol{\pi}]dS$, where $\boldsymbol{\pi}$ is tensor associated with contribution due to microscopic flow and π_{ij} as a component of this second order tensor in positive flux j momentum in positive i direction.

On the other hand, if this microscopic contribution of fluid to total transported momentum is considered as an external way of transporting momentum, the second approach of definition is gained. According to this impression, the conservation of momentum across fluid flowing with velocity of \mathbf{v} , crossing surface boundary dS , is conducted by bulk flow internally ($[\mathbf{n} \cdot \rho \mathbf{v} \mathbf{v}]dS$) and by applying additional forces, externally. This external force is consist of surface

surrounded fluid force ($\pi_n ds$) and body gravitational force ($\rho g dV$) (see Figure 2.6). Hence, with the current definition, former microscopic terms in mathematical definition ($[\mathbf{n} \cdot \boldsymbol{\pi}] ds$) shows itself as $\boldsymbol{\pi}_n ds$. This is ‘‘force vector exerted by fluid located in negative side of the surface dS on the fluid located on positive side of dS ’’. So, now it is wise to call $\boldsymbol{\pi}$ as total stress tensor or pressure tensor, and component of π_{ij} as a force per unit in positive j direction acting on the surface perpendicular to i direction (Bird, Curtiss et al. 1987).

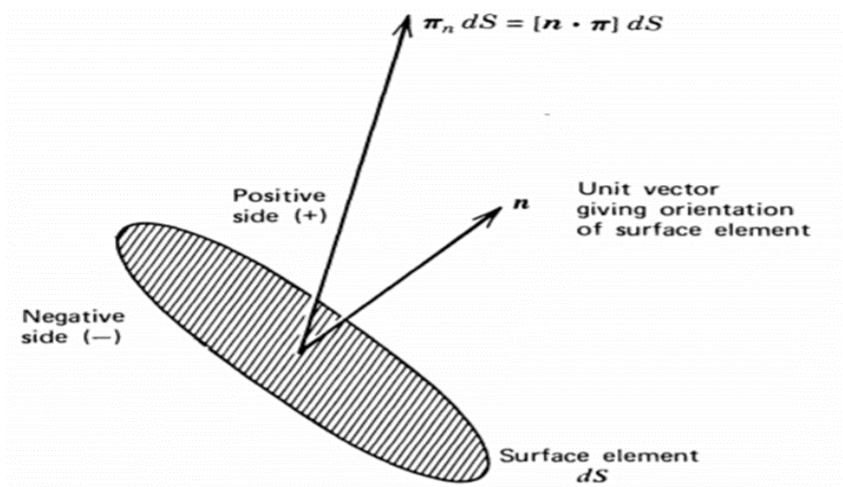


Figure 2.5. Element of dS across which a force $\boldsymbol{\pi}_n dS$ is transmitted (Bird et al., 1987)

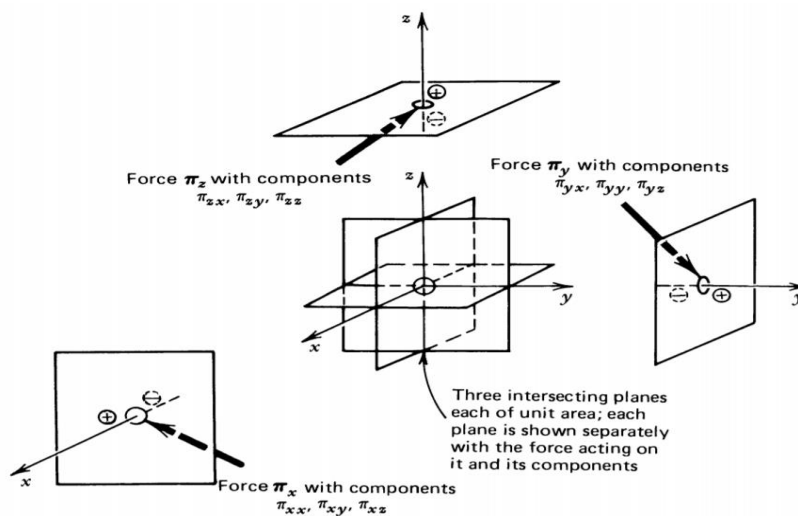


Figure 2.6. Sketch showing the sign convention and index convention for components of stress tensor $\boldsymbol{\pi}$ (Bird, Dotson et al. 1980)

2.3.4 Solving the equation of fluid dynamic (“Generalized Navier-Stokes equations”)

After obtaining required equation (equation of continuity and motion) for solving equation of fluid dynamic in previous parts, it is favorable to initiate an effort to solve it either analytically or numerically. Moreover, determination of $\boldsymbol{\pi}$ either as a total flux momentum displaced during flowing flow due to microscopic contribution or total stress tensor plays a key role in solving equation of fluid dynamic. It is convenient to drive $\boldsymbol{\pi}$ as (Bird, Curtiss et al. 1987, Shogin 2020)

$$\boldsymbol{\pi} = P\boldsymbol{\delta} + \boldsymbol{\tau} . \quad (2.12)$$

Where:

$\boldsymbol{\pi}$ is stress tensor [Pa]

P is thermodynamic pressure [Pa]

$\boldsymbol{\delta}$ is unit tensor [Pa]

$\boldsymbol{\tau}$ deviatoric, commonly called "extra stress tensor" [Pa]

Proceed to this point, almost all derived equations are also valid for non-fluids. So, this is the first time the fact that the substance is originally fluid is considered. This would enable us to extract isotropic (pressure) component from it.

Furthermore, equation 2.12 comprises of two independent components:

- isotropic part which is result of multiplication of a thermodynamic pressure (P) and ($\boldsymbol{\delta}$) as unit stress tensor.
- anisotropic or deviatoric part ($\boldsymbol{\tau}$) which makes a difference where fluid is out of rest. In fact, the anisotropic part of total stress tensor ($\boldsymbol{\tau}$) is vanished in rest state. Hence, at equilibrium condition fluid has isotropic pressure (equal pressure in every direction of flow) and substance that does not show this important property, is not fluid at all.

The equation which specify $\boldsymbol{\tau}$ is called constitutive equation. Newton derived a theoretical value for $\boldsymbol{\tau}$ which has shown good accordance with experimental data. This equation can be expressed as

$$\boldsymbol{\tau} = -\mu[\nabla\boldsymbol{v} + (\nabla\boldsymbol{v})^T] + \left(\frac{2}{3}\mu - k\right)(\nabla \cdot \boldsymbol{v})\boldsymbol{\delta}. \quad (2.13)$$

where:

- μ is called Newtonian viscosity [Pa s]
- $(\nabla\boldsymbol{v})$ is defined as nabla velocity tensor [m s⁻¹]
- $(\nabla\boldsymbol{v})^T$ is transpose of nabla velocity tensor [m s⁻¹]
- k is called additional transport quantity related to dilatational viscosity [-]

as it was noted in deriving continuity equation in part 2.3.2, in case of incompressible fluid ($\frac{d\rho}{dt} = 0$) we have $\nabla \cdot \boldsymbol{v} = 0$, and so the terms which contain k is eliminated, resulting in reduced equation

$$\boldsymbol{\tau} = -\mu[\nabla\boldsymbol{v} + (\nabla\boldsymbol{v})^T]. \quad (2.14)$$

Then it is convenient to reform equation 2.14 as

$$\boldsymbol{\tau} = -\mu\dot{\boldsymbol{\gamma}}. \quad (2.15)$$

Where:

$$\dot{\boldsymbol{\gamma}} = [\nabla\boldsymbol{v} + (\nabla\boldsymbol{v})^T], \quad (2.16)$$

And $\dot{\boldsymbol{\gamma}}$ is called rate- of - strain tensor [s⁻¹].

2.3.5 Definition of Newtonian and non-Newtonian fluid

Fluids which obey derived equation by Newton (equation 2.13) is called Newtonian fluid like most of liquid which are consist of quite small molecular, such as oil and water. All other fluid which do not obey this constitutive equation is called Non-Newtonian fluid such as polymers and drilling fluid (mud and cement). In fact, the difference in constitutive equation poses a major change in flow behavior which is explained more in next section (Bird, Curtiss et al. 1987, Shogin 2020).

2.4 Non-Newtonian phenomena in polymeric solution

As it was noted in Previous part, the difference in constitutive equation causes a major difference in motion and behavior between Newtonian and non-Newtonian fluid. In this section we will go through some experiments that clearly differentiate these differences.

Non-Newtonian phenomena in polymeric solution is divided to three categories (Shogin 2020)

- shear-dependent viscosity
- Normal stresses and their differences
- time-dependent phenomena

2.4.1 shear-dependent viscosity

Stress can be simply defined as an internal reaction of material relative to applying external pressure (force per unit area). The diagonal components of this generated stress ($\boldsymbol{\tau}$) called normal stress, while off-diagonal component of $\boldsymbol{\tau}$ called shear stress. Moreover, the rate at which this shear stress is created called rate-of-strain tensor ($\dot{\boldsymbol{\gamma}}$), and the scalar value of this tensor called shear rate ($\dot{\gamma}$). Now if fluid does obey classic physics rules (Newtonian fluid), then its viscosity (μ) which is defined as fraction of shear stress versus applied shear rate is constant for given temperature, pressure, and composition and not dependent on value of applied shear rate anymore. On the contrast, for fluid which does not follow classic physics their non-Newtonian viscosity (η) is not constant and dependent on applied shear rate. Thus, non-Newtonian fluid can show different behavior relative to applied shear rate (see Figure 2.7). In this respect, kind of fluid in which viscosity (the slope of shear stress versus shear rate in diagram) increases with increase in applied shear rate is called shear thickening fluid. On the other hand, kind of fluid in which viscosity (the slope of shear stress versus shear rate in diagram) decreases with increase in applied shear rate is called shear thinning. Polymers are well-known as a kind of fluid which show shear thinning behavior. Some representative phenomena which shows this properties has been summarized in following (Bird, Curtiss et al. 1987, Shogin 2020).

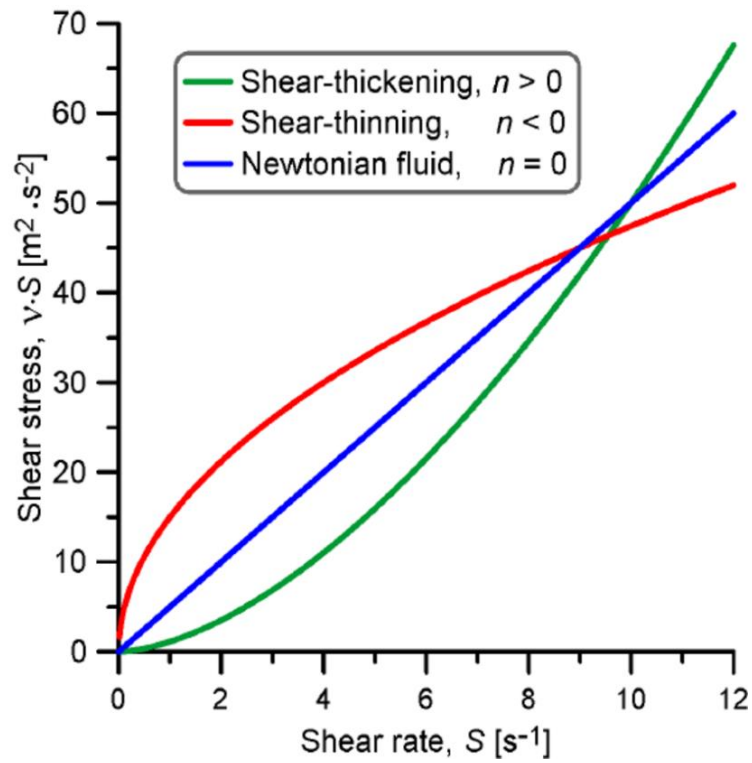


Figure 2.7. different behavior of different types of fluid regarding applied shear rate (Researchgate.com)

2.4.1.1 Tube flow

At this experiment we have two identical tube, both covered from bottom by same shape of plate, one filled with Newtonian fluid and another one filled by non-Newtonian polymeric fluid. (Figure 2.8).

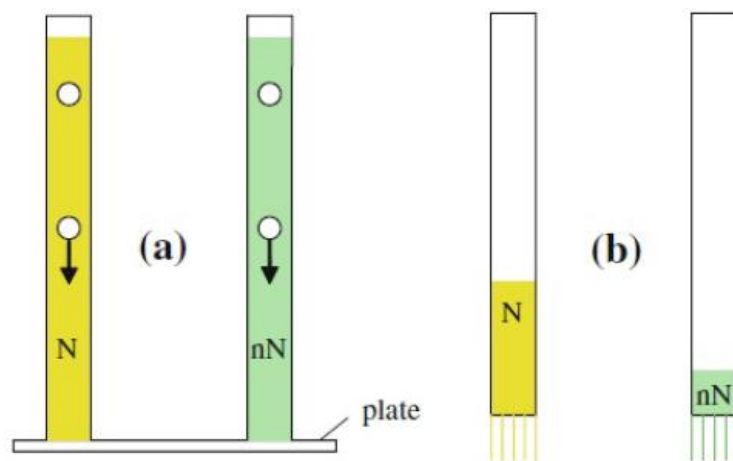


Figure 2.8. flow of Newtonian and non-Newtonian flow in a) in primary state (bottom covered) and b) in secondary state (removed bottom covered) (Bird et al., 1987)(Islam 2019)

First some high density identical small spheres are dropped into both fluids to make sure about having analogous viscosity at primary condition (when the covered plate has not removed yet). Covered plate is removed for both fluids in same velocity and same manner in secondary stage of this experiment. It is observed that non-Newtonian tube is drained much faster than Newtonian fluid. This clearly proves shear-dependent viscosity in polymeric solution, where viscosity decreases as shear rate increases (shear thinning behavior), while viscosity is constant in Newtonian fluid.(Bird, Curtiss et al. 1987)

2.4.2 Normal stress and their differences

Existence of normal stress and their differences is another property of polymer solution as noted in part 2.4. some of experiments which shows this property of polymeric solutions is summarized in below.

2.4.2.1 Rod climbing

Rod climbing phenomenon is one of the most outstanding phenomena in polymeric behavior. First two rotating rods is inserted in to two beakers, one of which is filled with Newtonian fluid and another one with non-Newtonian polymeric fluid. Completely opposite behaviors are observed when rotating rods start to rotate in these two beakers. The surrounded Newtonian fluid is pushed away in outward shape due to centrifugal force while polymer fluid moves toward the center of breaker and even climb up the rod in completely opposite behavior (Figure 2.9).The reason ,as it is explained extensively in material section part2.5, roots up in presence of extra tension along the direction of streamline caused by stretching and alignment of polymeric molecule. In fact, polymer molecules are stretched by flow along the streamline. A "restoring" force will therefore attempt to compress the fluid along the streamline, like what a stretched spring does. And, since fluid is incompressible, a "compression" along the streamline would result in an attempt of "extension" normal to the same streamline (another reason to call these stresses "normal")(Bird, Curtiss et al. 1987) .

Rod Climbing Effect

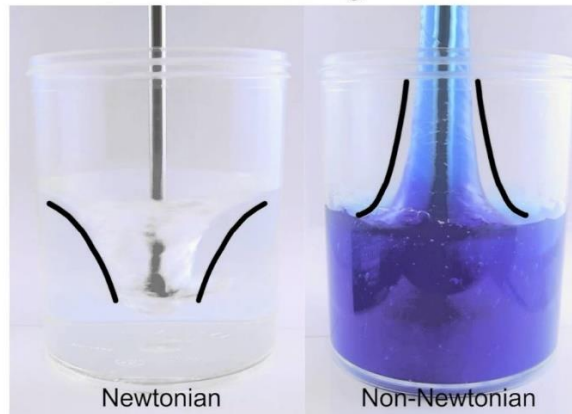


Figure 2.9. rod climbing phenomena (Youtube.com)

2.4.2.2 Extrude swell (die swell)

In the other simple experiment called die swell, the fluid is let to exit into air, from capillarity with diameter of D . As it is appeared in Figure 2.10, the result is impressive. it is observed that although there is almost no significant change in exit diameter of Newtonian fluid both in small and large Reynolds number laminar flow, the extrude diameter (D_e) of polymeric solution would increase up to 300 percent in comparison with capillarity diameter (D). Apart from elastic and memory properties (the ability of polymer to remember its some crucial properties like viscosity) of polymer that could be responsible for this phenomenon at least partially, the reason is believed to roots up again in extra tension along streamline. In fact, this extra tension shows clearly its effect when the flow is exiting from tube, at this point this extra tension cannot be tolerated anymore, which lead to fluid to be contacted axially and to be expanded radially (Bird, Curtiss et al. 1987).

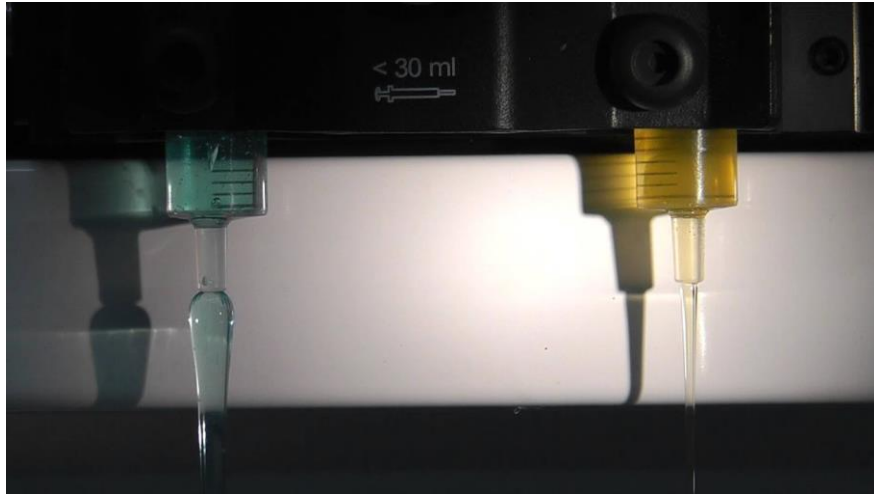


Figure 2.10. Die swelling phenomena in right (Newtonian) and left (polymeric) solution (Youtube.com)

2.4.3 Time-dependent phenomena

Time dependent properties of polymers are those properties that are dependent on the time of experiment. One of the most important time-dependent properties of material is called “memory” properties which is defined as the ability of material to remember and maintain some its initial properties like viscosity. This property of polymer is highly dependent on elastic properties of polymer such that as it has been clarified in Bird book (Bird, Curtiss et al. 1987), the probability of exhibiting memory properties is relatively low, in case flow does not show an elastic behavior. Moreover, since polymers are not cross-linked material, their memory property is considered as a temporary one, in which memory is faded as time elapses (Bird, Curtiss et al. 1987). Some most important representative of time-dependent properties of polymeric solution has been summarized below.

2.4.3.1 Cutting an Aluminum soap solution

Cutting an Aluminum soap solution in half is one of funniest and most representative of the time-dependent properties in polymeric solution. At this experiment conducted first by Lodge in 1964 (Lodge 1964), first according to Figure 2.11 the Aluminum soap is poured out from breakers in initial condition (a). Then the polymeric solution is cut in half during secondary stage (b). Finally it is observed that only flow above the cut point falls down to the container and the flow below the cut point returns again into breaker in third stage of experiment (c) (Bird, Curtiss et al. 1987).

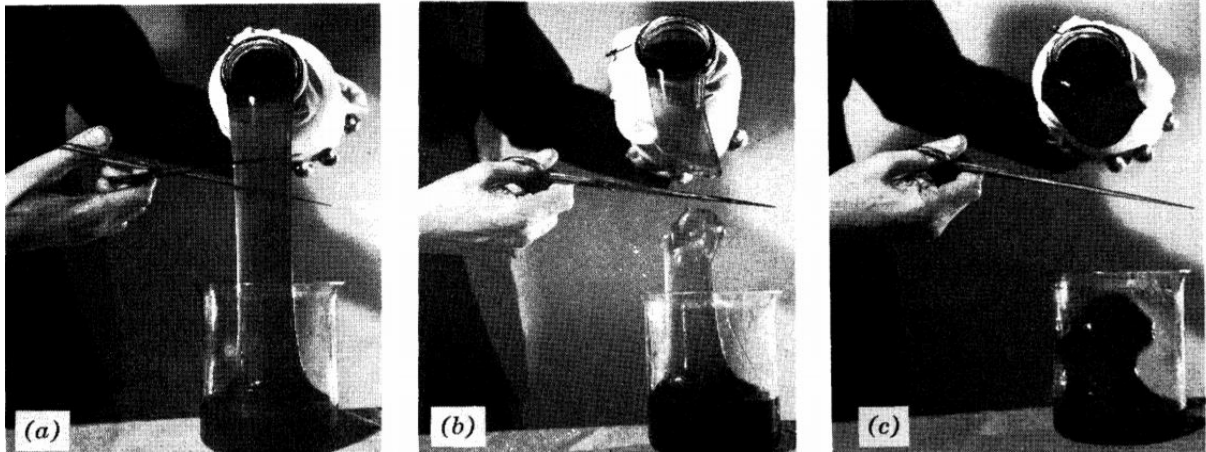


Figure 2.11. Cutting an Aluminum soap solution phenomena first conducted by Lodge (Lodge 1964) taken from (Bird et al., 1987)

2.4.3.2 Filament of low-density Polyethylene

In other interesting experiment, elastic recoil properties of polymeric solution (“the tendency of fluid to snap back to its original state upon removing the extra forces”) was tested first by Meissner (Meissner 1971). First one centimeter of filament of low-density Polyethylene is stretched up to 30 cm at temperature of 423 K, and then suddenly it is set to free state. It is observed that it returns up to 3 cm of its initial lengths, which clearly shows the fact that complete memory concept is somehow ideal in polymeric solution. Moreover, it is observed during this experiment that the length of recovery is highly time dependent such that the more you wait after stretching the filament, the less recovered lengths is observed. This recalls the concept of fading memory mentioned in the introduction (Bird, Curtiss et al. 1987).

2.4.3.3 The tubeless siphon

The tubeless siphon is one of the simplest but outstanding representative of time dependent properties in polymeric solution. In this experiment, as it is appeared in Figure 2.12, two fluids, one Newtonian and one polymeric are being sucked from their container. After running siphon for sometimes, suddenly the operation is stopped by lifting the tubes. It is observed that in case of Newtonian fluid the flow is stopped immediately, whereas for polymeric fluid the flow persists for short time. Polymer-polymer interactions and time dependent properties are the key factors here. Therefore, this phenomenon is not observed in dilute polymeric solutions.

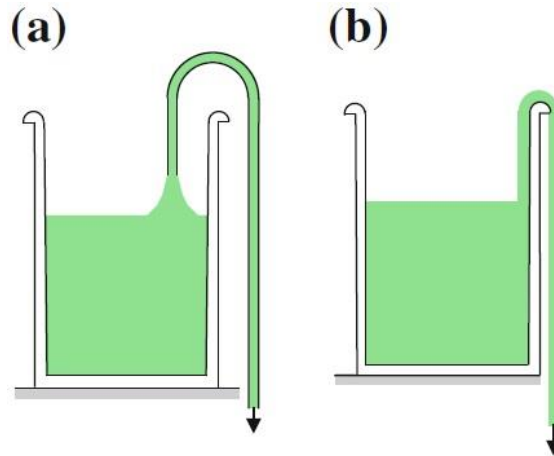


Figure 2.12. Tubeless siphon phenomenon in (a) Newtonian and(b) polymeric solution (Islam 2019)

2.5 Material function

From last part 2.4, we learned that there are fundamental differences between motion of Newtonian and non-Newtonian fluid rooted in fundamental difference in their constitutive equation. This shows its effects in different experiments conducted on last section. In fact, serious issue regarding measuring the inconstant viscosity arises due to lack of constitutive equation analogous to equation 2.13 and existence of normal stresses in polymeric fluid. Hence, some scientist tried to first drive the constitutive equation representative for non-Newtonian fluid. And, then solve this equation to drive the functions that describe material properties (shear and normal stress) during deformation. These functions are called material function collectively. These material functions are of great importance specially regarding fluid classification, where each type of flow has its exclusive material function (Bird et al., 1987). In the following, shear flow itself and its different branches, namely steady shear flow, start-up and cessation of steady shear flow is explained.

2.5.1 Shear flow

2.5.1.1 Shear flow Characteristic

Now let us consider the flow between two parallel plates with axial distance of b in which upper plate can move with velocity of v while lower plate is kept in static condition (see Figure 2.13). In the simplest way, velocity field for this type of flow can be expressed as a below

$$\mathbf{v} = \begin{cases} v_x = \dot{\gamma}_{yx}y, \\ v_y = 0, \\ v_z = 0. \end{cases} \quad (2.17)$$

Where ($\dot{\gamma}$) is called rate-of-strain or velocity gradient and it is dependent on time, though it is constant in simple shear steady flow pattern.

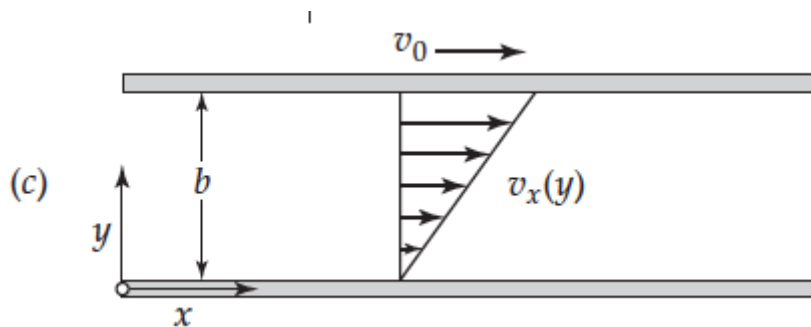


Figure 2.13. represented shape of shear flow (chegg.com)

2.5.1.2 Shear flow stress tensor

there is three directions , locally at any type of flow in shear flow (Bird, Curtiss et al. 1987, Shogin 2020):

- 1st direction: the direction in which flow is flowing
- 2nd direction: the direction in which the velocity changes
- 3rd direction: the neutral direction in which nothing will change

Take flow in Figure 2.13 (flow between two parallel infinite plate in 2D space) as an example, following conclusions can be made

- 1st direction: x
- 2nd directions: y
- 3rd directions: z

Alline with above introduction, total stress tensor required for initiating shear flow is compares of both normal and shear stress and in case of having isotropic fluid (there is no suppository

regarding fluid properties in different direction of flow ‘’other than the direction introduced by flow itself ‘’(Bird, Curtiss et al. 1987)) it can be described as symmetric independent matrix based on equation 2.12 as

$$\boldsymbol{\pi} = P\boldsymbol{\delta} + \boldsymbol{\tau} = \begin{bmatrix} P + \tau_{xx} & \tau_{xy} & 0 \\ \tau_{yx} & P + \tau_{yy} & 0 \\ 0 & 0 & P + \tau_{zz} \end{bmatrix}. \quad (2.18)$$

Then following can be extracted from above tensor as

$$\begin{cases} \tau_{xy} = \text{shear stress,} \\ \tau_{xx} - \tau_{yy} = \text{First normal stress differences,} \\ \tau_{yy} - \tau_{zz} = \text{Second normal stress differences.} \end{cases} \quad (2.19)$$

These three quantities are called viscoelastic properties collectively.

On the other hand, the shear stress is the only component of total stress tensor in shear flow of Newtonian fluid. In other words existence of shear stress is sufficient to create shear flow in Newtonian fluid, while apart from shear stress , implementation of normal stress are essential to generation of shear flow in non-Newtonian fluid such as polymer (Bird, Curtiss et al. 1987)

2.5.2 Steady shear flow

2.5.2.1 Steady shear rate material function

Material functions of shear steady flow are only relying on absolute value of rate- of-strain ($\dot{\gamma}$) called shear rate ($\dot{\gamma}$). These material functions have been summarized in below

$$\begin{cases} \tau_{xy} = -\eta(\dot{\gamma})\dot{\gamma}_{yx}, \\ \tau_{xx} - \tau_{yy} = -\Psi_1(\dot{\gamma})\dot{\gamma}_{yx}^2, \\ \tau_{yy} - \tau_{zz} = -\Psi_2(\dot{\gamma})\dot{\gamma}_{yx}^2. \end{cases} \quad (2.20)$$

Where:

- Ψ_1 is first normal stress differences coefficient [Pa s²]
- Ψ_2 is second normal stress differences coefficient [Pa s²]

- **Steady shear rate Non-Newtonian viscosity (η)**

Lots of experiments has been conducted on measuring non-Newtonian viscosity which makes this quantity as a well-known viscoelastic properties in literature. The changing trend of non-Newtonian viscosity of low-density polyethylene melts versus applying different steady shear rate(called shear steady ramping) in different temperature is depicted in Figure 2.14. As it appears in the Figure 2.14, Non-Newtonian viscosity shows Newtonian behavior (constant viscosity(η_0)) at low shear rate region (also called lower Newtonian region).Then it starts its shear thinning behavior when shear rate increase in the middle region (also called power-law region) .And, finally it switches back again to Newtonian behavior (constant viscosity(η_∞)) at very high shear rate region (also called upper Newtonian region),though this region is not seen in log-log scale of figure (Bird, Curtiss et al. 1987, Dunstan 2019).

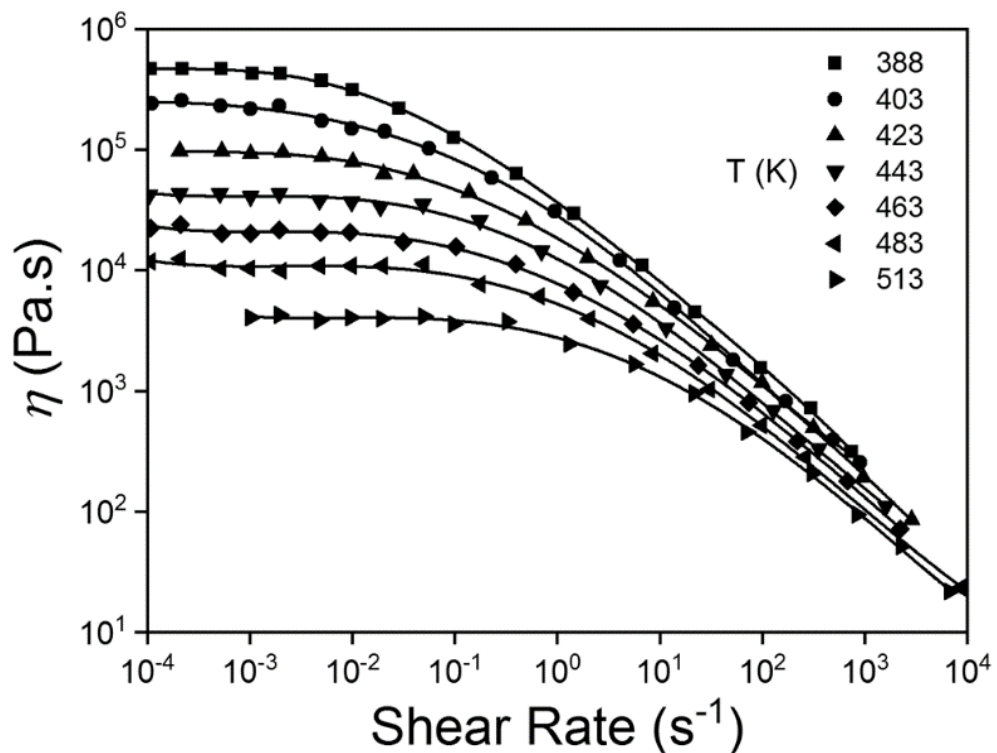


Figure 2.14. Non-Newtonian viscosity(η) of low-density melted polyethylene versus shear rate(γ) in different temperature in log-log scale axis(Dunstan 2019)

Moreover, if logarithmic viscosity ($\log \eta$) versus logarithmic shear rate ($\log \gamma$) is plotted, the former power-law region is appeared as a linear reduction region, and according to Bird (Bird, Curtiss et al. 1987) the slope of this linear reduction is between $m= -0.4$ and $m= -0.9$ for typical polymer solution.

- **Steady shear rate first normal stress differences coefficient (Ψ_1)**

As it has shown in Figure 2.15 , the typical changing trend of first normal stress difference coefficient (Ψ_1) versus shear rate is similar to those of viscosity trend. First, it is positive and constant in lower Newtonian region, then it starts to decrease more rapidly in comparison with viscosity in power-law region. Finally, it again reaches to constant value (zero) in lower Newtonian region. (Bird, Curtiss et al. 1987) .

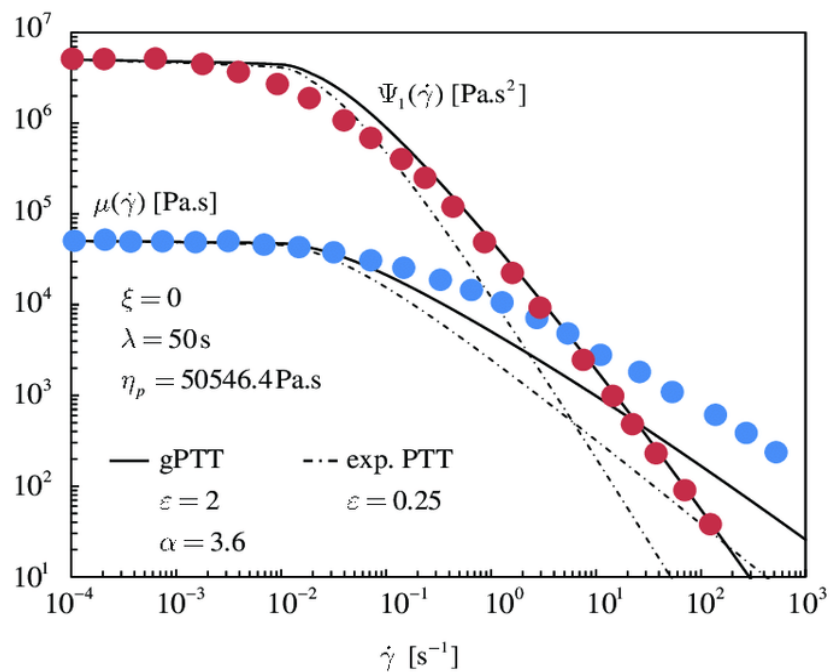


Figure 2.15. The typical changing trend of first normal stress coefficient(Ψ) versus reduced applied shear rate ($\dot{\gamma}$) for a low density polyethylene melt (Ribau, Ferrás et al. 2019)

- **Steady shear rate second normal stress differences coefficient (Ψ_2)**

It is negative and much smaller than first normal stresses coefficient ($\Psi_2 \sim 0.1 \times (\Psi_1)$), though it experiences completely similar reduction trend versus increase of shear rate. Modern rheometers allow for measurement of second normal stress differences, though it is still not an easy task. So, information on second normal stress coefficient (Ψ_2) are rare to find in literature specially in very low shear rate and very high shear rate region (Carreau, Choplin et al. 1985, Bird, Curtiss et al. 1987).

2.5.3 start-up of steady shear flow

2.5.3.1 start-up of steady shear flow characteristic

For this experiment as it is depicted in Figure 2.16, the flow is on rest state before starting this experiment (for all time $t < 0$). And, then constant initial shear rate (called step-rate) is applied for $t > 0$ to investigate on how shear stress shifts to its steady state value (Bird, Curtiss et al. 1987). From physical point of view, this experiment is similar to put a weight on the spring and see how it is expanded from its initial state length (L_0) to its steady state expanded length (L_S) possibly after some oscillations around L_S .

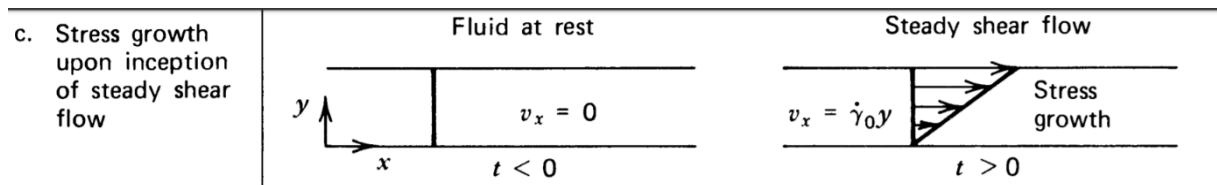


Figure 2.16. Simple schematic of startup flow (Bird et al., 1987)

2.5.3.2 Material function of startup of steady shear flow

the material function of start-up of steady shear flow is summarized in below (Bird, Curtiss et al. 1987)

$$\begin{cases} \tau_{xy} = -\eta^+(t, \dot{\gamma}_0) \dot{\gamma}_0, \\ \tau_{xx} - \tau_{yy} = -\Psi_1^+(t, \dot{\gamma}_0) \dot{\gamma}_0^2, \\ \tau_{yy} - \tau_{zz} = -\Psi_2^+(t, \dot{\gamma}_0) \dot{\gamma}_0^2. \end{cases} \quad (2.21)$$

So, it is seen that they are identical to their corresponding equation in steady shear rate flow, except all material functions are now function of time (t). Moreover, the positive sign (+) in the formula is just an indication of the fact that the steady rate is only applied for positive time. Alternatively, "+" can stand for the increase (growth) of stresses (Bird, Curtiss et al. 1987).

- **Shear stress growth function of start-up of steady shear flow (η^+)**

Figure 2.17, shows shear stress growth function of start-up of steady shear flow for melted low-density polyethylene regarding different initial shear rates. It can be seen that only for very low shear rate called linear viscoelastic envelope (the curve below which all other stress growth curves lie) the shear stress reaches to its steady state value in monotonous increasing fashion. But from some critical boundary called the linear viscoelastic limit (around $\dot{\gamma} = 1.5$ for low-density melted polyethylene) the significant divergence from linear viscoelastic envelope is appeared. This is the region where the data first increases up to their maximum (also called overshoot), then it starts to decrease and reaches to its steady state value, possibly with some oscillation around this steady state value. The more step-rate the sooner data is deviated from linear viscoelastic envelope (Bird, Curtiss et al. 1987).

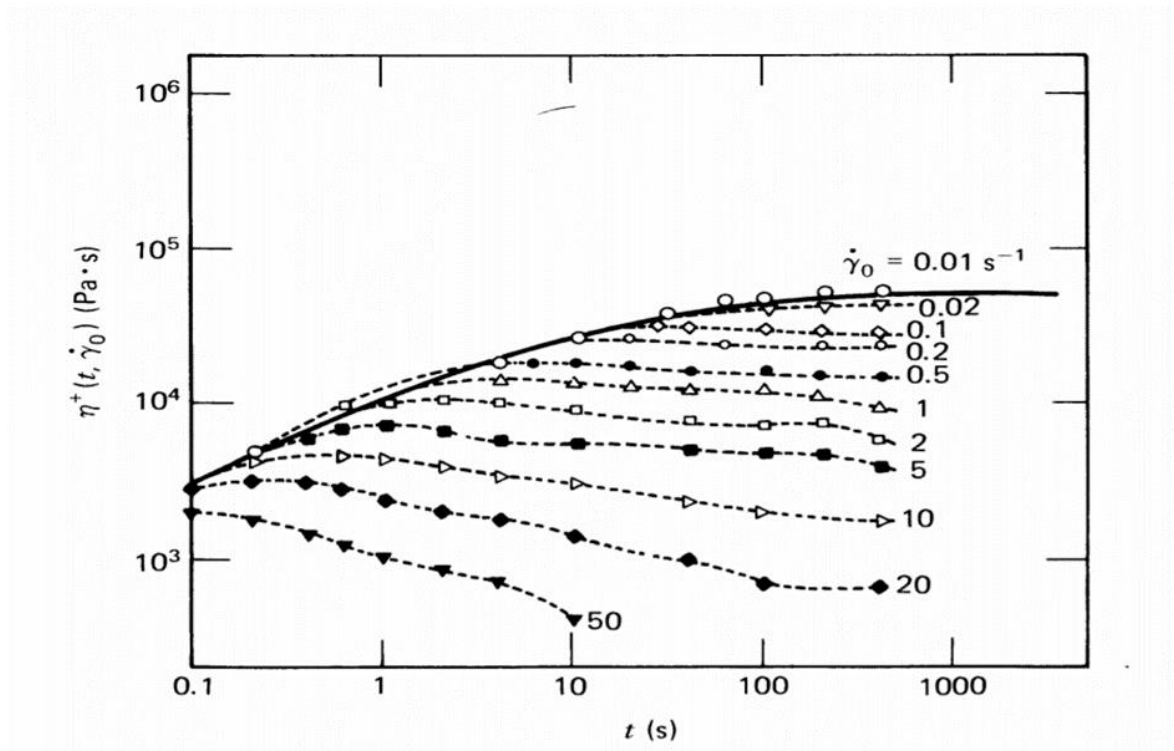


Figure 2.17. shear stress growth ($\eta^+(t, \dot{\gamma}_0)$) versus of time (t) for melted low-density polyethylene with respected to different initial shear rate (Bird et al., 1987)

below Figure 2.18 also shows same quantity for polyacrylamide in 50/50 mixture weight of water and glycerin, but here the data have been normalized with respect to steady state value of shear stress growth such that the overshoot value is easier to be observed

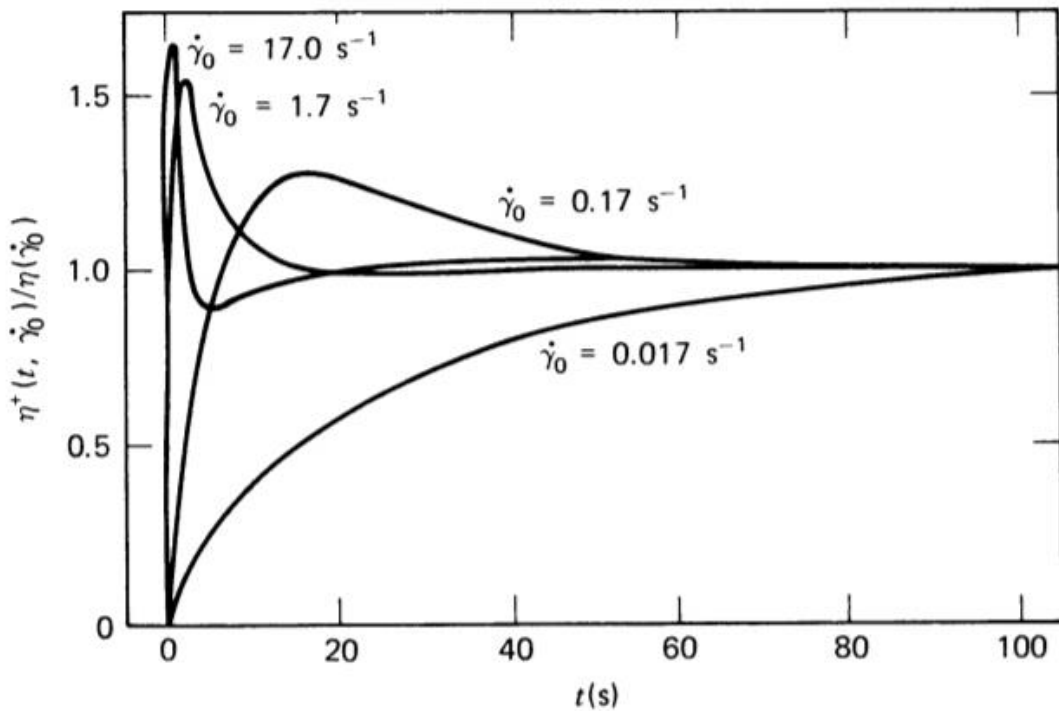


Figure 2.18. Normalized shear stress growth ($\frac{\eta^+(t, \dot{\gamma}_0)}{\eta(\dot{\gamma}_0)}$) versus time(t) for 1.5% polyacrylamide in 50/50 mixture by weight of water and glycerin (Bird, Curtiss et al. 1987)

- **First normal stress differences growth coefficient of start-up of shear steady flow (Ψ_1^+)**

The below Figure 2.19, shows first normal stress differences growth coefficient of coefficient growth (Ψ_1^+) of melted low-density polyethylene over elapsed time (t). As it is obvious from chart the first normal stress also experiences completely similar trend toward steady state value regarding application of different shear rate. But here the major difference is time of reaction which is much slower than shear stress growth. Moreover, the size of overshoot is much greater than those of shear stress (Bird, Curtiss et al. 1987).

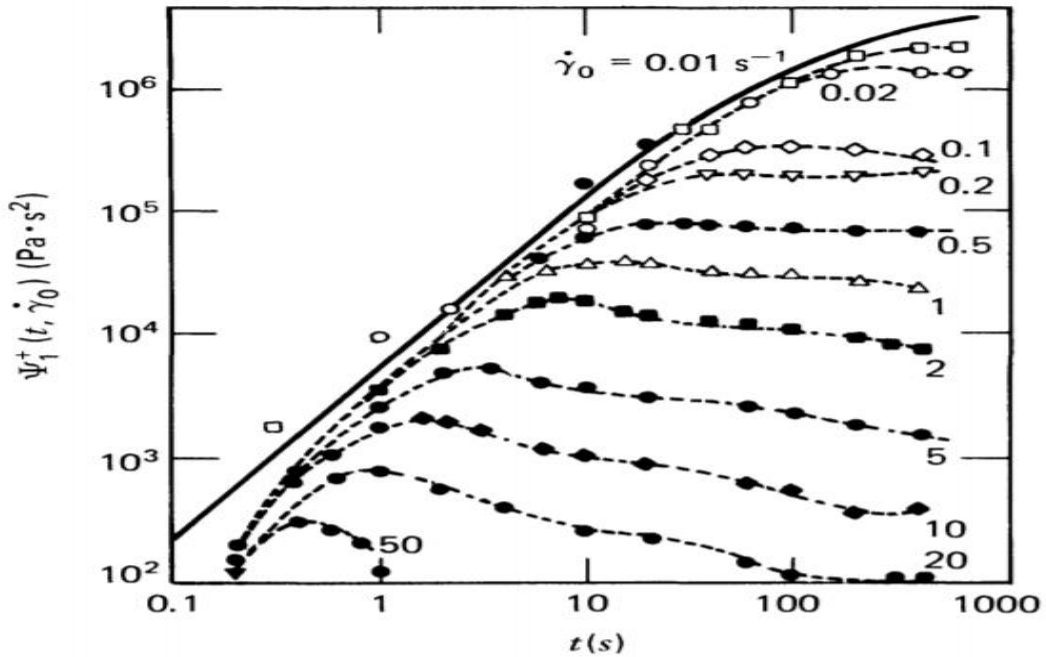


Figure 2.19. shows first normal stress coefficient growth ($\Psi_1^+(t, \dot{\gamma}_0)$) of melted low-density polyethylene over elapsed time (Bird et al., 1987)

2.5.4 Cessation of steady shear flow

2.5.4.1 Cessation of steady flow characteristic

In this experiment which is in complete opposition with startup experiment, the constant initial shear rates is applied to the flow only for time before relaxation period ($t < 0$). Then for $t > 0$ there is sudden stop of initial shear rate to observe how flow relax its shear stress toward zero (Bird, Curtiss et al. 1987). Recall to spring example it is similar to release the mentioned weight from spring to see how it returns to its initial length state (L_0) from its extended stable state length (L_s).

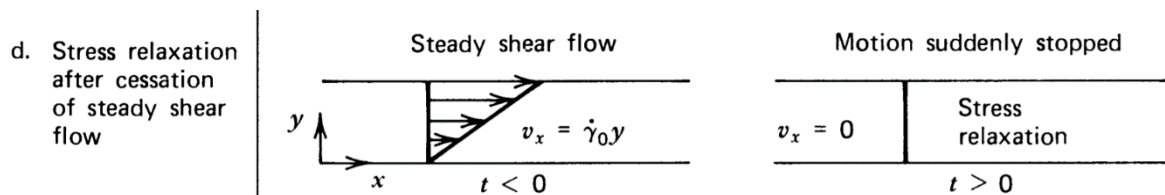


Figure 2.20. Simple schematic of relaxation flow (Bird et al., 1987)

2.5.4.2 cessation of steady shear rate flow material function

as it is appeared in equation 2.22, material function of cessation of steady shear rate is again identical to those of shear steady regime except now all material functions are dependent on time (t) and negative sign(−) only shows the fact that constant shear rate has been applied only for time $t < 0$. Material functions of cessation of steady shear rate flow material function can be expressed as (Bird, Curtiss et al. 1987)

$$\begin{cases} \tau_{xy} = -\eta^-(t, \dot{\gamma}_0)\dot{\gamma}_0, \\ \tau_{xx} - \tau_{yy} = -\Psi_1^-(t, \dot{\gamma}_0)\dot{\gamma}_0^2, \\ \tau_{yy} - \tau_{zz} = -\Psi_2^-(t, \dot{\gamma}_0)\dot{\gamma}_0^2. \end{cases} \quad (2.22)$$

- **Shear stress relaxation function of cessation of steady shear flow relaxation flow**
(η^-)

Again, the objective of this experiment is set up to observe shifting change of material function toward zero in relaxation state, after cession of initial constant shear rate (step-rate). Figure 2.21, shows the typical expected result of shear stress relaxation of cessation of steady shear flow. Following observation can be made (Bird, Curtiss et al. 1987):

- Again, it takes times for polymeric solution to get implemented changes due to their “laziness” and elastic memory properties. While the Newtonian fluid behaves in opposite way and takes implemented changes immediately after implementation.
- The monotonous decreasing trend toward zero is seen in all curves regarding different step-rate. And again, all curves lie below the linear viscoelastic envelope.
- Though, two different slope of reduction is observed in typical ways of showing data (linear-log scale) . In fact, the reduction in earlier time (also called “non-exponential region”) is much faster than late time (also called exponential region). This exponential region shows itself as a straight line in linear-log scale, though it is exponential in linear-linear scale. Moreover, the slope of reduction is independent of step-rate in exponential region. On the contrast, this slope accelerates as step-rate increases in non-exponential region. So, the more step-rate the sooner polymer lost its stored energy in early time region.

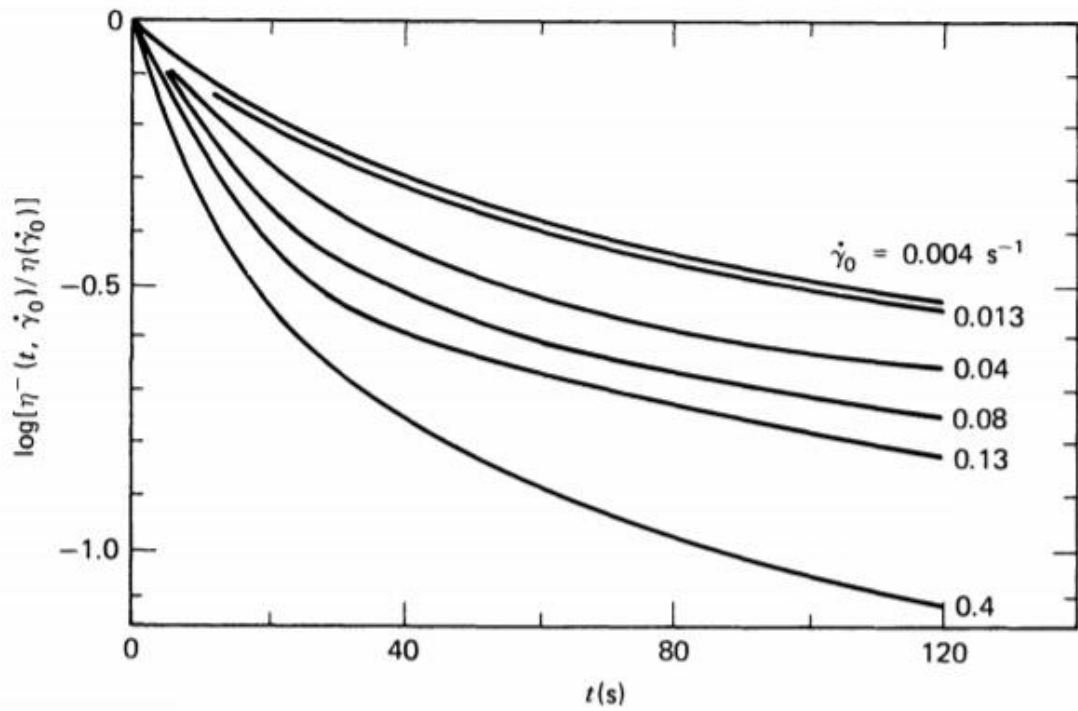


Figure 2.21. Normalized logarithmic shear stress relaxation ($\log \frac{\eta^-(t, \dot{\gamma}_0)}{\eta(\dot{\gamma}_0)}$) versus time(t) of low density polyethylene implementation of different initial shear rate taken from (Bird et al., 1987)

- **First normal stress differences relaxation coefficient of cessation of steady shear flow (Ψ_1^-)**

According to below Figure 2.22, the first normal stress difference relaxation coefficient in cessation of steady shear flow shows exactly similar trend of reduction toward zero, but it is again so “lazy” that reacts to implemented change much slower than shear stress (Bird et al., 1987)

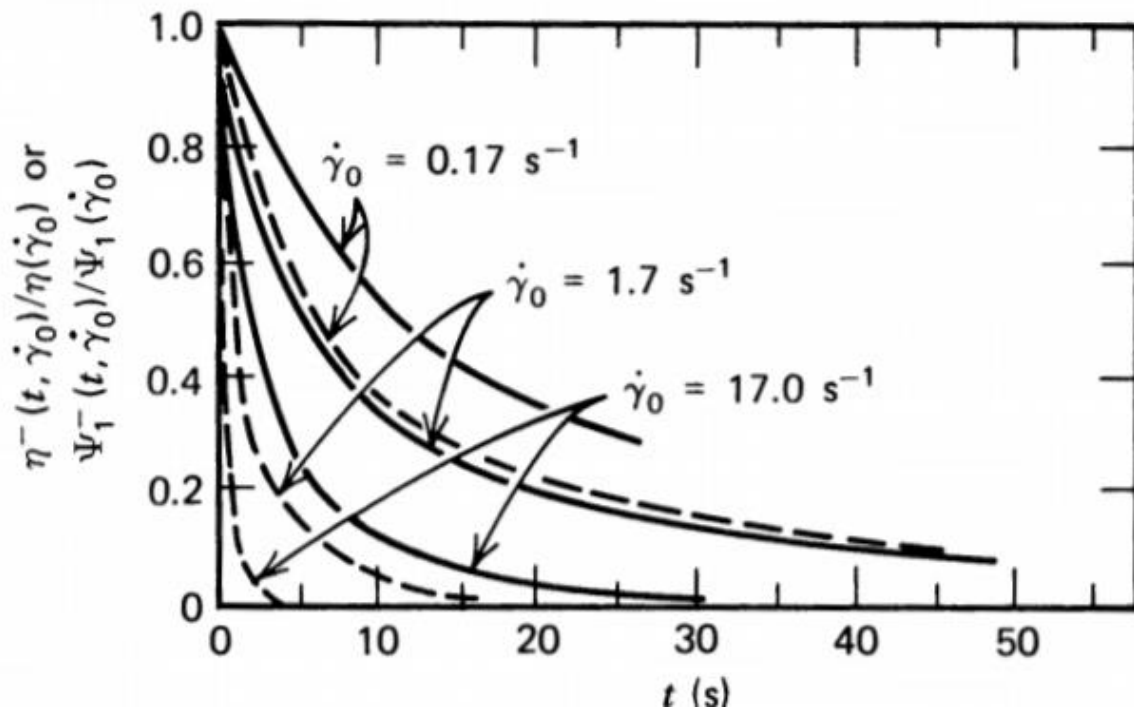


Figure 2.22. Systematic comparison for relaxation mood between shear stress (shown with —) first normal stress differences coefficient(shown with - - -) (Bird, Curtiss et al. 1987)

2.6 Modeling part

After obtaining basic knowledge about material function of polymer both in steady and transient flow in last part, it would be favorable to initiate an effort to model these functions. In fact, lots of scientist tried to make behavioral models for polymers. At the first stages huge number of pure mathematical models were proposed. Mathematical models can give amazing predictions at certain circumstances, but they are not general. They "fail" in certain situations or for certain flow patterns, while work perfectly for the others.

Then the advent of physical models proved to be successful to predict polymeric behaviors at least partially. Here first we summarize most important one of polymeric mathematical models and then will go through some physical outstanding models (Bird, Curtiss et al. 1987, Shogin 2020)

2.6.1 Mathematical modeling

2.6.1.1 “The generalized Newtonian fluid model”

As noted, before, the viscosity is constant in the Newtonian fluid for given temperature, pressure, and composition. So, if the elementary flow velocity field is assumed to be

$$\mathbf{v} = \begin{cases} v_x = v_x y \\ v_y = 0 \\ v_z = 0 \end{cases} \text{), Newtonian viscosity relation with shear stress can be expressed as (Bird,}$$

Curtiss et al. 1987)

$$\tau_{yx} = -\mu \frac{dv_x}{dy}. \quad (2.23)$$

Where:

- τ_{yx} is shear stress [Pa]
- μ is Newtonian viscosity [Pa s]
- $\frac{dv_x}{dy}$ is velocity gradient [m s^{-1}]

Then modification of equation 2.23 such that it allows for viscosity change when velocity gradient changes, was first attempt to obtain representative relationship for Non-Newtonian fluid. This modified (called generalized) Newtonian viscosity can be expressed as

$$\tau_{yx} = -\eta \left(\frac{dv_x}{dy} \right) \frac{dv_x}{dy}. \quad (2.24)$$

Where:

$\eta \left(\frac{dv_x}{dy} \right)$ is non-Newtonian viscosity dependent on velocity gradient $\left(\frac{dv_x}{dy} \right)$ [Pa s].

The negative sign in each formula is just to make sure that the change in viscosity is only dependent on magnitude of velocity gradient not its direction. Then the idea in of equation 2.23 can be further extended to obtain the formula which can describe all steady shear flow velocity field (v_x, v_y, v_z) . For incompressible fluid it can be written as

$$\boldsymbol{\tau} = -\mu \dot{\boldsymbol{\gamma}}. \quad (2.25)$$

Where, $\dot{\boldsymbol{\gamma}}$ is rate-of-strain tensor is defined by equation 2.16 ($[\nabla\boldsymbol{v} + (\nabla\boldsymbol{v})^T]$). In case the fluid is non-Newtonian then equation 2.25 can be rewritten as

$$\boldsymbol{\tau} = -\eta(\dot{\boldsymbol{\gamma}})\dot{\boldsymbol{\gamma}}. \quad (2.26)$$

2.6.1.2 “The Power-law model” of Ostwald and de Waele (with m and n parameters)

Power-law model is one type of the generalized Newtonian (time independent non-Newtonian) model. The power law relationship can be expressed as (De Waele 1923, Ostwald 1923, Ostwald 1929)

$$\eta = m\dot{\boldsymbol{\gamma}}^{n-1}. \quad (2.27)$$

Where:

- m model parameter called consistency index [Pa s^n]
- $\dot{\boldsymbol{\gamma}}$ is shear rate [s^{-1}]
- n is model parameter, called the power-law index [-]

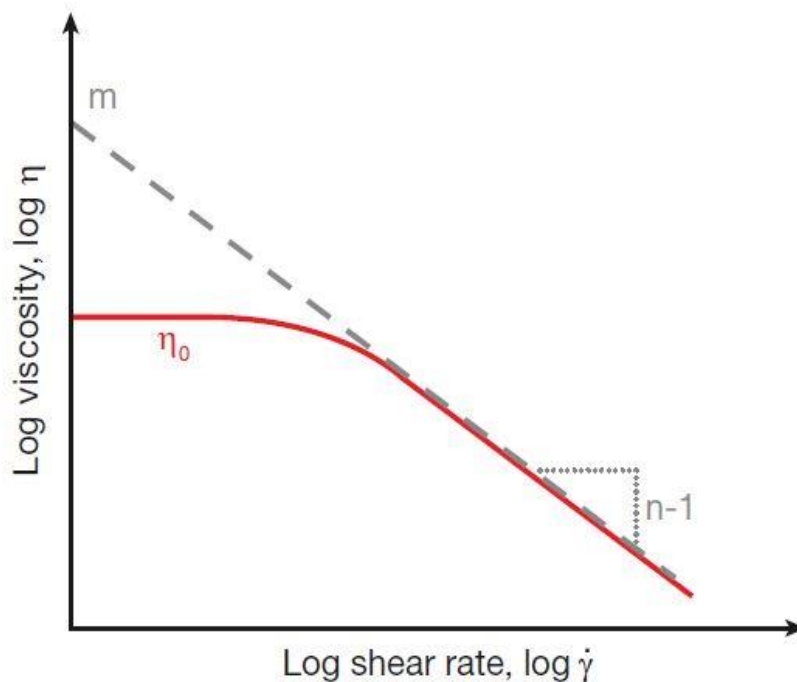


Figure 2.23. Viscosity curve (solid line) and approximation by the Power Law model (dashed line) in Eq. 41 (Rudolph and Osswald 2014) (De Waele 1923, Ostwald 1923, Ostwald 1929)

So, as it is seen from Figure 2.23 ,power-law model is linear in log-log scale setup .Moreover, it shows good accuracy in flow prediction both regarding shear thinning and shear thickening phenomena. The model is also simple and works with only two parameters (m,n), though it is unable to describe both lower and upper Newtonian region in very small and very large shear rate, respectively. This model also has a difficulty in description of Non-Newtonian time dependent phenomena (Bird et al., 1987).

On the other hand, power law model can be generalized to predict other type of flow behavior (Figure 2.24). for example, it is seen that Newtonian fluid set up, can be obtained with $m = \mu$ and $n = 1$.Furthermore, as it is seen in Figure 2.24 , In case $n > 1$ the non-Newtonian power-law fluid, called ‘‘dilatant fluid’’ with shear thickening behavior would be gained, whereas in case $n < 1$ other common type of non-Newtonian fluid (‘‘pseudo-plastic fluid’’) with shear thinning behavior would be recovered. One should also remember that Bingham plastic fluid shown in Figure 2.24 is not classified as a fluid, because it can withstand stress.

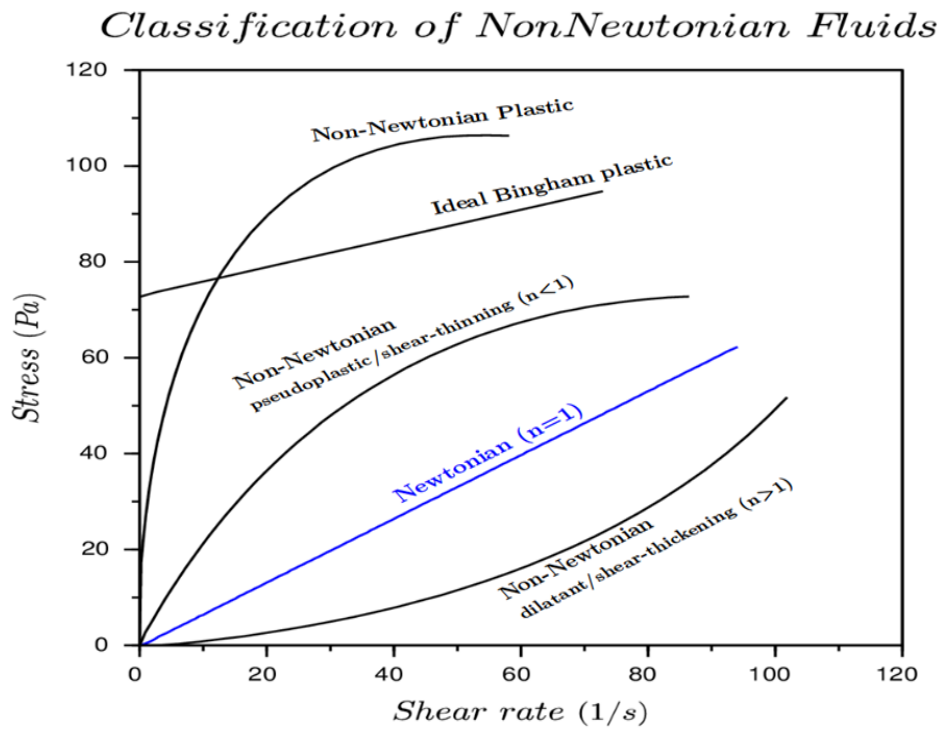


Figure 2.24. Concept of generalized fluid model for all different kind of flow ("What are the properties of non-Newtonian fluids,")

2.6.1.3 The Bird-Carreau-Yasuda Model (with η_∞ , η_0 , λ , a , n parameters)

The Bird-Carreau-Yasuda Model (see Figure 2.25) is one of other type of generalization of Newtonian models. This model proved to be more accurate than power-law model. The model relate stress with applied shear rate as a below (Bird, Curtiss et al. 1987, Andrade, Petronílio et al. 2007)

$$\eta = \eta_\infty + (\eta_0 - \eta_\infty)[1 + (\lambda\dot{\gamma})^a]^{\frac{n-1}{a}}, \quad (2.28)$$

Where:

- η_∞ is infinite -shear- rate Non-Newtonian viscosity [Pa s]
- η_0 is zero- shear- rate Non-Newtonian viscosity [Pa s]
- λ is time constant [s]
- a is model constant [-]
- n is power-law region exponent (since it describes the slope of $(\frac{\eta-\eta_\infty}{\eta_0-\eta_\infty})$) [-]

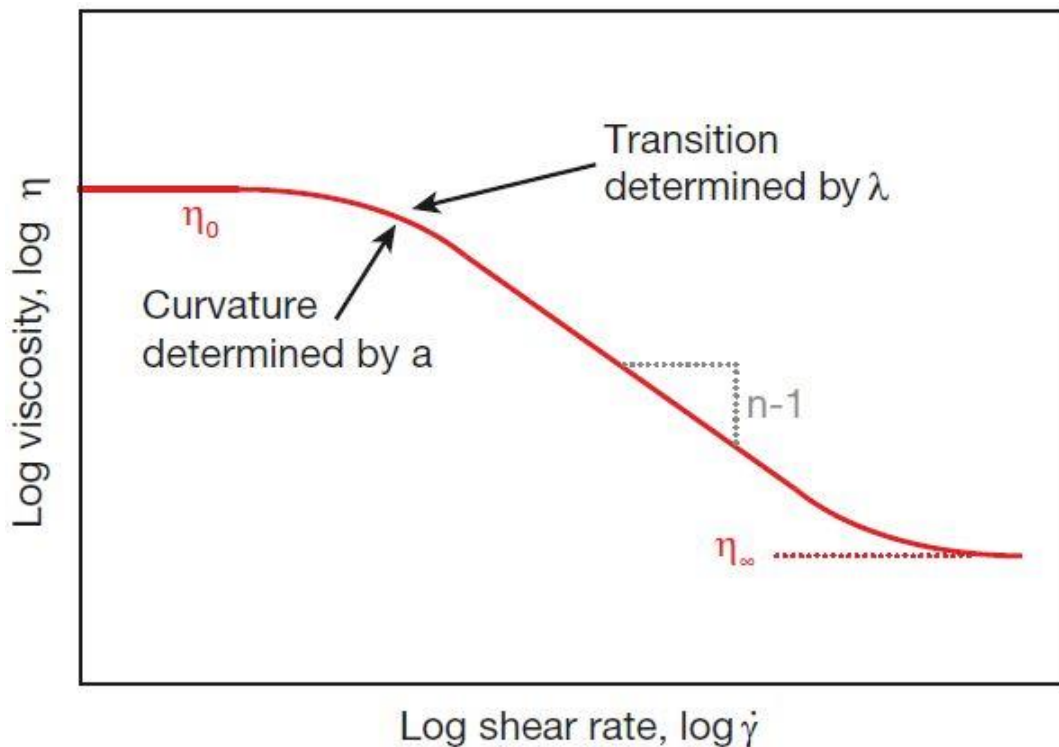


Figure 2.25. The Bird-Carreau-Yasuda Model schematic (Rudolph and Osswald 2014)

So, the zero- shear- rate viscosity (η_0) and infinite-shear-rate viscosity (η_∞) has been included in this model to get better description of these upper and lower Newtonian region which is one of the main disadvantage of power-law model. In fact, the model was proposed first with four parameters by Carreau with constant parameter $a = 2$ and then the dimensions parameter a was introduced to this model by Yasuda to gain better description of transitional region between zero-shear-rate viscosity and power-law region (Bird et al., 1987). Thus, this model has a better performance in comparison with the power-law model specially regarding prediction of upper and lower Newtonian region in very high and very low shear rate, respectively. But it still has fundamental drawbacks for prediction of time dependent flow properties like memory effect and also it does not predict normal stresses at all (Shogin 2020) (Bird, Curtiss et al. 1987).

2.6.2 Physical modeling

As has been mentioned in earlier stage in this master thesis, usage of the mathematical models proved to be insufficient for prediction of polymeric behavior. So, scientist pushed to combine mathematics with physical models to achieve more reliable models. Physical model is categorized in two classifications, physical models applicable for dilute solutions (kinetic theory) and physical models applicable for concentrated solution (network theory) (Shogin 2020) (Bird, Curtiss et al. 1987).

- **Physical model applicable for dilute solution (Kinetic theory)**

As it was noted beforehand the kinetic theory in which solvent is dominate and the concentration of polymer is such low that polymeric molecules more interact with solvent rather than each other, has been used for description of dilute solution (Bird, Curtiss et al. 1987, Shogin 2020).

- **Dumbbell based models**

The idea of simplification of polymers molecule to an elastic dumbbell with two beads, each of them with mass (m), attached by a spring (elastic dumbbell) or by rigid rod (rigid dumbbell), was first introduced to physical modeling by Kramers. This idea is simple but useful since this assumed dumbbell can justify some most representative properties of polymers. In fact, dumbbells can orient, stretch, contract and aligned like what is done by real polymer molecule. Then if two beads marked with label (“1”) and label (“2”) (Figure 2.27) and their location relative to one reference point (R_1) in space nominated as r_1 and r_2 respectively, the “connector

vector” (the vector which connect \mathbf{r}_1 to \mathbf{r}_2) is defined mathematically as $\mathbf{Q} = \mathbf{r}_2 - \mathbf{r}_1$. This connector vector is of great importance since it clearly shows the dumbbell “state”. “State” implies orientation and stretching and as it was noted it is specified by connector vector \mathbf{Q} (Bird, Curtiss et al. 1987, D. Shogin1 2020). Some dumbbell-based models have been summarized below.

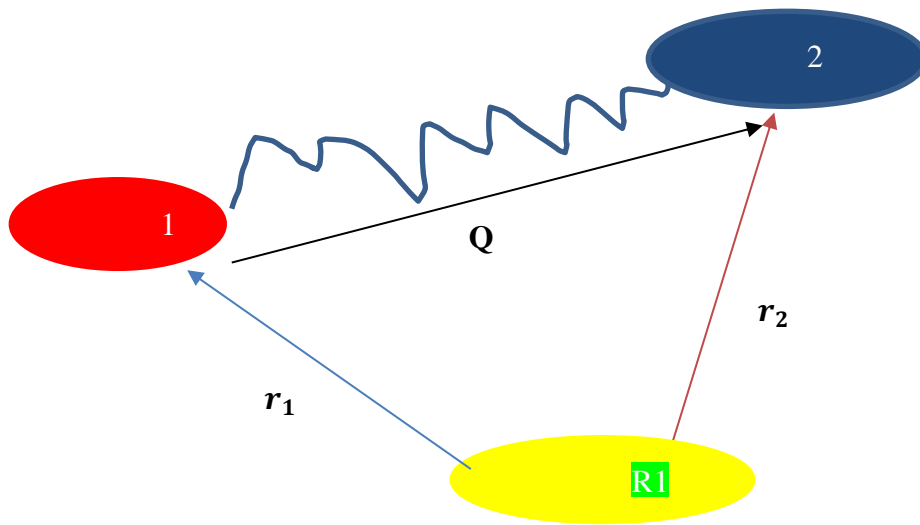


Figure 2.26. Dumbbells model schematic

2.6.2.1 Hookean Dumbbells model

Up to this point we have not yet specified the type of connector or spring (linear or nonlinear). But the type of connection (spring) is assumed to be linear in Hookean Dumbbells model. So, the connector force (the force which is resulted of beads interactions) obeys Hook law such that the below relation is verified (Bird, Curtiss et al. 1987, D. Shogin1 2020)

$$\mathbf{F}_c = H\mathbf{Q}. \quad (2.29)$$

Where:

- \mathbf{F}_c is connector force [N]
- H is stiffness of the spring [N m⁻¹]
- \mathbf{Q} is connector vector [m]

This model had some serious disadvantages which caused to be not valid for describing polymeric flow and forces anymore. First, this model is simple, and it is not able to describe shear thinning phenomena (it predicts constant shear viscosity). Then, by formulating model and start investigating its properties, one would find out that in extensional flow (shear free flow), the molecules (dumbbells) are infinitely stretched at a finite elongation rate. This, of course, cannot happen to a real molecule. (Van Heel, Hulsen et al. 1998, Shogin 2020).

2.6.2.2 Finitely Elongated Nonlinear Elastic (FENE) Dumbbell

The proposal of considering non-linear elastic spring which can extend only to maximum value ($Q = Q_0$) has been offered by Warner (Warner Jr and Fundamentals 1972) based on simple approximation of the inverse Langevin function. Based on such Idea the related relationship between molecular force and connector vector can be expressed as

$$F_c = \frac{HQ}{1 - \frac{Q^2}{Q_0^2}} \quad (2.30)$$

Where:

- Q is length of dumbbell extension (or the absolute value of connector force) [m]
- H is Warner spring coefficient [N m^{-1}]
- Q_0 is maximum length of dumbbell extension [m]
- \mathbf{Q} is connector vector [m]

as it is appearing from the equation, the initial amount of force is zero in $Q = 0$, then when Q increases up to its maximum value ($Q \rightarrow Q_0$) the force blows up to infinity and never reaches its maximal value which simply does not exist.

Similar to other kinetic based physical model the deviatoric ($\boldsymbol{\tau}$) stress tensor for this model is expressed as a sum of solvent contribution ($\boldsymbol{\tau}_s$) and polymer contribution ($\boldsymbol{\tau}_p$). In case the solvent is assumed to be Newtonian, its contribution ($\boldsymbol{\tau}_s$) is well understood, and therefore one concentrates on the polymer part ($\boldsymbol{\tau}_p$).

The polymer contribution ($\boldsymbol{\tau}_p$) is expressed by two different form called Kramer's form and Gieseku's form, respectively as (Shogin and Amundsen 2020)

$$\boldsymbol{\tau}_p = -n\langle \mathbf{Q}\mathbf{F}_c \rangle + nkT\boldsymbol{\delta}, \quad (2.31)$$

$$\boldsymbol{\tau}_p = \frac{1}{4}n\zeta\langle \mathbf{Q}\mathbf{Q} \rangle_{(1)}, \quad (2.32)$$

Where:

n is number concentration of dumbbells [m^{-3}]

k is Boltzmann's constant [J K^{-1}]

T is thermodynamic temperature [K]

$\boldsymbol{\delta}$ is unit stress tensor [Pa]

ζ is hydrodynamic drag coefficient [Kg s^{-1}]

“The angular brackets also shows the configuration -space averaging and subscript “(1)” stands for the upper-convected time derivative, introduced by Oldroyd to shows the rate of change in tensor properties of a fluid element in a coordinate system deforming with the fluid”(Shogin and Amundsen 2020).

Then adopting Kramer's form and substituting connector force proposed by FENE model, one can arrived at

$$\boldsymbol{\tau}_p = -nH \left\langle \frac{\mathbf{Q}\mathbf{Q}}{1 - (Q/Q_0)^2} \right\rangle + nKT\boldsymbol{\delta}. \quad (2.33)$$

This equation is called FENE constitutive equation.

2.6.2.3 FENE-P dumbbell model (with (nkT) , b , λ_H model parameters)

Although infinite elongation concept which was one of the main disadvantageous of the Hookean dumbbells model has been totally addressed in FENE model, the model constitutive equation cannot be written in close form. In fact, the average term in the constitutive equation of FENE model should be obtained by averaging with respect to the configuration'' distribution function'' $\Psi(\mathbf{Q}, t)$ in each single point which is very difficult task .The distribution function comes from statistical physics and shows the probability of finding a particular dumbbell in a

given state in each single point. R.Bird and his colleagues (Bird, Dotson et al. 1980) initiated an effort to eliminate averaging term in FENE constitutive equation and thus arriving at closed-form constitutive equation based on idea proposed by Peterlin .So,P in model nomination stand as a honor for Peterlin. He proposed following approximation (also called pre-averaging) for averaging part

$$\left\langle \frac{\mathbf{Q}\mathbf{Q}}{1 - \left(\frac{Q}{Q_0}\right)^2} \right\rangle \approx \frac{\langle \mathbf{Q}\mathbf{Q} \rangle}{1 - \frac{\langle Q^2 \rangle}{Q_0^2}}. \quad (2.34)$$

Moreover, mean-square relative dumbbell extension (x) is defined as

$$x = \frac{\langle Q^2 \rangle}{Q_0^2}. \quad (2.35)$$

Inserting equation 2.34, 2.35 and into equation 2.33 one can obtain

$$\boldsymbol{\tau} = -nH \frac{\langle \mathbf{Q}\mathbf{Q} \rangle}{1 - x} + nKT\boldsymbol{\delta}. \quad (2.36)$$

By defining Z factor such as

$$Z = \frac{1}{1 - x}, \quad (2.37)$$

equation 2.36 can be written as:

$$\boldsymbol{\tau} = -nHZ\langle \mathbf{Q}\mathbf{Q} \rangle + nKT\boldsymbol{\delta}. \quad (2.38)$$

One can still proceed the simplification process by first take taking the Oldroyd derivatives of both sides of the equation, and then using Giesekus form of constitutive equation to eliminate the averaging term($\langle \mathbf{Q}\mathbf{Q} \rangle$),resulting in below equation

$$Z\tau_p + \lambda_H\tau_{p(1)} - \lambda_H\{\tau_p - nkT\delta\} D \ln \frac{Z}{D_t} = -nkT\lambda_H\dot{\gamma} . \quad (2.39)$$

This equation is called FENE-P constitutive equation. Where Z factor is defined by equation 21 of Dmitry Shogin and Amundsen article (Shogin and Amundsen 2020), t is the time variable, while D stands for the material derivative and λ_H is time constant to return to the original state after deformation based on FENE-P model, defined as

$$\lambda_H = \frac{\zeta}{4H}. \quad (2.40)$$

R.Bird (Bird, Dotson et al. 1980) also related experimental time constant λ_e (time constant to return to the original state after deformation based on experiment) and λ_Q (time constant to return to the original state after deformation for rigid dumbbell) to λ_H such that

$$\lambda_e = \lambda_H \frac{b}{(b+3)} = \frac{3\lambda_Q}{b+3}. \quad (2.41)$$

Where, b is dimensions parameter (also called nonlinearity parameter) defined as

$$b = \frac{HQ_0^2}{kT}. \quad (2.42)$$

Figure below figure, summarize model prediction regarding steady shear rate dimensionless viscosity ($\frac{\eta-\eta_\infty}{\eta_0-\eta_\infty}$) versus dimensionless shear rate ($\lambda_e \dot{\gamma}$) based on defined equation 21 in the Bird article (Bird, Dotson et al. 1980):

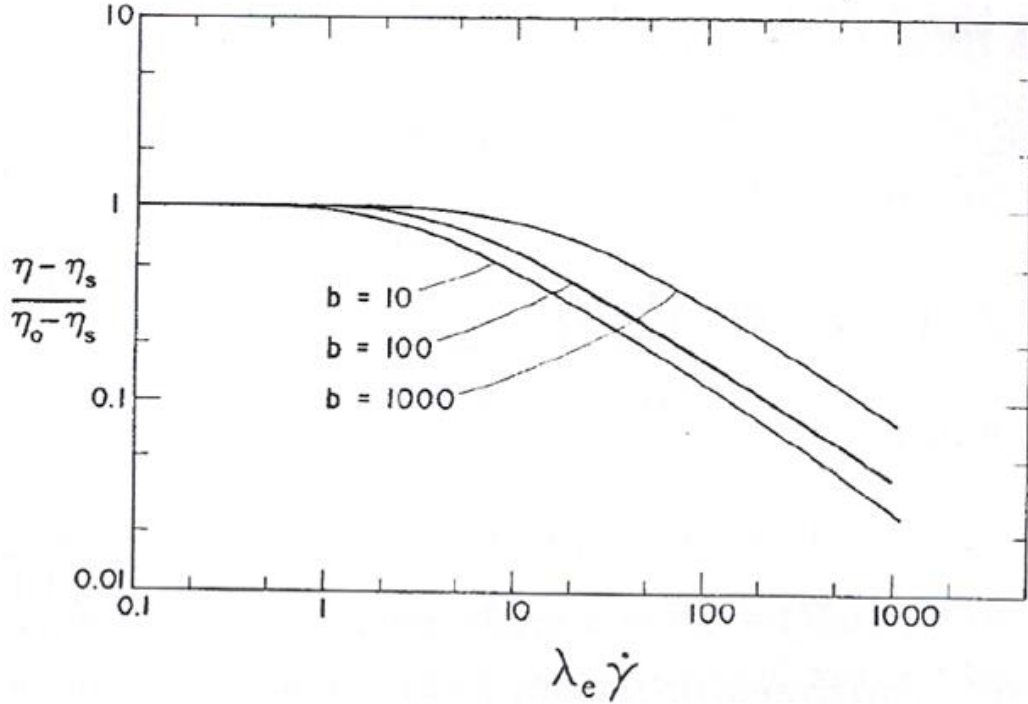


Figure 2.27. dimensionless viscosity($\frac{\eta-\eta_s}{\eta_0-\eta_s}$) versus dimensionless shear rate ($\lambda_e \dot{\gamma}$) for dilute solution of FENE-P Dumbbells based on equation(21) in (Bird, Dotson et al. 1980)

Now it can be seen that as it is appearing in the Figure 2.27 , the viscosity curves are dependent on model parameter (b) , so variety of curves can be created with change in model parameter b. To obtain one master curve (the curve which is only dependent on one parameter) the shear rate is converted to dimensionless shear rate by multiplying it in to converting coefficient ($C_{convert}$) which has same unit as relaxation time (s) and is defined such that change in b shows itself in this converting factor.it can be mathematically expressed as

$$C_{convert} = \frac{3\sqrt{3}}{\sqrt{2 + (b + 3)^3}} \lambda_Q \quad (2.43)$$

So, in case Weissenberg number ($w_i = \lambda_Q \dot{\gamma}$) is introduced, then dimensionless shear rate is defined as ($\dot{\gamma}_D$) is

$$\dot{\gamma}_D = C_{convert} \dot{\gamma} = \frac{3\sqrt{3}}{\sqrt{2 + (b + 3)^3}} \lambda_Q \dot{\gamma} = \frac{3\sqrt{3}}{\sqrt{2 + (b + 3)^3}} w_i \quad (2.44)$$

The resulted master curve based on been shown in following.

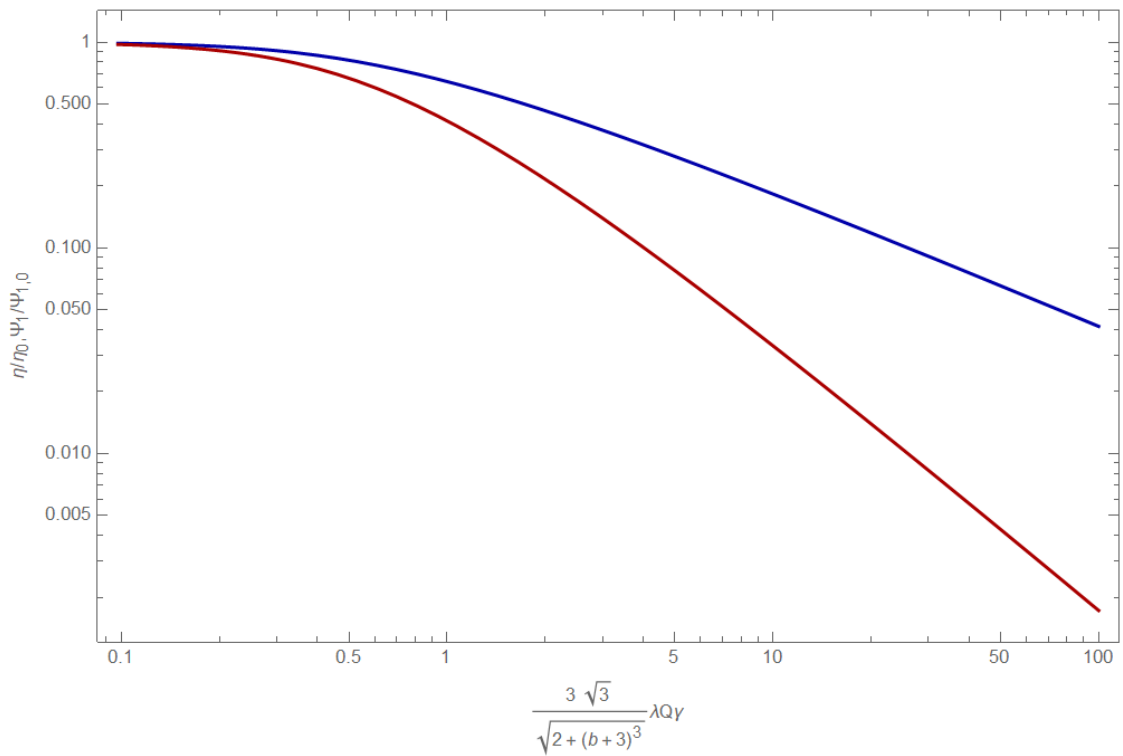


Figure 2.28. Master curve of dimensionless viscosity ($\frac{\eta}{\eta_0}$) (shown with blue curve) and normalized first normal stress coefficient (shown with red curve) versus dimensionless shear rate ($\dot{\gamma}_D = C_{Convert} \cdot \dot{\gamma}$)

The FENE-P model also predicts shear stress relaxation as a function of time in cessation of steady shear flow, based on equation (49) of (R. Bird et al., 1980). The resulted diagram has been summarized in below:

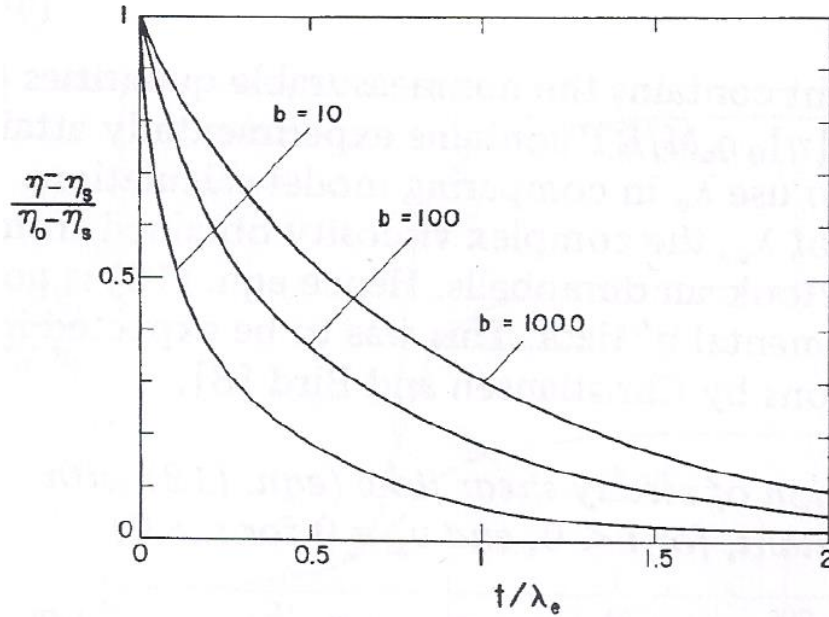


Figure 2.29. dimensionless shear Stress relaxation ($\frac{\eta - \eta_s}{\eta_0 - \eta_s}$) as a function of dimensionless time ($\frac{t}{\lambda_e}$) after cessation of steady shear flow for FENE-P dumbbells, from equation (49) of (Bird, Dotson et al. 1980)

As it can be seen from diagrams, the proposed model predicts shear thinning behavior of shear flow in satisfactory state. But the slope of shear thinning region is proposed to be constant amount ($-\frac{2}{3}$) which can be considered as drawback. Furthermore, the model cannot describe the wide distribution of relaxation time that real polymer shows. (Wedgewood, Ostrov et al. 1991).

2.6.2.4 C-FENE-P Dumbbell Model (with (nkT) , b , λ_H and E model parameters)

The FENE-P model is not able to describe ‘‘charged’’ dilute polyelectrolyte solutions. The charged implies the repulsive force between charged parts of a polyion, one can take the repulsive force between negatively charged part of HPAM polymer (Carboxyl COO^-) as an example. This fact was addressed by Shogin and Amundsen in 2020, where they tried to modify former FENE-P model such that it could describe the rheological properties of polyelectrolyte solutions, again based on kinetic theory. They called their model C-FENE-P (C stands for charged) and started to modify former FENE-P connector force. In fact, ‘they assumed the beads to carry identical effective charges q , interacting via an electrostatic Coulomb force’ Now, the modified connector force in this model can be expressed as (Shogin and Amundsen 2020)

$$F = \frac{HQ}{1 - \frac{Q^2}{Q_0^2}} + \frac{q^2}{4\pi\epsilon_0\epsilon} \frac{Q}{Q^3} \quad (2.45)$$

Where:

- ϵ is relative permittivity of the solvent [-]
- ϵ_0 is permittivity of vacuum [F m⁻¹]
- q is effective charge [C]

Then to take the strength of the electric interactions into their account, they defined new parameter (E) as

$$E = \frac{q^2}{(4\pi\epsilon_0\epsilon Q_0)KT} \quad (2.46)$$

And ,then they repeated all the procedures described in driving FENE-P constitutive equation except they used modified connector force (equation2.45) in all procedure. And they arrived at C-FENE-P constitutive equation as

$$\frac{b}{3}Z\tau_p + \lambda\tau_{p(1)} - \lambda\{\tau_p - nkT\delta\}D_t \ln Z = -nkT\dot{\gamma}, \quad (2.47)$$

Where $Z_{C-FENE-P}$ can be defined as

$$Z = \frac{1}{1-x} - \frac{E}{b} \frac{1}{x^2} = \frac{(Z_{FENE} - 1)}{F(Z_{FENE} - 1, \frac{E}{b})}. \quad (2.48)$$

Where, F is mathematical function defined by equation 21 of Dmitry Shogin and Amundsen article (Shogin and Amundsen 2020) and also Z_{FENE} factor is defined by equation 21 of same article.

So, the C-FENE-P constitutive equation is analogous to corresponding FENE-P equation in form. But here the key distinction is the modified Z factor in which the E parameters has been included. This E can vary from $E = 0$ to $E = \infty$,and it has an inverse relationship with salinity .”The reason roots up in “ionic interaction between polyions and counterions ,e.g. from dissolved salt resulting in reduction of repulsive force, and consequently more flexible polyiones”(Shogin and Amundsen 2020) .Hence E is responsible of stiffness of the assumed spring between beads such that, as it can be seen from constitutive equation ,when it decrease

to zero ($E \rightarrow 0$) in high level of salinity, the repulsive force reaches to its minimum amount (the most flexible state) and uncharged FENE-P model is recovered. On the contrast, when E increase up to its maximum margin ($E \rightarrow \infty$) in the lowest salinity, the repulsive force gets its maximum value and the most rigid dumbbell is recovered. The model prediction regarding dimensionless steady shear rate viscosity versus dimensionless shear rate, dimensionless stress growth as function of dimensionless time after start-up of steady shear stress and dimensionless stress relaxation as a function of dimensionless time after cessation of steady shear flow has been summarized in following figures respectively (Shogin and Amundsen 2020):

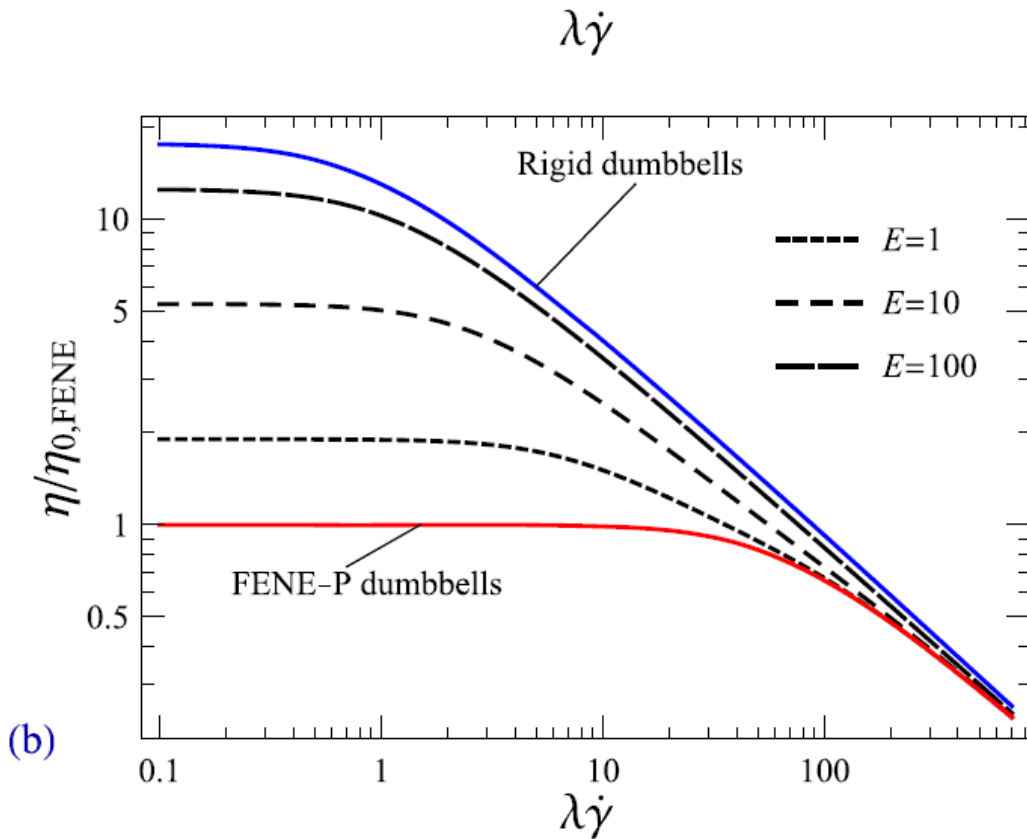


Figure 2.30. non-Newtonian viscosity (b) of C-FENE-P dumbbells, plotted as a function of dimensionless shear rate ($\lambda\dot{\gamma}$), for different values of E . The limiting cases $E = 0$ (uncharged FENE-P dumbbells) and $E \rightarrow \infty$ (rigid dumbbells) are marked. The nonlinearity parameter, b , is set to a moderate value of 50. (Shogin and Amundsen 2020)

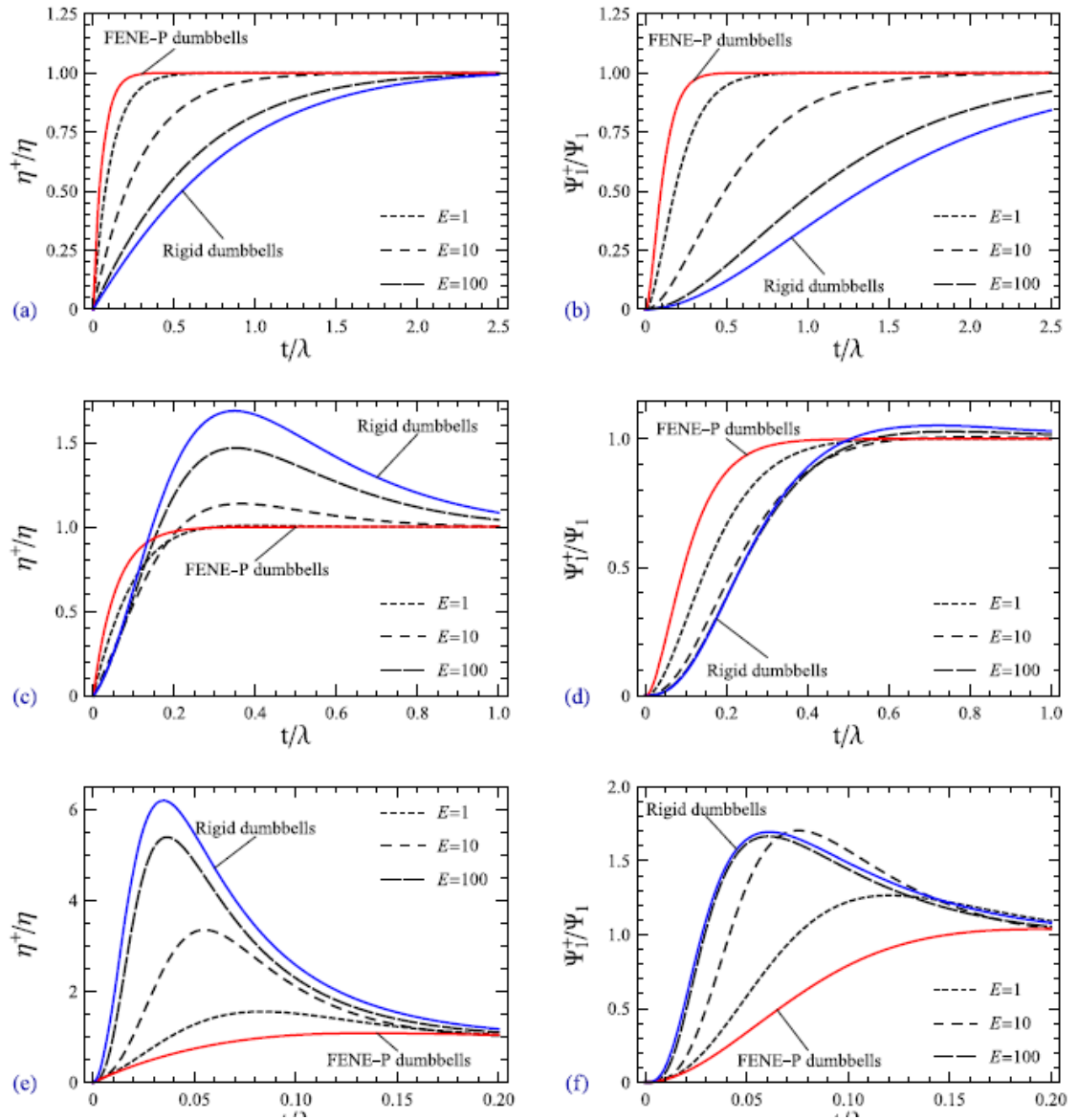


Figure 2.31. Normalized polymer contribution to shear stress [(a), (c), and (e)] and first normal stress difference [(b), (d), and (f)] growth functions of C-FENE-P dumbbells, plotted against dimensionless time, t/λ , for different values of parameter E at $\lambda\dot{\gamma} = 0.5$ [(a) and (b)], $\lambda\dot{\gamma} = 5$ [(c) and (d)], and $\lambda\dot{\gamma} = 50$ [(e) and (f)]. The limiting cases $E = 0$ (FENE-P dumbbells) and $E \rightarrow \infty$ (rigid dumbbells) are shown. All curves are plotted at $b = 50$ (Shogin and Amundsen 2020)

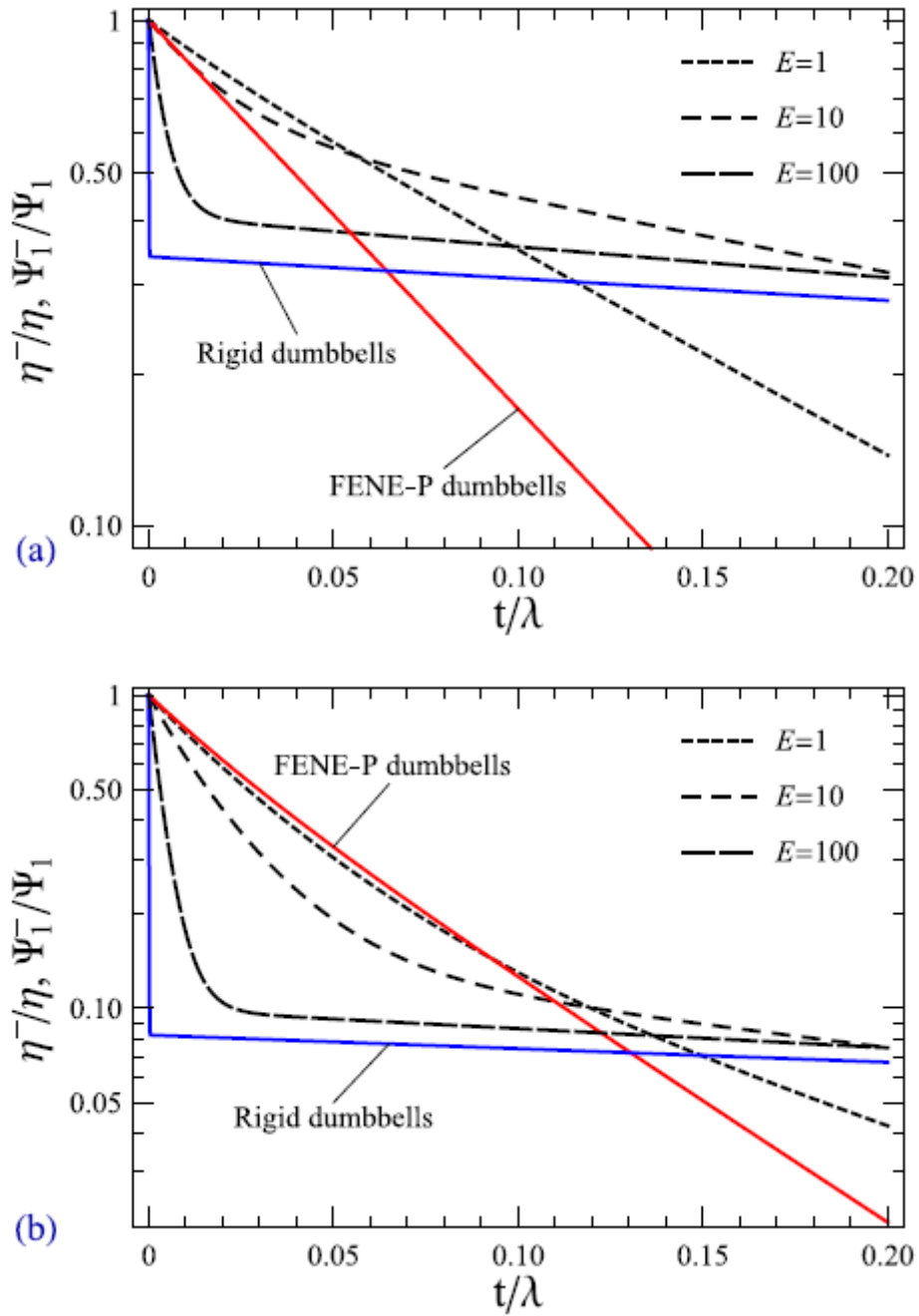


Figure 2.32. Normalized polymer contribution to shear stress and first normal stress difference relaxation functions of C-FENE-P dumbbells, plotted against dimensionless time t/λ at $\lambda\gamma = 5$ (a) and $\lambda\gamma = 50$ (b) for different values of E . The FENE-P limit, $E = 0$, and the RDB limit, $E \rightarrow \infty$, are also shown. The value of b is set to 50 (Shogin and Amundsen 2020)

- **Physical model applicable for Concentrated solution (network theory)**

The network theory was proposed to describe the material function of concentrated solution, where the concentration of solution is such that the solution is dominated by solution rather than solvents, and polymeric molecules interact more with each other rather than solvent molecules.

2.6.2.5 Phan-Thien-Tanner model (PTT) (*with ϵ, ξ, λ and η_0 model parameters*)

In 1977 Theien and Tanner initiated an effort to derive constitutive representative equation for description of material function of concentrated polymeric solution based on network theory and idea proposed by Lodge (Lodge 1968). The representative example of this network theory is shown in Figure 2.33 .Where polymer solution is shown as ‘‘a networks of junctions in this theory and each ‘network strand’’ is represented by vector ρ between junction’’. The full version (also called non-affine) of this model has only two free (independent) parameters ϵ and ξ . ϵ is the extensional parameter of the order 10^{-2} - 10^{-1} and $0 < \xi < 1$ is the affinity parameter, such that at $\xi = 0$, the model is affine with only one free parameters (ϵ) .Model constitutive equation can be expressed as(Thien and Tanner 1977) :

$$Z(\text{tr}\boldsymbol{\tau})\boldsymbol{\tau} + \lambda\boldsymbol{\tau}_{(1)} + \frac{\xi}{2}\{\dot{\boldsymbol{\gamma}} \cdot \boldsymbol{\tau} + \boldsymbol{\tau} \cdot \dot{\boldsymbol{\gamma}}\} = -\eta_0\dot{\boldsymbol{\gamma}}. \quad (2.49)$$

Where:

- λ is relaxation time[s]
- $\dot{\boldsymbol{\gamma}}$ is rate-of- strain tensor [s^{-1}]
- η_0 is zero -shear- rate viscosity [Pa s]

In case of affine PPT, this constitutive equation can be expressed as

$$Z(\text{tr}\boldsymbol{\tau}) \boldsymbol{\tau} + \lambda\boldsymbol{\tau}_{(1)} = -\eta_0\dot{\boldsymbol{\gamma}}. \quad (2.50)$$

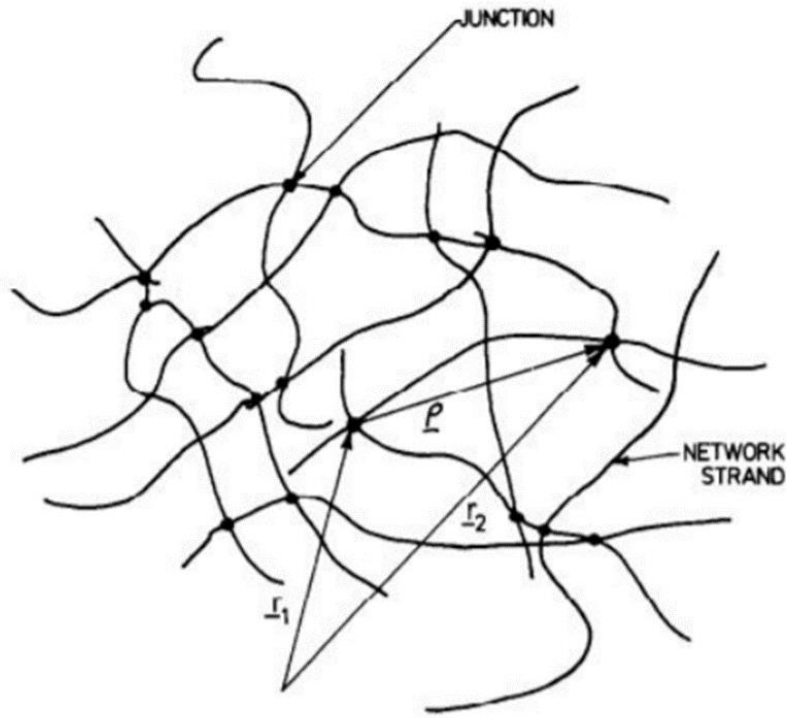


Figure 2.33. Simple representative of Phan-Thien-Tanner model (PTT) (Thien and Tanner 1977)

The model also has two branches called linear PPT (LPPT) and exponential PPT (EPPT) which are basically same in fundamental. Here The major difference is the representative equation for Z factor. Z factor can be expressed either as

$$Z = 1 - \epsilon\lambda \frac{(\text{tr}\tau)}{\eta_0}, \quad (2.51)$$

Or

$$Z = e^{-\epsilon\lambda \frac{(\text{tr}\tau)}{\eta_0}}. \quad (2.52)$$

In case first approach (the linear relation) is implemented for obtaining Z factor, the whole model is called linear PPT (LPPT) ,but if the second approach (exponential relationship) is implemented ,second branch of model called exponential PPT (EPPT) is recovered (Phan-Thien 1978). t is worth to mention some distinguishing properties of all these model branches at this stage of this research. Affine LPTT is somewhat similar to FENE-P, with power-law shear-thinning exponent of order 2/3. On the contrast, affine EPTT does not give a power-law at all,

predicting a polylogarithmic shear-thinning. But non-affine versions predict the non-zero second normal stress differences. Non-affine LPTT exhibits some "weird" properties though. It shear-thins with a very large negative exponent (-2): this leads to shear stress being not monotonic in shear rates but having a maximum, which is kind of sick. The model has a "constitutional instability" because of that, as described by Alves et al (2001) in their "Study of steady pipe and channel flows of a single-mode Phan-Thien-Tan " article (Alves, Pinho et al. 2001). On the other hand non-affine EPTT, is a really good model which has shown fantastic predictions for concentrated solutions and melts, especially the "multimode" version (Shogin 2020). 'Multimode' implies having different relaxation time (λ_e) that collaborates in constitutive equation such that as Dmitry Shogin has shown in his recent article for LPPT model (Shogin 2020), the resulted constitutive equation is the result of contribution from all spectrum of these different relaxation time. it is also worth to note that the maximum amount of overshoot prediction by LPPT single-mode based model is mathematically proven to not exceeding 1.14 which is considered as a drawback in case the larger overshoot is observed within data range (Shogin 2020).

The following diagrams summarized some LPP model predictions regarding steady shear ramping dimensionless viscosity versus dimensionless shear rate.

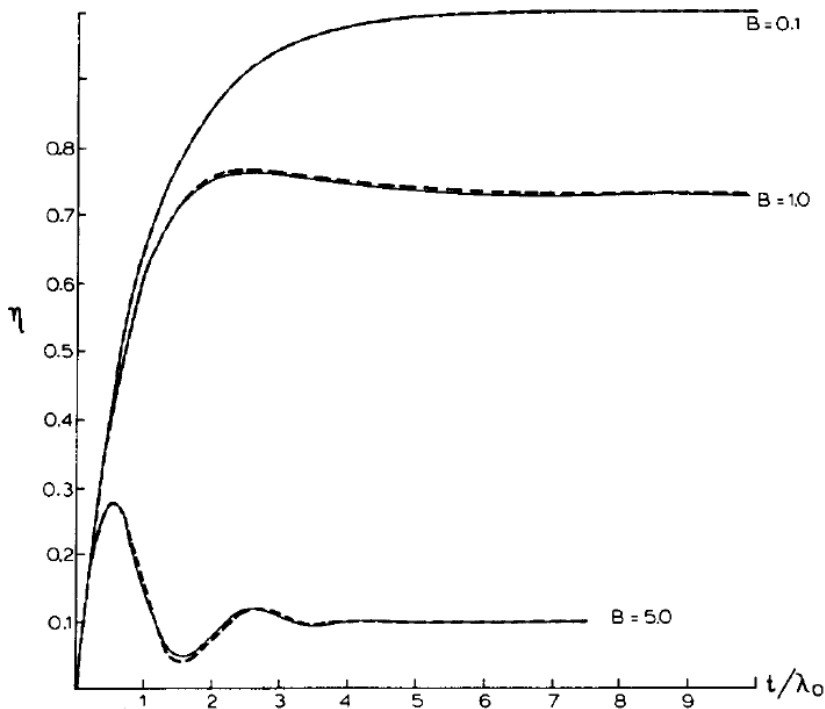


Figure 2.34.. Dimensionless viscosity. $B = \lambda_0 \dot{\gamma}$, dimensionless shear rate. for $\epsilon = 0.01$, for $\epsilon = 0.2$

Again, above diagram can be shown with one master curve based on dimensionless shear rate ($\dot{\gamma}_D$) for affine LPPT model as

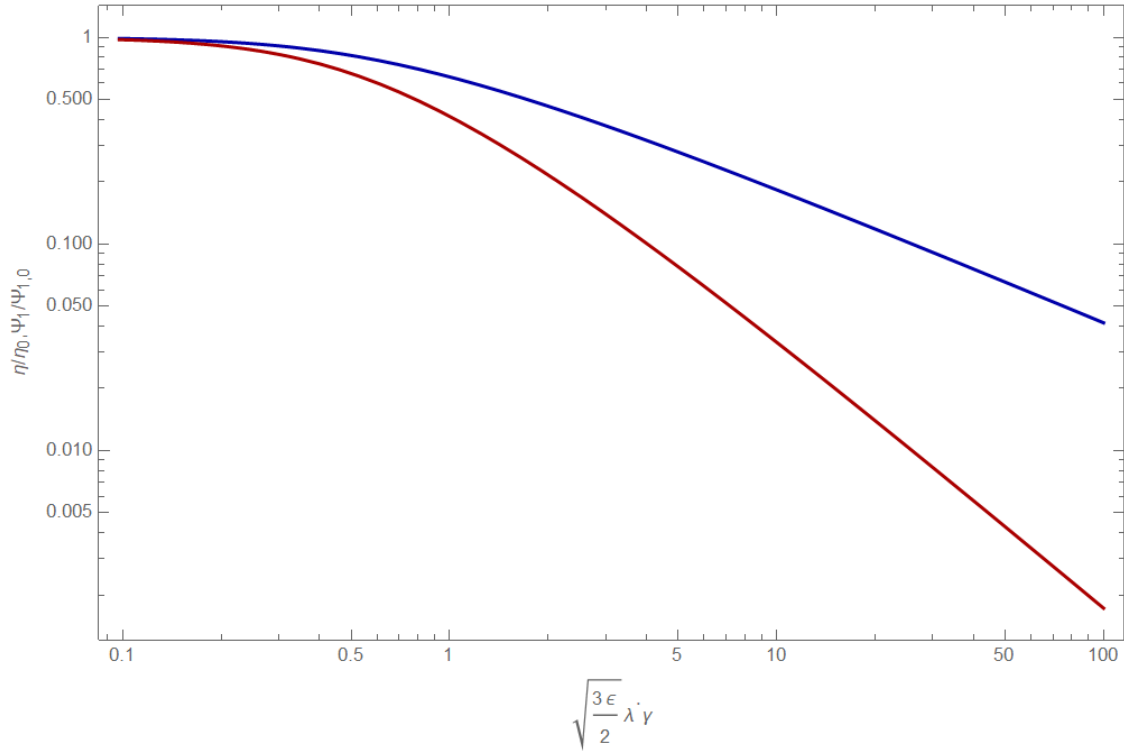


Figure 2.35. Master curve of dimensionless viscosity ($\frac{\eta}{\eta_0}$) (shown with blue curve) and normalized first normal stress coefficient (shown with red curve) versus dimensionless shear rate ($\dot{\gamma}_D = C_{convert} \cdot \dot{\gamma}$) for affine LPPT model

So again, it is observed that there is a coefficient ($C_{convert}$) which convert shear rate to dimensionless shear rate ($\dot{\gamma}_D$). It is defined by LPPT parameters terminology as

$$C_{convert} = \sqrt{\frac{3\epsilon}{2}} \lambda \dot{\gamma} \quad (2.53)$$

One should also remember that the Weissenberg number (w_i) here is simply defined as $w_i = \lambda \dot{\gamma}$. Moreover, although as mentioned beforehand, different theory has been used in deriving PPT constitutive equation, the constitutive equation of PPT model is interestingly equals to corresponding equation of FENE-P at least in all shear steady flows and extensional flows. PPT model parameters can be converted to FENE-P model as (Shogin 2020)

$$\eta_0 \leftrightarrow \frac{b}{b+3} nkT\lambda_H, \quad (2.54)$$

$$\lambda \leftrightarrow \frac{b}{b+3} \lambda_H, \quad (2.55)$$

$$\epsilon \leftrightarrow \frac{1}{b+3}. \quad (2.56)$$

This fact was relatively unknown for some period in literature. Tanner himself learned this fact only in 2019 and therefore could not mention it in 1977.(Poole, Davoodi et al. 2019),(Bird, Dotson et al. 1980). Moreover, the main advantages of PPT model is that it is only rely on two parameters (ϵ and ξ) which can be extracted by experiment (Thien and Tanner 1977) It is also worth to mention that according to theory, model parameter λ for affine LPPT, can be gained from the slope of exponential decay (m_{relax}) in cessations of steady shear ramp test such that

$$\lambda = -\frac{1}{m_{relax}}. \quad (2.57)$$

3 Experimental workflow

3.1 Quick introduction on experimental workflow

As it was mentioned beforehand, the objective of this study was set to focus on more analysis, instead of doing laboratory experiments in extensive way. So only one mother solution (not modified HPAM) with $M_w=5.10^5$ g/mole studied in three different concentrations $C_c=3.10^4$ ppm, $C_c=2.10^4$ ppm and $C_c=1.5 .10^4$ ppm

Laboratory workflow regarding preparing the solution can be summarized in below .

- **First stage: Preparation of mother solution**
preparation of mother solution based on predefined concentration and Mathematica program codes
- **Second step: Dilution of mother solution**
dilution of mother solution and making lower concentration solutions again based on predefined dilute concentrations and Mathematica program codes
- **Final stage: Conducting tests**
making rheology measurements with Anton Paar rheometer in three different experiments namely, steady shear ramping and start-up of steady shear flow and cessation of steady shear flow.

3.1.1 First step: Preparation of mother solution

In this part the goal is set to prepare mother solution with predefined concentration of $C_c=3.10^4$ ppm such that lower concentration solutions can be obtained from this mother solution.

Following Steps were taken to prepare mother solution.

- **First:**

Pouring about 500 ml desilted water into graduated cylinder and measuring the pour weight of water by scale number 2

- **Second:**

At the next stage, the required weight of polymer solution is measured based on desired polymeric concentration (concentrations $C_c=3.10^4$ ppm) with usage of following formula

$$M_P = \frac{C_c \cdot M_S \cdot 10^{-6}}{1 - (C \cdot 10^{-6})} \quad (3.1)$$

Where:

M_P is required mass of polymer [g]

C_c is Concentration of polymer [ppm]

M_S is Measured mass of solvent [g]

- **Third:**

Then in the next stage called practical calculation, taken weight of polymer in practice is measured (by scale number 2) as it is almost impossible to take exact theoretical amount of polymer powder calculated in former stage. Then real concentration of mother solution (C_{rel}) can be obtained as

$$C_{rel} = \frac{M_{Pa}}{M_{Pa} + M_S} \cdot 10^6 \quad (3.2)$$

Where:

C_{rel} is true concentration of resulted solution [ppm]

M_{Pa} is Practical mass of polymer taken in practice [g]

- **Final stage:**

In the final stage of experiment, polymer powder is mixed with distilled water about two hours by mixer to gain desired concentration. Then the resulted polymeric solution is mixed with magnetic stirrer for 24 hours, while it has been covered with parafilm to prevent water from evaporating.



Figure 3.1. from left; graduated cylinder, measuring spoon, scale number 1 and scale number 2



Figure 3.2 from left; HPAM polymer powder ,mother solution $C_c=3.10^4$ ppm, mixer for mixing polymer powder and water and magnetic mixer

3.1.2 Dilution of mother solution

At this stage lower concentrations ($C_c=2.10^4$ ppm, $C_c=1.5.10^4$ ppm) is derived from mother solution. The procedure defined by Mathematica software and by following stages

- **First:**

the theoretical mass of the concentrated solution required for making dilute solution is obtained from following as

$$M_c = \left(\frac{C}{C_0} \cdot m_d \right). \quad (3.3)$$

Where:

M_c is theoretical mass of concentrated polymer [g]

C is desired concentration of dilute polymer [ppm]

C_0 is true concentration of concentrated polymer [ppm]

m_d is desired mass of dilute solution [g]

- **Second:**

Then in the next stage the total true mass of dilute solution with desired concentration gained based on the mass of concentrated polymer taken in practice, as again it is almost

Impossible to take exact amount of polymer calculated in former stage according to Following

$$m_t = \left(\frac{M_c \cdot C_0}{C} \right). \quad (3.4)$$

Where:

m_t is total mass of dilute solution required [g]

M_c is mass of concentrated solution taken in practice [g]

C_0 is true concentration of concentrated polymer [ppm]

C is desired concentration of dilute polymer [ppm]

- **Third stage:**

In the third stage, finally the evaluation of true concentration of dilute solution is done based on the measured total mass of dilute solution in practice via

$$C = \left(\frac{M_{cp} \cdot C_0}{m} \right). \quad (3.5)$$

Where:

C is final and true concentration of dilute polymer [ppm]

M_{cp} is mass of concentrated solution taken in practice [g]

C_0 is the true concentration of concentrated polymer [ppm]

m is measured total mass of dilute solution required [g]

- **Final stage:**

Then magnetic components are put in resulted dilute solution and it is mix with magnetic stirrer for about 15 minutes and then it can be poured into sample container and put in the refrigerator.

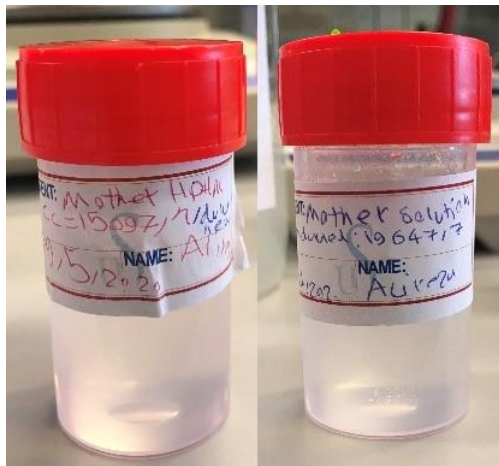


Figure 3.3. HPAM polymer with concentration from left; $C_c = 1.5 \cdot 10^4$ ppm, $C_c = 2 \cdot 10^4$ ppm

So, the predefined and true concentrations of HPAM polymer $C_c=3.10^4$ ppm, $C_c=2.10^4$ ppm and $C_c=1.5.10^4$ ppm solution can be compacted as a below

Table 3.1: *Predefined concentration versus concentration on practice*

Name of solution	Predefined concentration	Concentration on practice
HPAM Solution	$C_c=3.10^4$ ppm	$C_c=3.16.10^4$ ppm
HPAM solution	$C_c=2.10^4$ ppm	$C_c=1.96 .10^4$ ppm
HPAM Solution	$C_c=1.5 .10^4$ ppm	$C_c=1.5 .10^4$ ppm

3.1.3 Conducting tests

Before explaining the mechanism and setting adjustment by which the experiments has been done, it is worth to go through some more details on the rheometer instrument and how it measures the viscoelastic properties.

3.1.3.1 Introduction on Rheometer

The Anton Paar rheometer (MCR302) was used in this experiment. This kind of rheometer can work with different kind of attached instrument, each are suitable for especial kind of flow listed below(Mezger 2006):

- Concentric cylinder measuring system
- Parallel plate measuring system
- Mooney-Evart measuring system
- Cone-and-plate measuring system

The cone-and-plate attached system has been used in this research as it can maintain constant shear rate due to its special geometric figuration.

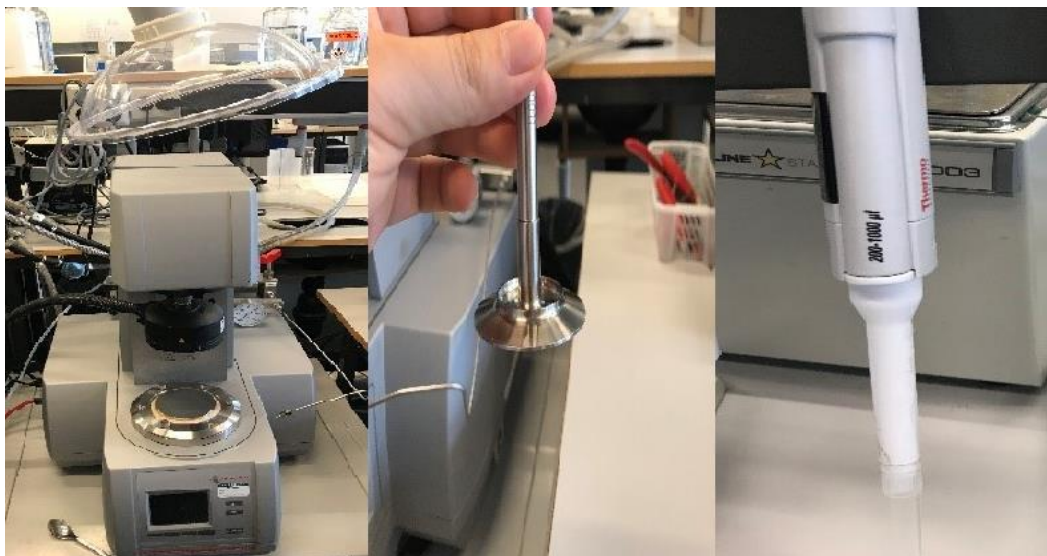


Figure 3.4. from left; Anton paar rheometer, cone-and-plate attachment, graduated pipette for poring polymer into rheometer

3.1.3.2 shear ramping test

As it can be seen from nomination, at this experiments the viscosity of polymer is measured relative to the applied shear rate which ramps up from very low shear rates ($\dot{\gamma} = 10^{-3} \frac{1}{s}$) to extremely high shear rates ($\dot{\gamma} = 10^3 \frac{1}{s}$). As it is depicted in Figure 3.5, the setting part is adjusted in such a way that 25 viscosity points is measured in shear rates interval ranging from $10^{-3} \geq \dot{\gamma} \leq 10^3$. But as it is shown in Figure 3.5, more time is dedicated for lower shear rates measurements (120 s/measurement for mother solution and 60 s/measurement for lower concentrations) and less time for higher shear rates (7 s/measurement). The reason roots up in the fact that more time is required for gaining consistent results in lower shear rates region. Thus, the obtained viscosity data from the shear ramping experiments in measuring shear rates can be considered as a steady shear rates value of the specific steady shear rates.

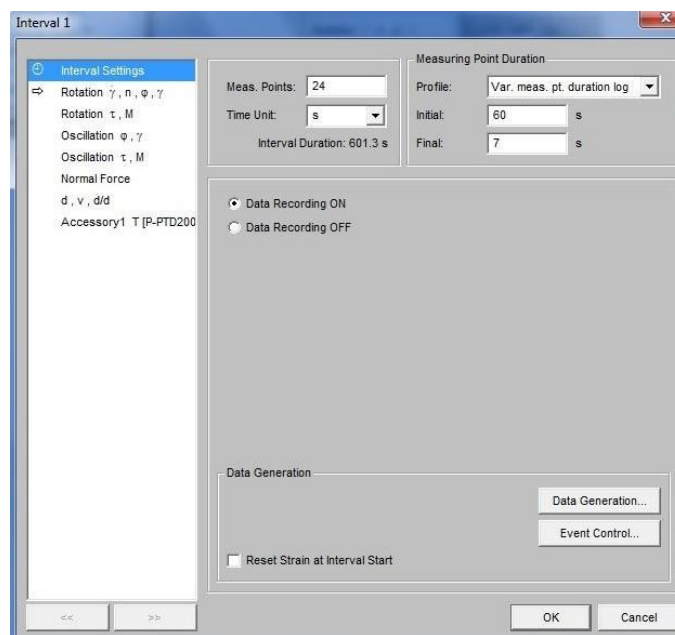


Figure 3.5. Setting parameter of shear ramping test

3.1.3.3 startup of steady shear rate experiment

As noted in chapter 2 the start-up of steady shear rate experiment is kind of experiment in which the constant shear rate is applied to fluid only from start point of experiment ($t > 0$) and fluid is on rest for all time before starting point of experiment (for all $t < 0$). So, as it is depicted in Figure 3.6, the setting options should be changed such that it able us to reach specific constant shear rate whiten specific amount of time from starting point of experiment ($t=0$). Thus, 40 measuring points were implemented such that less time per measurement (0.001 s/measurement) is dedicated for initial time interval and more time per measurement (0.25 s/measurement) for final time interval.

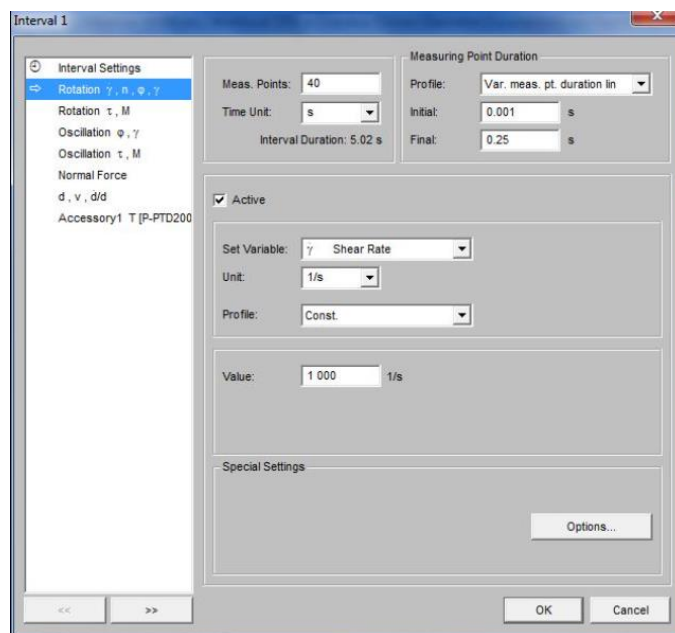


Figure 3.6. Setting parameter of startup of steady shear rate experiment

3.1.3.4 Cessation of steady shear rate test

As it was noted in chapter 2 in this experiment which is in complete opposition compare to start-up of steady shear flow test, the constant shear rate is only applied to fluid for time before starting the experiment ($t < 0$) and then there is sudden stop of applied shear rate for all $t > 0$ to see how fluid relaxes its stored shear stress. So, to have constant shear rate before starting point (for all $t < 0$) this experiment conducted immediately after startup experiment. Moreover setting parameters should be arranged exactly similar to Figure 3.6 except the shear rate value is set up to zero from starting point of this experiment (for all $t > 0$) where there is a sudden stop in applied constant shear rate to obtain measure 40 measuring relaxation points.

4 Data analysis

4.1 Data analysis without considering physical models

As it was discussed in the project objective, at the first stage, the obtained data in experiments part is plotted and fitted to their representative trends (linear, power-law, etc.) via both quantitative and qualitative analysis without considering physical representative model.

It is also worthwhile to mention that all figures represented in this part of thesis produced with the help of Wolfram Mathematica software.

4.1.1 Shear ramping experiments

4.1.1.1 Viscosity analysis (η)

The below Figure 4.1, is produced representative of viscosity versus shear rates for HPAM polymer in three different concentrations, $C_c=3.10^4$ ppm, $C_c=2.10^4$ ppm and $C_c=1.5 \cdot 10^4$ ppm.

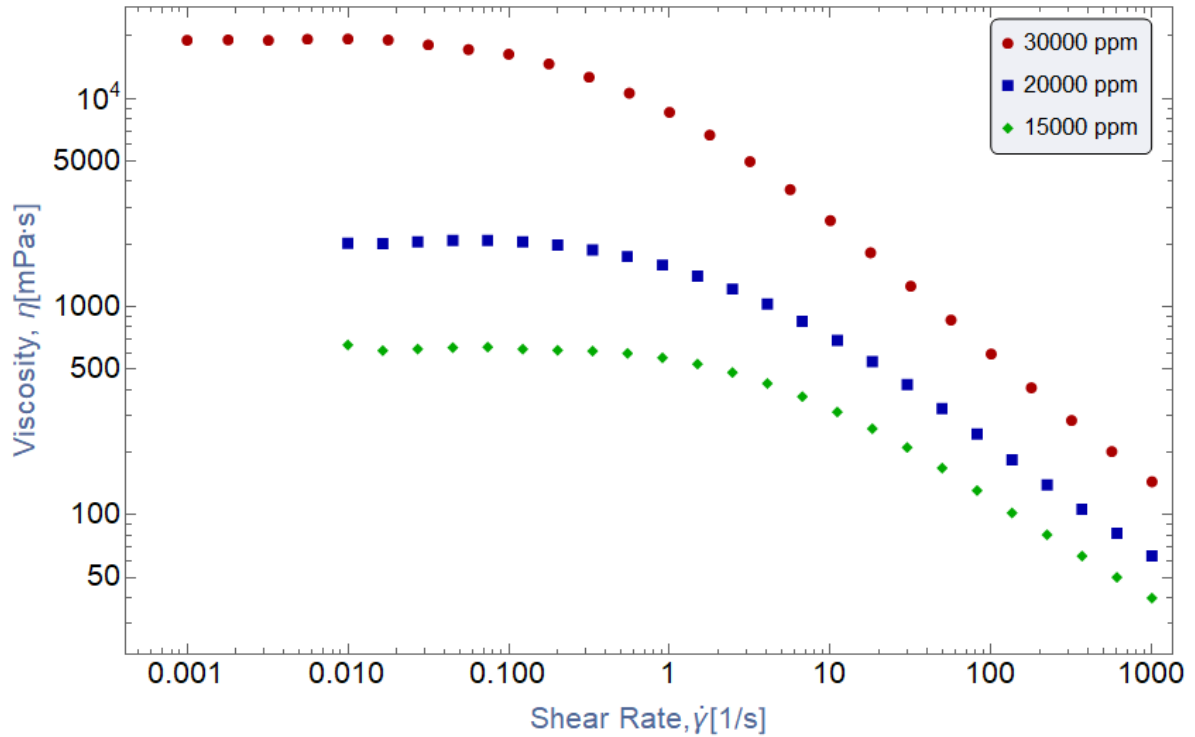


Figure 4.1. Produced graph of viscosity (η) versus shear rate ($\dot{\gamma}$) for $Cc=3.10^4$ ppm, $Cc=2.10^4$ ppm and $Cc=1.5 \cdot 10^4$ ppm HPAM polymer solution in log-log axis scale

So, there is no surprising regarding above trends. In other words, what is observed from this diagram is in great accordance with what was reviewed extensively in chapter 2, from main reference book (Bird, Curtiss et al. 1987).

Then above data normalized relative to upper Newtonian region viscosity value ($\frac{\eta}{\eta_0}$) and fitted to representative lines from Figure 4.2 to Figure 4.4. Finally, the slope of power-law region or linear reduction in log-log scale (m) was extracted from these fitted lines to investigate more about the relation and trend between slope of reduction and dilution degree of the solution.

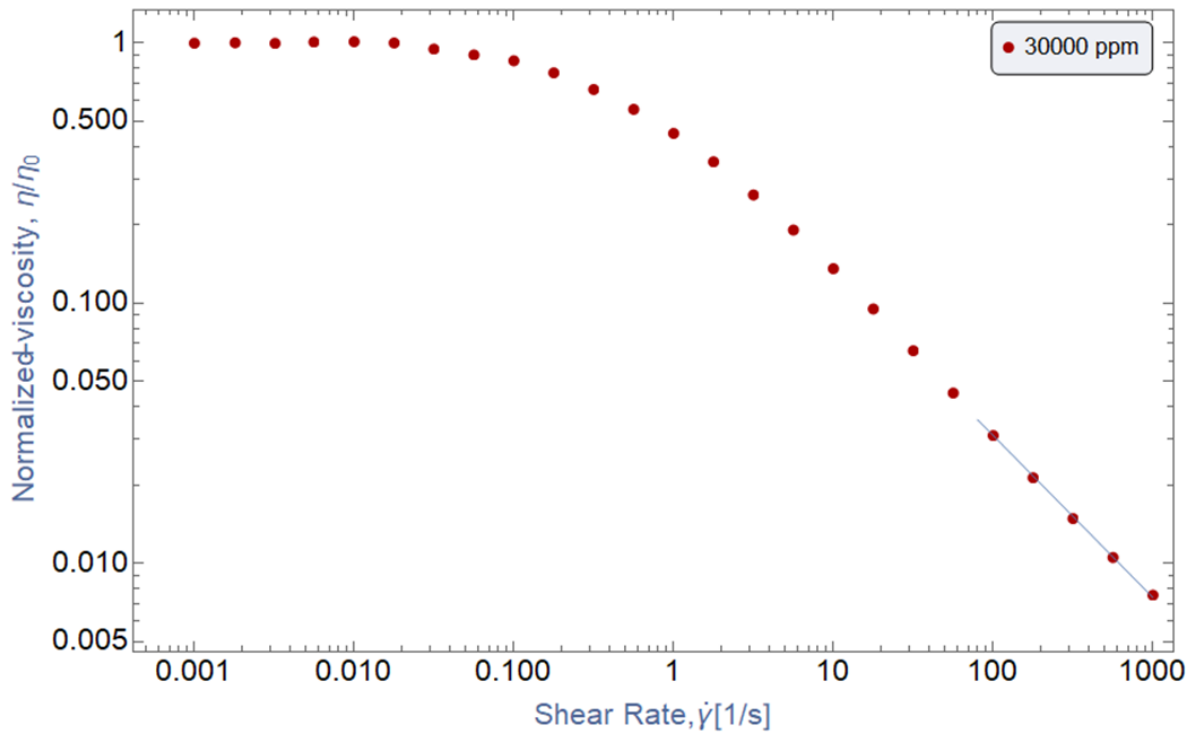


Figure 4.2. Normalized viscosity ($\frac{\eta}{\eta_0}$) versus applied shear rate ($\dot{\gamma}$) for $Cc=3.10^4$ ppm HPAM polymer solution in log-log axis

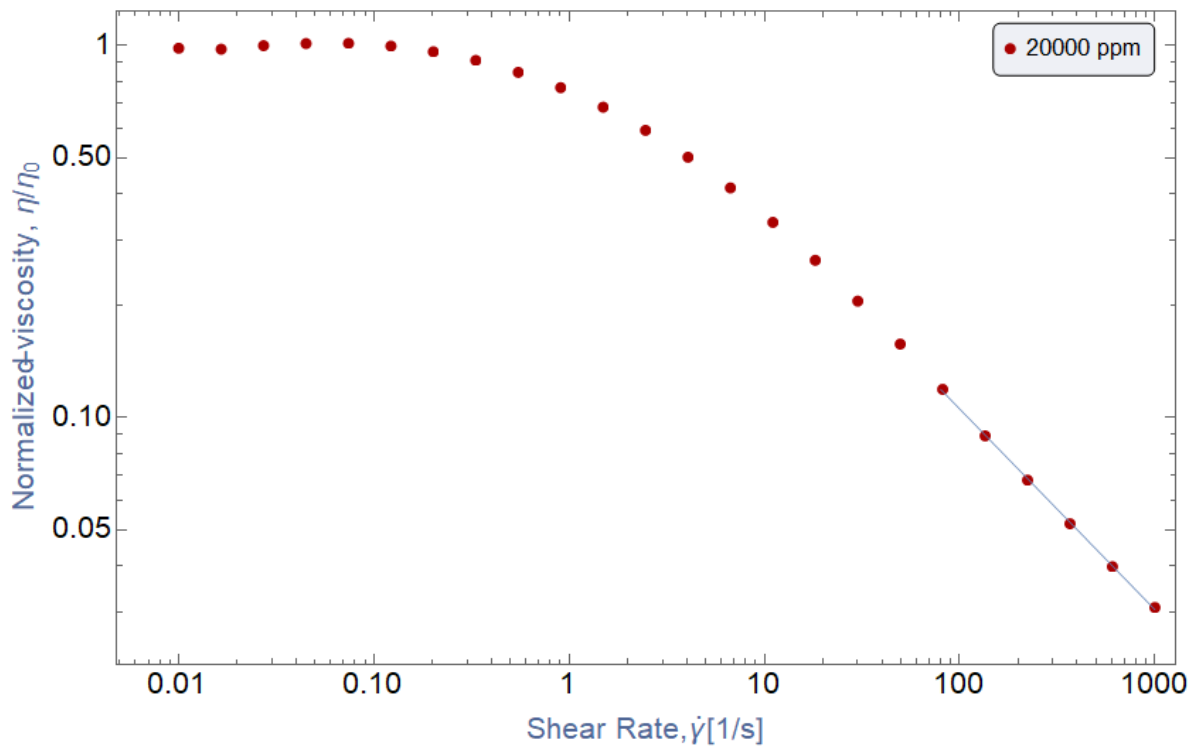


Figure 4.3. Normalized viscosity ($\frac{\eta}{\eta_0}$) versus applied shear rate ($\dot{\gamma}$) for $Cc=2.10^4$ ppm HPAM polymer solution in log axis

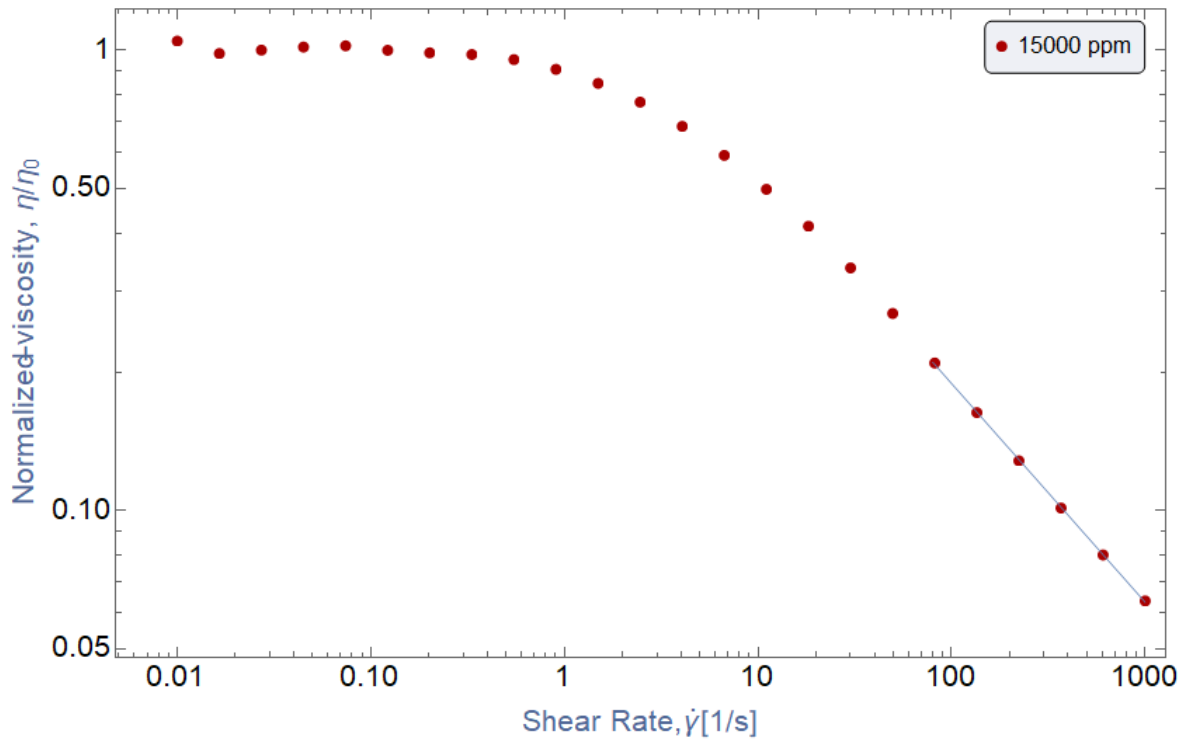


Figure 4.4. Normalized viscosity ($\frac{\eta}{\eta_0}$) versus applied shear rate ($\dot{\gamma}$) for $C_c=1.5 \cdot 10^4$ ppm HPAM polymer solution in log-log axis

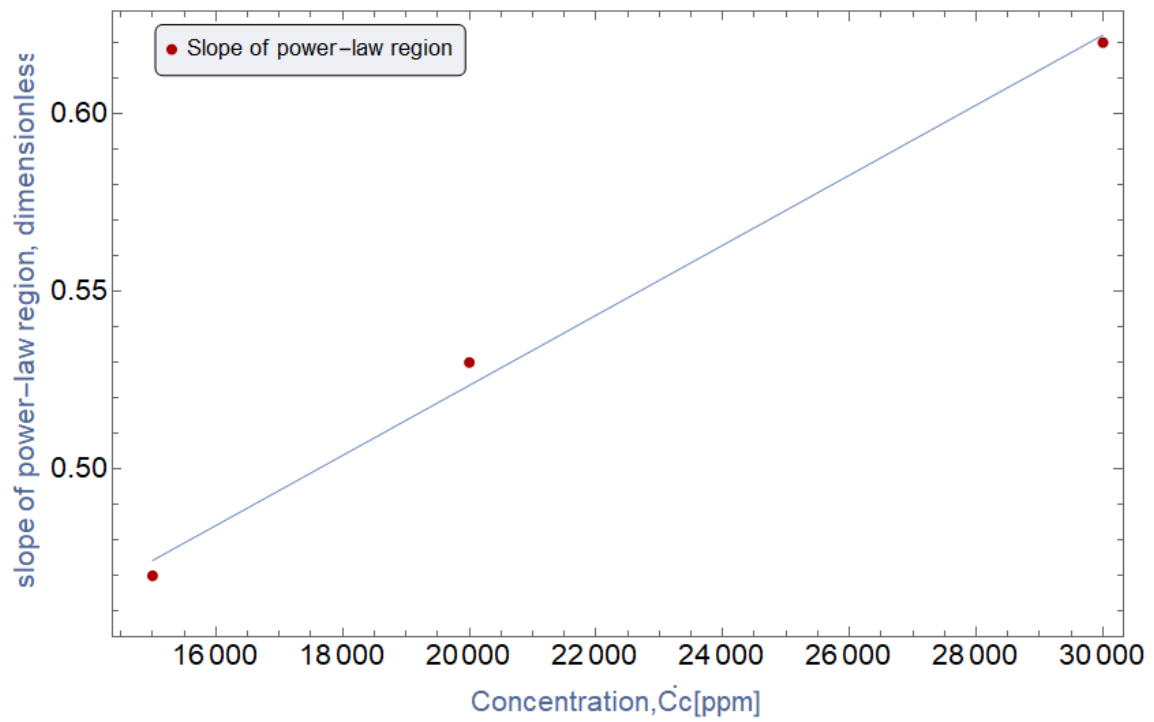


Figure 4.5. Cumulative result of Figure 4.2 to Figure 4.4

From Figure 4.5 it is seen that;

- first, the slope of power-law region for HPAM polymer in all concentration level lies in the typical range for polymeric solution ($-0.4 < m < -0.9$)
- then it also seen that the slope of reduction slows down as the concentration decreases.

4.1.1.2 First normal stress differences coefficient (Ψ_1) analysis

As it has been mentioned in literature review, low level of practical information on first normal stress differences coefficient (Ψ_1), is a great motivation to study this quantity in this research. Though, it is not easy task to measure this coefficient especially for low shear rate, where the forces involved are small, therefore the instrumental error becomes significant compared with what we measure. Also, sensitivity of the rheometer in the normal direction is another issue which needs to be addressed. Figure 4.6 to Figure 4.8 show first normal stress differences coefficient (Ψ_1) versus applies shear rate ($\dot{\gamma}$) of HPAM polymer in three concentration, $C_c=3.10^4$ ppm, $C_c=2.10^4$ ppm and $C_c=1.5.10^4$ ppm.

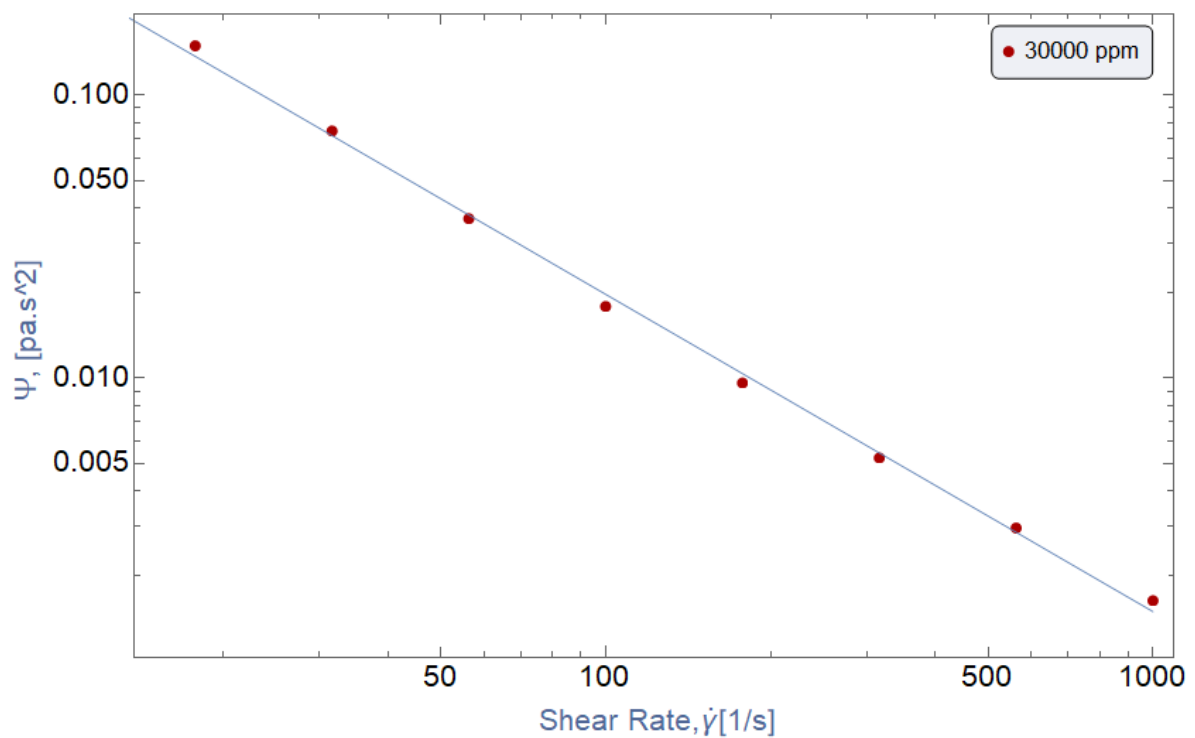


Figure 4.6. first normal stress differences coefficient (Ψ_1) versus shear rate ($\dot{\gamma}$) of $C_c=3.10^4$ ppm HPAM polymer solution in log-log axis

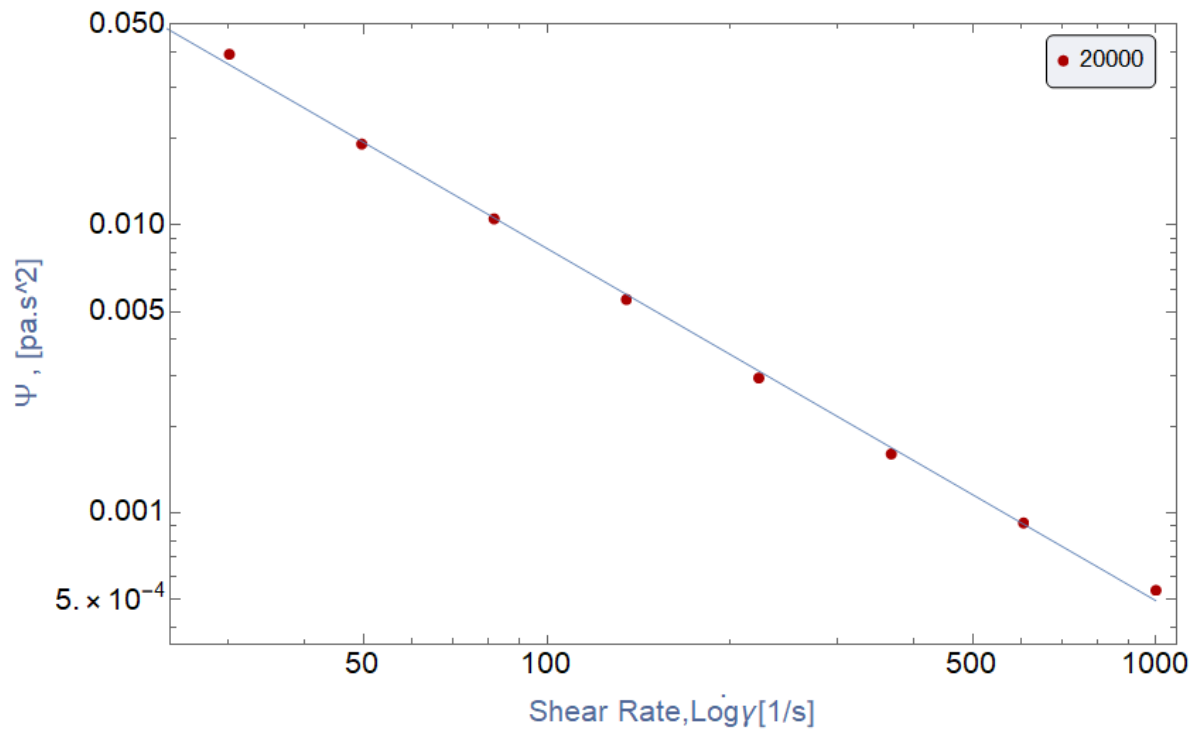


Figure 4.7. first normal stress differences coefficient (Ψ_1) versus shear rate ($\dot{\gamma}$) of $C_c=2.10^4$ ppm HPAM polymer solution in log-log axis

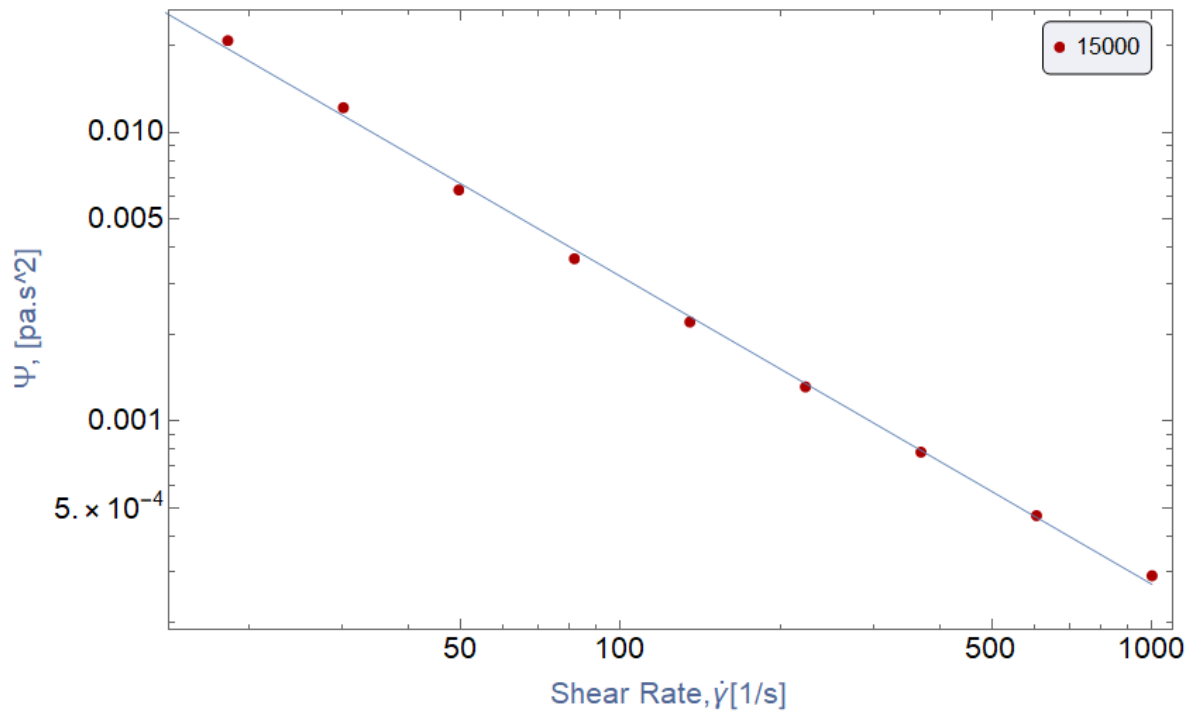


Figure 4.8. first normal stress differences coefficient (Ψ_1) versus shear rate ($\dot{\gamma}$) of $C_c=1.5 \cdot 10^4$ ppm HPAM polymer solution in log-log axis

Following observation about first normal stress difference coefficient (Ψ_1) can be made from above diagrams:

- It is seen as it was expected, first normal stress difference coefficient (Ψ_1) versus shear rate trend is similar to what was observed regarding viscosity.
- Though, the slope of fitted line in power-law region ($m= -1.12$, $m= -1.22$ and $m= -1.06$, for $C_c=3 \cdot 10^4$ ppm, $C_c=2 \cdot 10^4$ ppm and $C_c=1.5 \cdot 10^4$ ppm, respectively) shows that Ψ_1 decreases much more intensively in comparison with viscosity.
- Almost constant slope of fitted lines in power-law region of all three concentrations also shows that the slope of power-law region of first normal stress difference coefficient (Ψ_1) is not dependent on concentration at all, whereas it was observed in viscosity part, the slope of power-law region is dependent on level of concentration.

4.1.2 Startup of steady shear flow experiment

There are two fundamentally different ways regarding data analysis for this experiment. One is sorting data based on concentration of the fluid, and another one is relying on initial applied shear rate (step-rate). Second approach has been applied in below Figure 4.9 to Figure 4.15.

Below Figure 4.9 to Figure 4.15 show normalized shear stress growth $(\frac{\eta^+(t, \dot{\gamma}_0)}{\eta(\dot{\gamma}_0)})$ versus elapsed time (t) related to different applied shear rate ($\dot{\gamma}$), for HPAM polymer in three concentration $C_c=3 \cdot 10^4$ ppm, $C_c=2 \cdot 10^4$ ppm and $C_c=1.5 \cdot 10^4$ ppm.

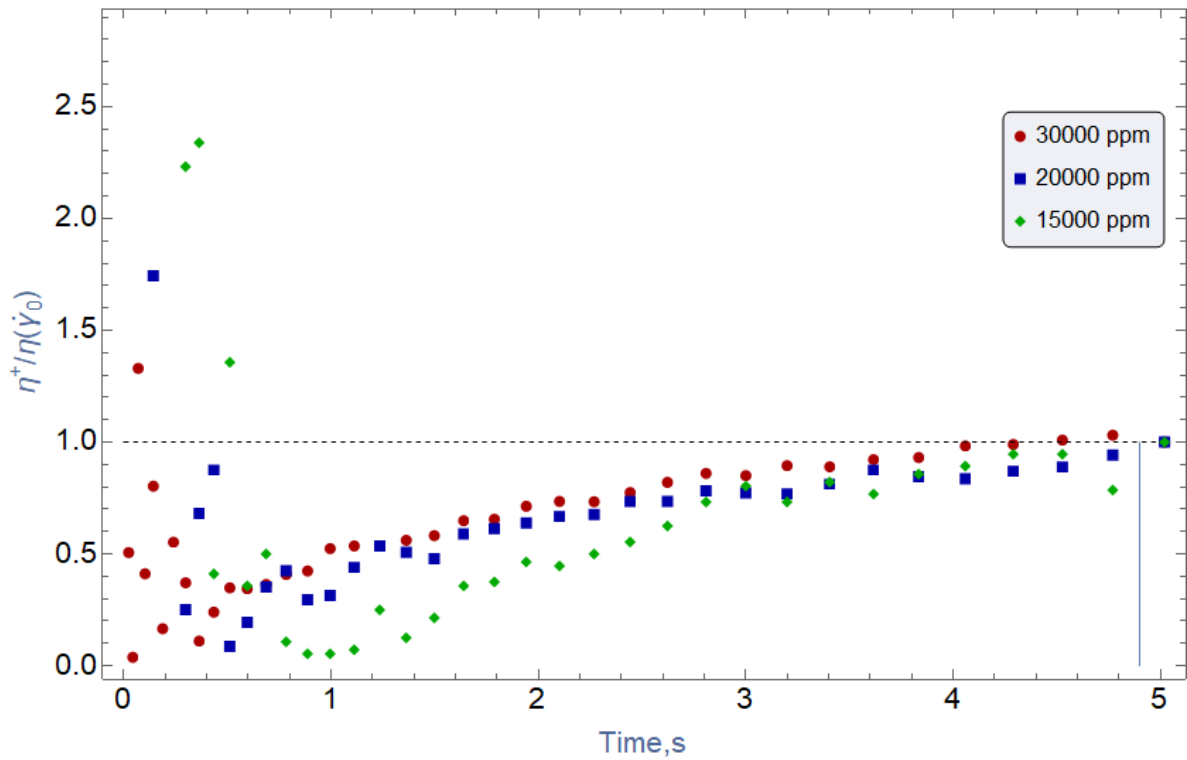


Figure 4.9. Normalized start up growth $(\frac{\eta^+(t, \dot{\gamma}_0)}{\eta(\dot{\gamma}_0)})$ versus time (t) for shear rate $\dot{\gamma} = 0.01$

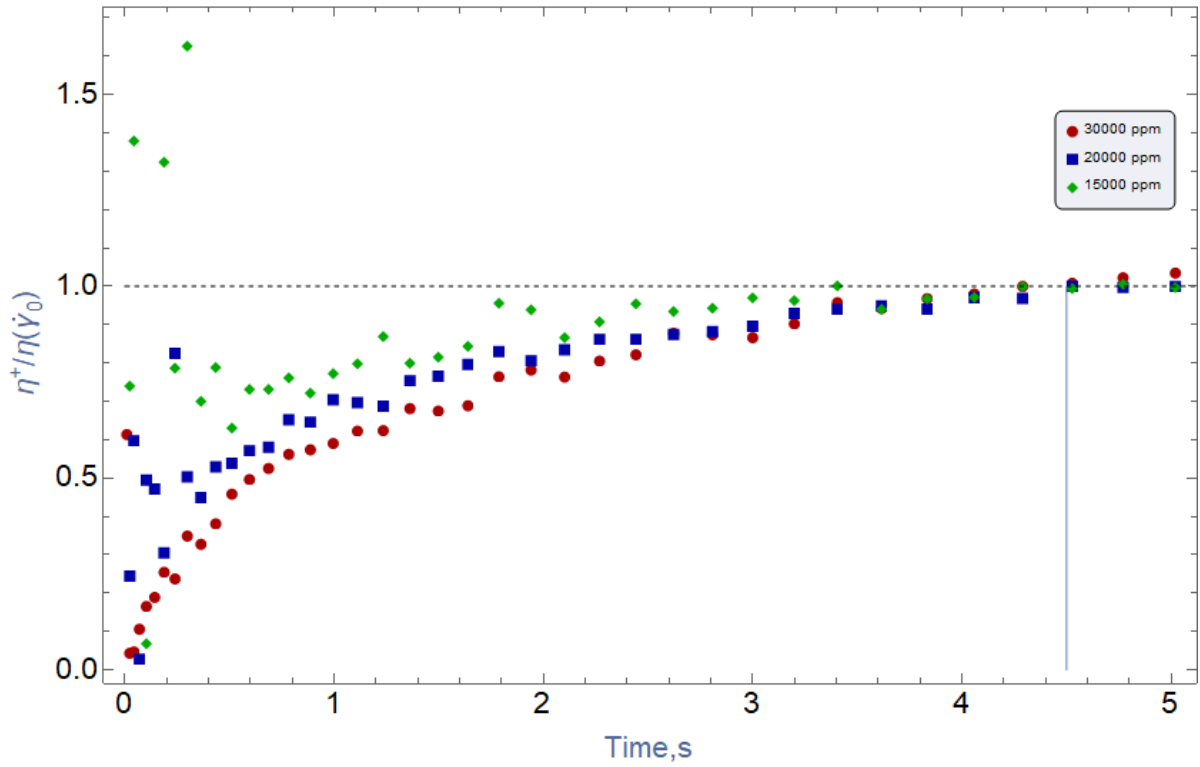


Figure 4.10. Normalized start up growth $\left(\frac{\eta^+(t, \dot{\gamma}_0)}{\eta(\dot{\gamma}_0)}\right)$ versus time (t) for shear rate $\dot{\gamma} = 0.1$

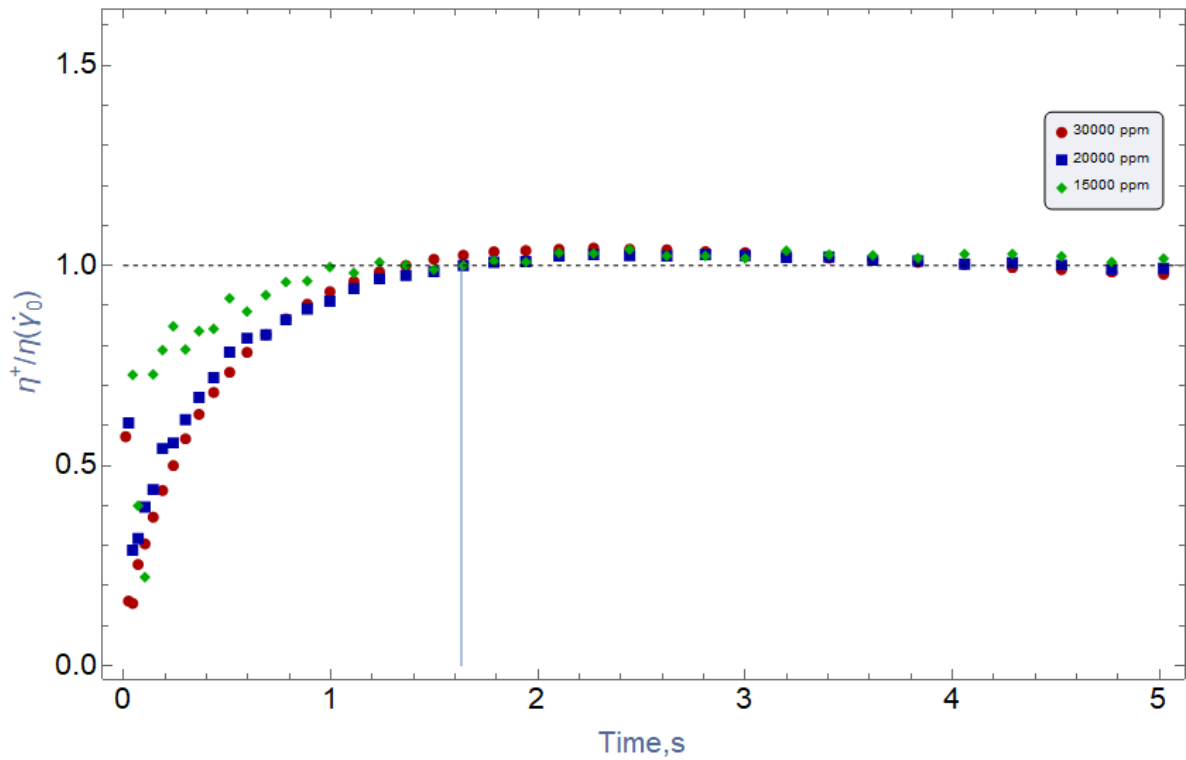


Figure 4.11. Normalized start up growth $\left(\frac{\eta^+(t, \dot{\gamma}_0)}{\eta(\dot{\gamma}_0)}\right)$ versus time (t) for shear rate $\dot{\gamma} = 1$

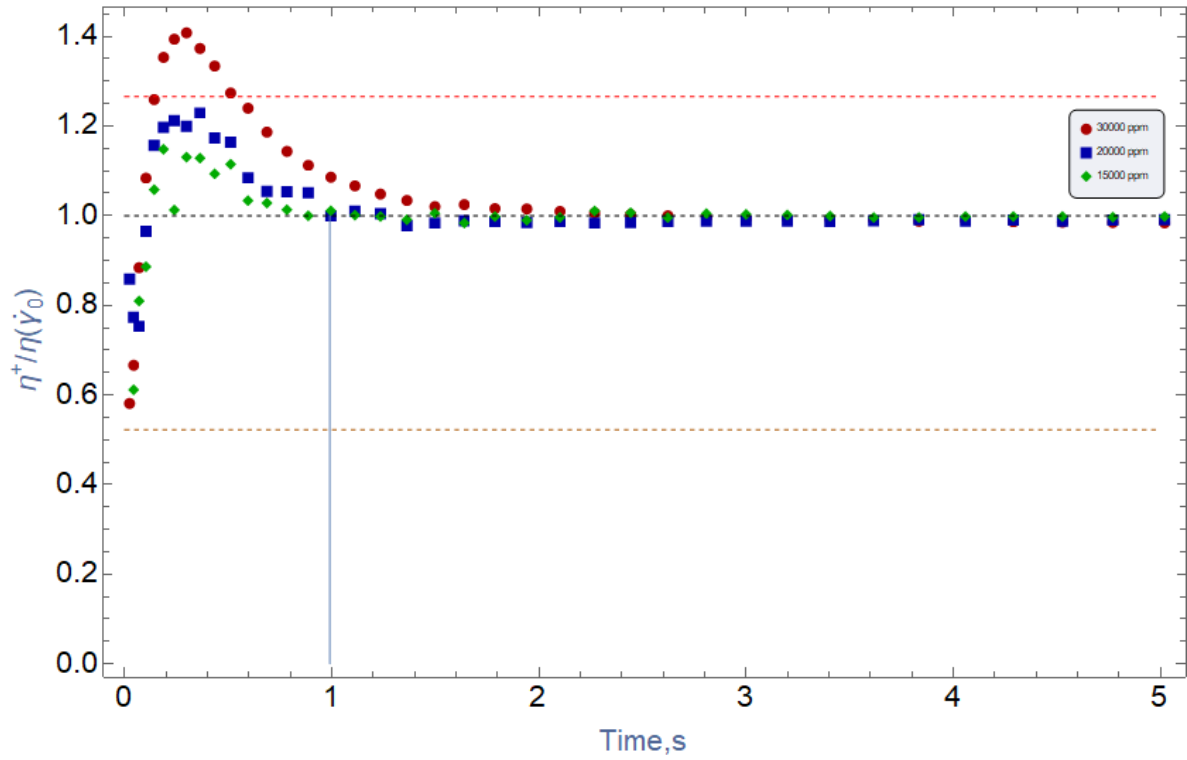


Figure 4.12. Normalized start up growth $\left(\frac{\eta^+(t, \dot{\gamma}_0)}{\eta(\dot{\gamma}_0)}\right)$ versus time (t) for shear rate $\dot{\gamma} = 10$

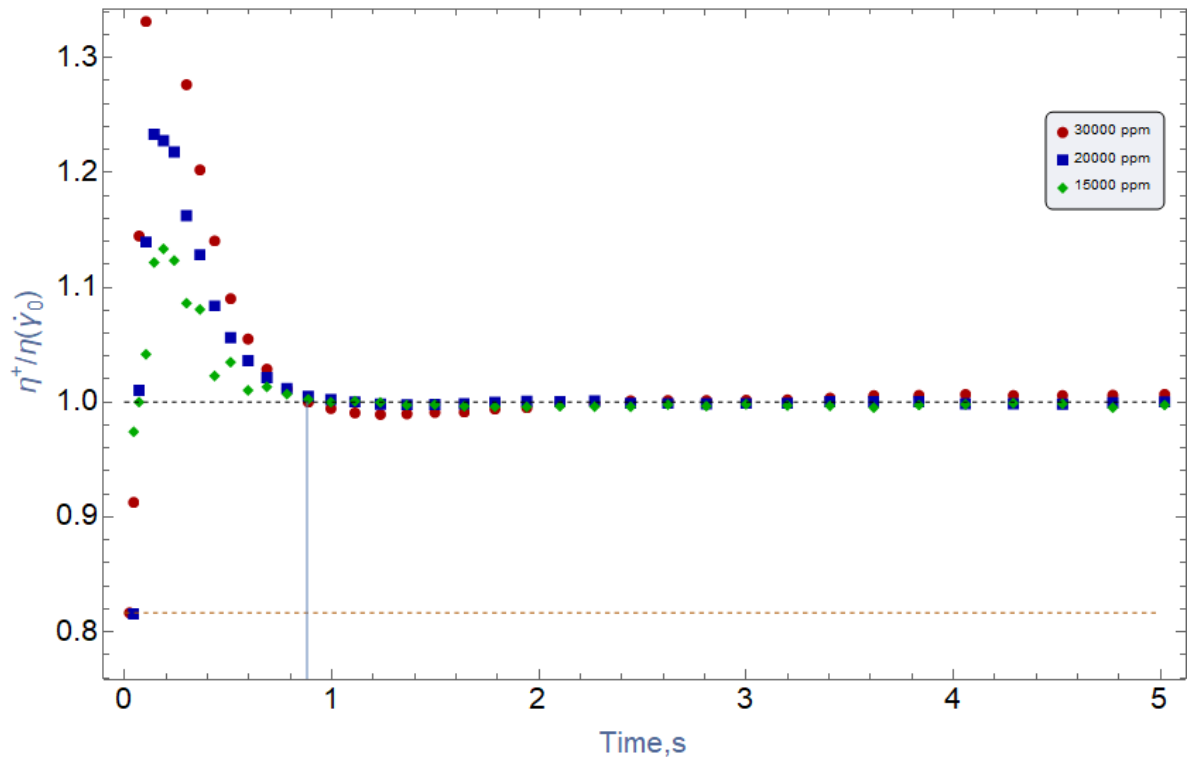


Figure 4.13. Normalized start up growth $\left(\frac{\eta^+(t, \dot{\gamma}_0)}{\eta(\dot{\gamma}_0)}\right)$ versus time (t) for shear rate $\dot{\gamma} = 20$

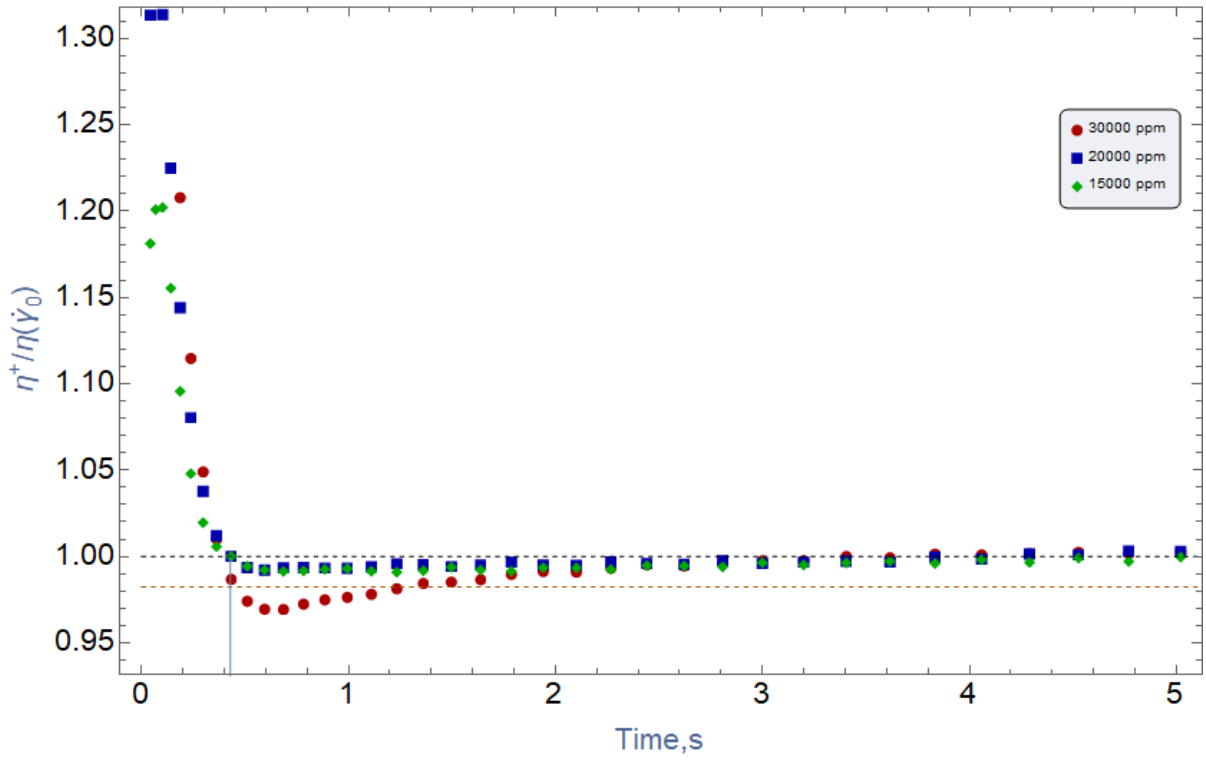


Figure 4.14. Normalized start up growth ($\frac{\eta^+(t, \dot{\gamma}_0)}{\eta(\dot{\gamma}_0)}$) versus time (t) for shear rate $\dot{\gamma} = 60$

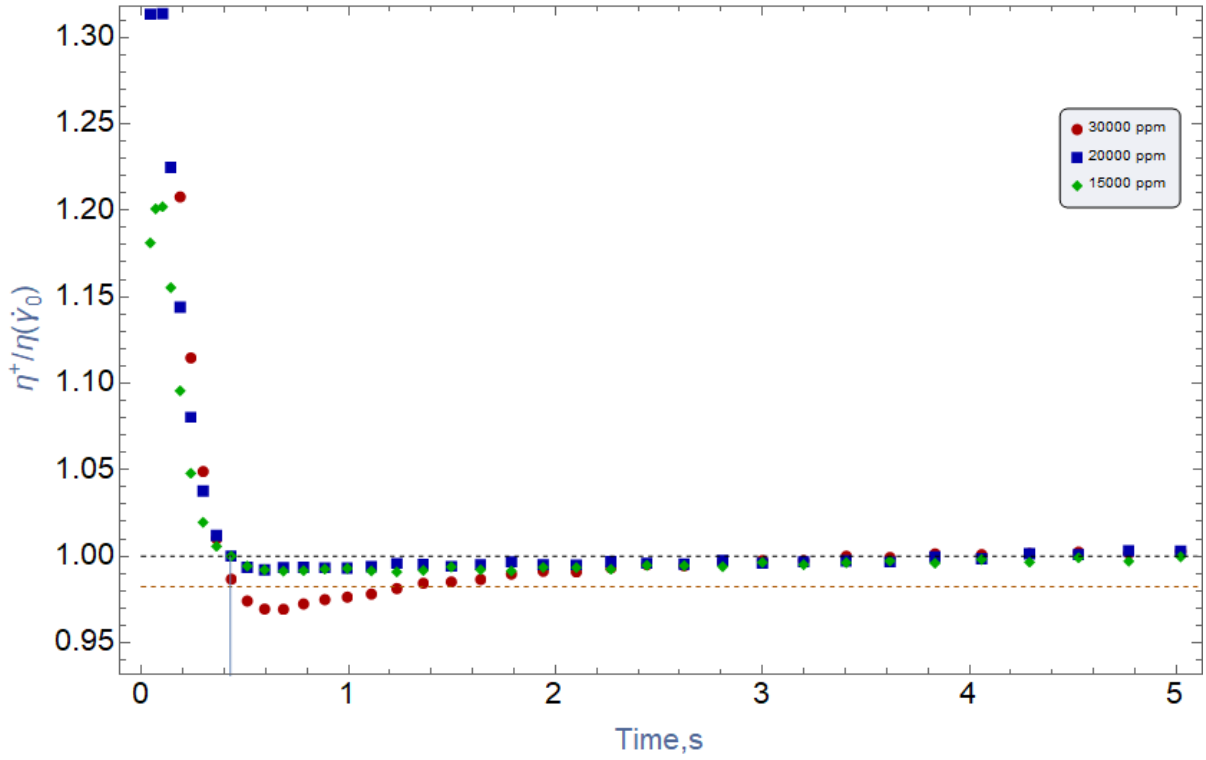


Figure 4.15. Normalized start up growth ($\frac{\eta^+(t, \dot{\gamma}_0)}{\eta(\dot{\gamma}_0)}$) versus time (t) for shear rate $\dot{\gamma} = 100$

Following impression can be made from above figures:

1. the completely similar trend is observed regarding all level of concentration for fixed initial constant shear rate. For example, both the position of overshoot relative to time and the time required to arrive at steady state value seems to be only dependent on initial shear rate and independent of concentration in fixed step-rate (some small discrepancy seen in the plot is within uncertainty) .This is the fact that was observed also by Islam in his thesis (Islam 2019) .
2. Though, there is some differences by which these three concentrations can be differentiated:
 - **Size of overshoot:**

As it is seen also from Figure 4.16, in fix initial applied shear rate (step-rate) size of overshoot is highly dependent on value of step-rate (which was already known from Bird (Bird, Curtiss et al. 1987) and concentration. In fact, size of overshoot increases with increase in concentration in monotonous fashion. So, the former hypothesis on non-monotonous dependency of the size of overshoot on the concentration, made by Islam in his thesis (Islam 2019) is not observed for HPAM polymer. In fact, he noticed some abnormal points about the dependency of overshoot size on concentration in fixed shear rate. And then he proposed the non-monotonous theory based on some chemical-based justifications. But as noted before, no abnormal point can be observed for HPAM polymer at least for three tested concentrations.
 - **Level of noise:**

It is seen that as the concentration and shear rate increase, unfavorable data (both outlier and noises) will reduce considerably. There is a simple explanation for this. When the fluid is subject to high shear rates, the stresses are also high. That makes the instrumental noise small compared to the quantities one can measure
3. in the first three diagrams (Figure 4.9 to Figure 4.11) regarding very low shear rates $\dot{\gamma} = 0.01$, $\dot{\gamma} = 0.1$ and $\dot{\gamma} = 1$ respectively, the shear stress grows monotonously toward its steady state value.
4. Then when shear rate increases up to $\dot{\gamma} = 10$ and $\dot{\gamma} = 20$ (Figure 4.12, Figure 4.13 respectively) such that it exceeds the critical shear rate (called linear viscoelastic limit), the significant deviation from linear viscoelastic envelope occurs within short time ($t < 1$ s). So, the shear stress first grows up to some maximum amount (overshoot), then it starts to reduce up to steady state value.

5. For ultimate shear rates $\gamma = 60$ and $\gamma = 100$ (Figure 4.14, Figure 4.15 respectively) it is seen that data deviate from linear envelope even in shorter period ($t < 0.5$ s) such that the increasing region toward overshoot value is almost impossible to be observed.

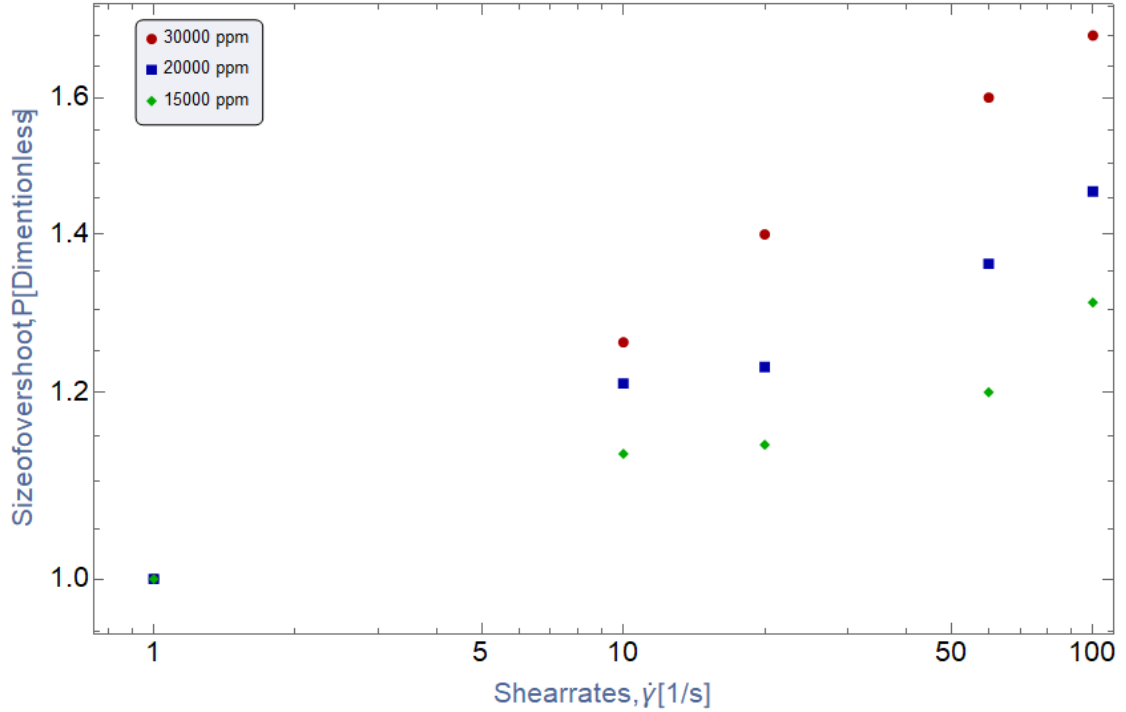


Figure 4.16. Cumulative comparison on size of overshoot regarding different initial shear rates and concentrations

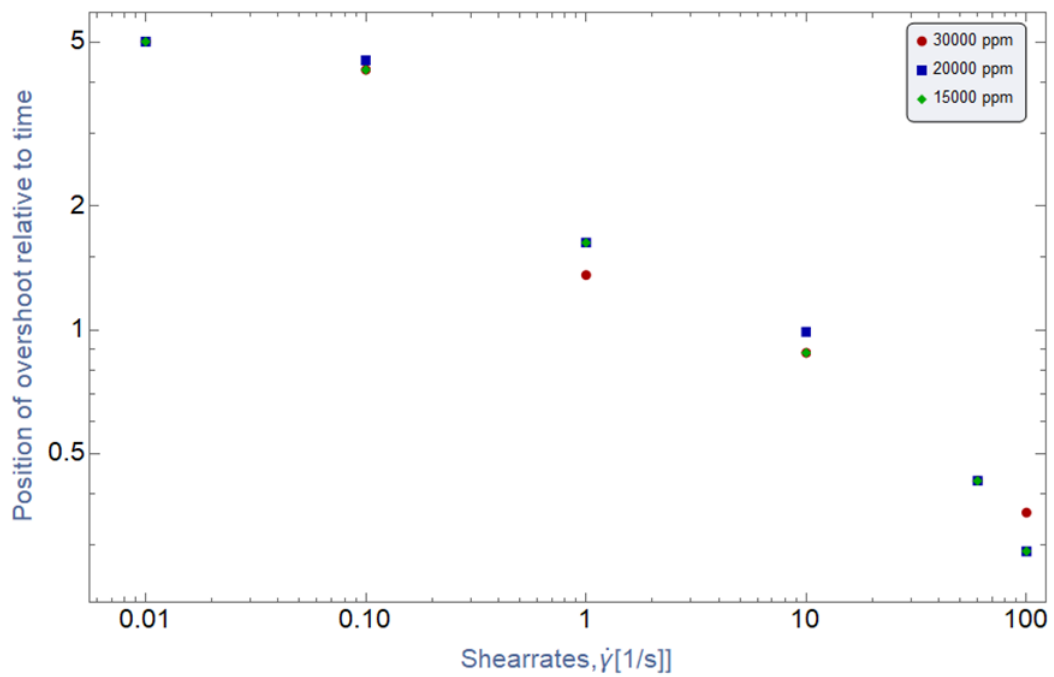


Figure 4.17. Cumulative comparison on deviation time regarding different initial shear rates and concentrations.

4.1.3 cessation of steady shear flow experiment

Here to see the effect of applying different step-rates the resulted data are first sorted based on fixed concentration regarding different applied step-rate proceed to cession, in vertical logarithmic, horizontal linear scale of axis. The data again has been normalized relative to steady state value (Figure 4.18 to Figure 4.20).

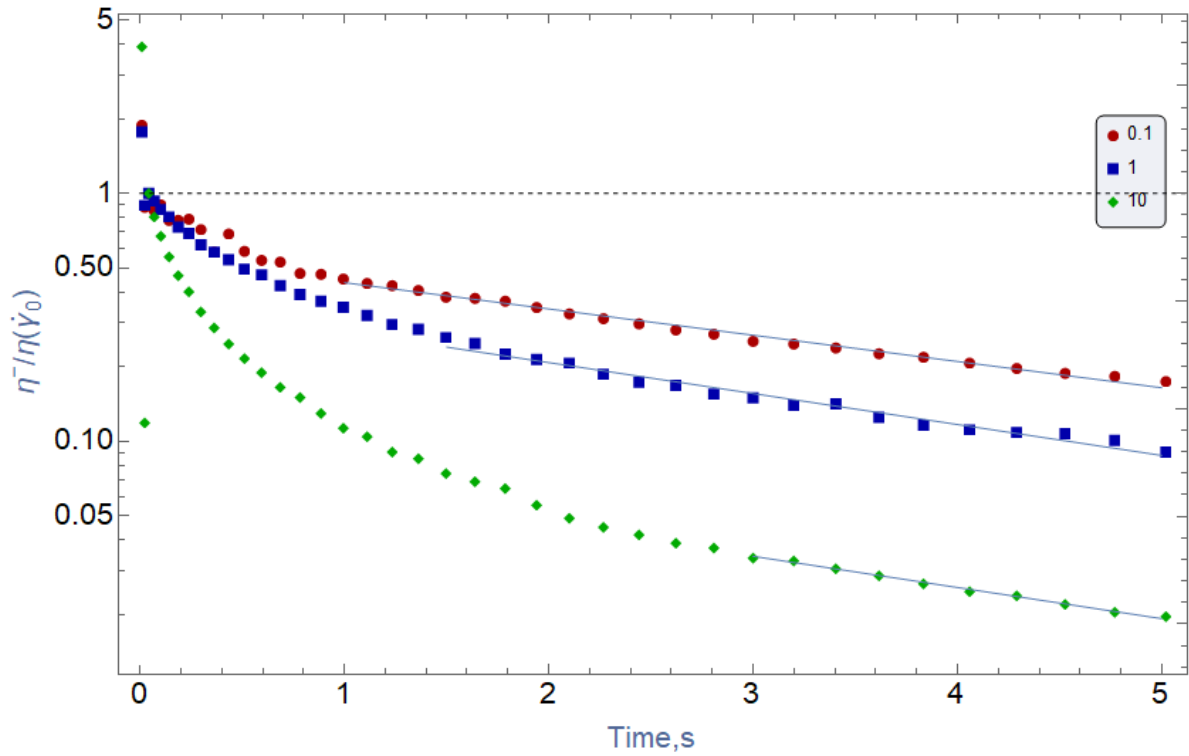


Figure 4.18. Normalized stress relaxation ($\frac{\bar{\eta}(t, \dot{\gamma}_0)}{\eta(\dot{\gamma}_0)}$) of HPAM polymer $C_c=3.10^4$ ppm versus time(t) regarding different initial shear rate before cession in log-linear scale axis.

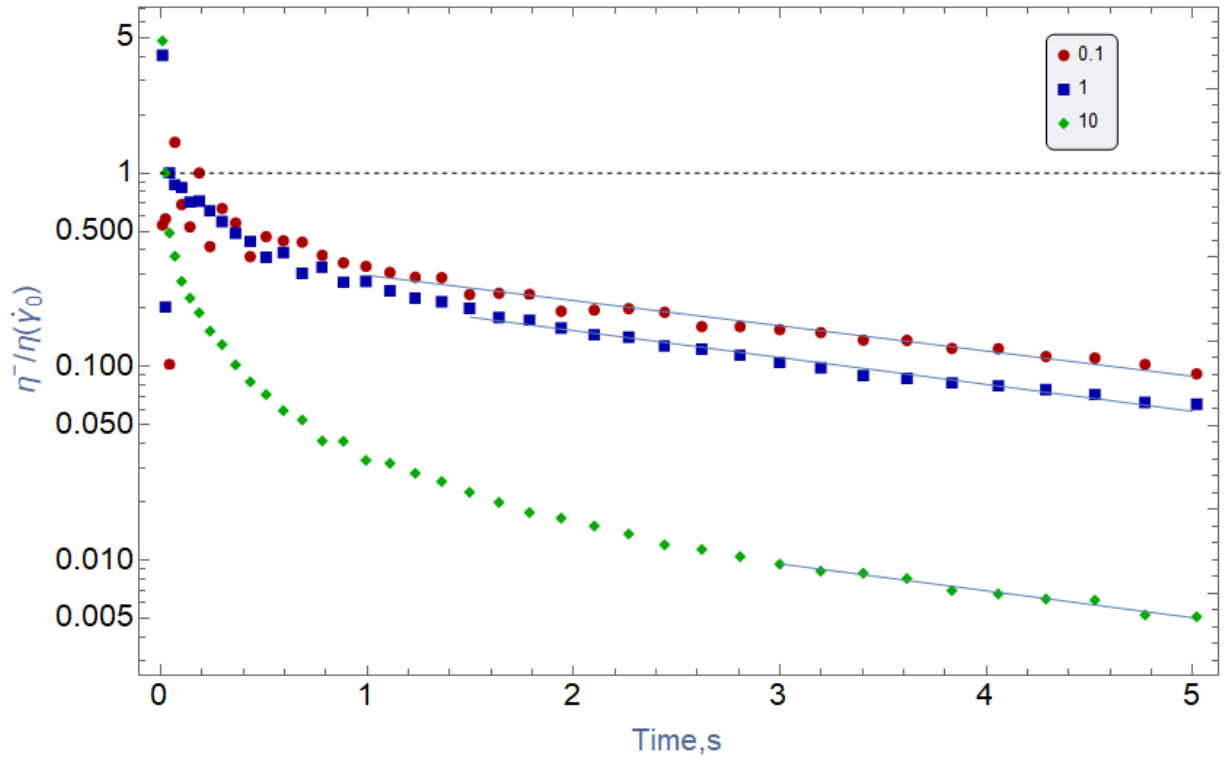


Figure 4.19. Normalized stress relaxation ($\frac{\eta^-(t,\dot{\gamma}_0)}{\eta(\dot{\gamma}_0)}$) of HPAM polymer $Cc=2.10^4$ ppm time(t) regarding different initial shear rate before cession in log-linear scale axis

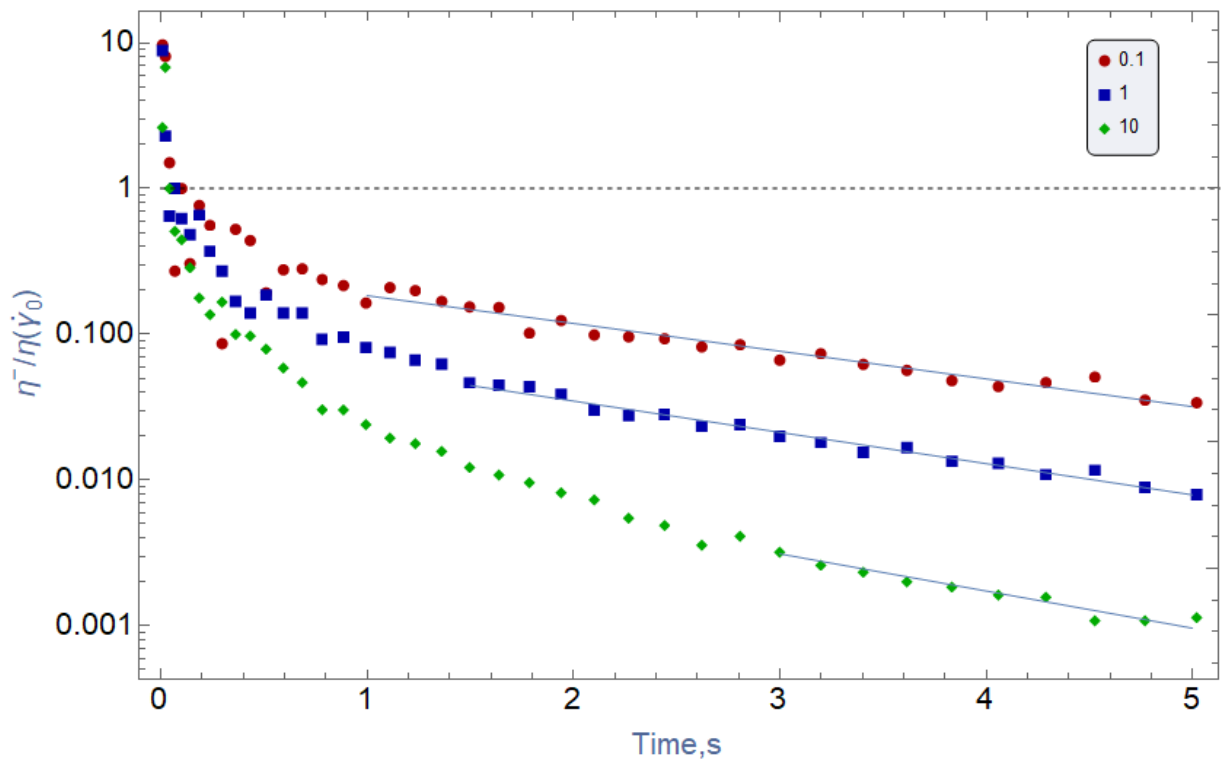


Figure 4.20. Normalized stress relaxation ($\frac{\eta^-(t,\dot{\gamma}_0)}{\eta(\dot{\gamma}_0)}$) of HPAM polymer $Cc=1.5.10^4$ ppm versus time(t) regarding different initial shear rate before cession in log-linear scale axis

Following impressions can be made from above Figure 4.18 to Figure 4.20:

1. As it was expected, in all concentration and applied shear initial shear rate, shear stress relaxes from its steady state value in monotonous fashion.
2. Though, as it was also predictable, this monotonous reduction is occurred with two different slopes in two different regions, namely “non-exponential “ region and exponential region (appears as line in the log-linear scale). In fact, shear stress data decays more rapidly in non-exponential region for early times in comparison with exponential region for late times. Moreover, the non-exponential stage of decay becomes more pronounced at higher step-rates. But in the exponential regime, the slope is almost independent of the step-rate (in Figure 4.18 to Figure 4.20 three blue lines are almost parallel).

The resulted data has been analyzed also based on initial applied shear rate before cession, in order to conduct more investigation on the effect of concentration through below Figure 4.21 to Figure 4.23 .

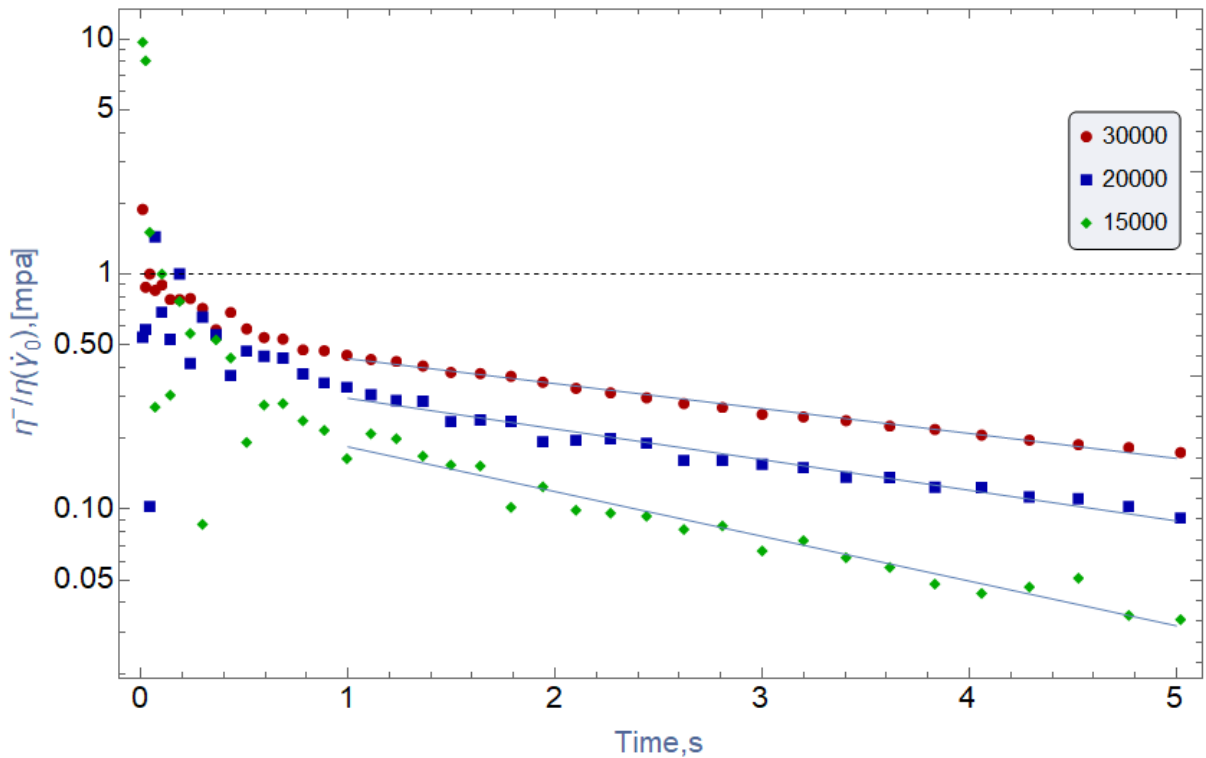


Figure 4.21. Normalized stress relaxation $\left(\frac{\eta^-(t, \dot{\gamma}_0)}{\eta(\dot{\gamma}_0)}\right)$ versus time (t) of different concentration regarding initial shear rate ($\dot{\gamma} = 0.1$)

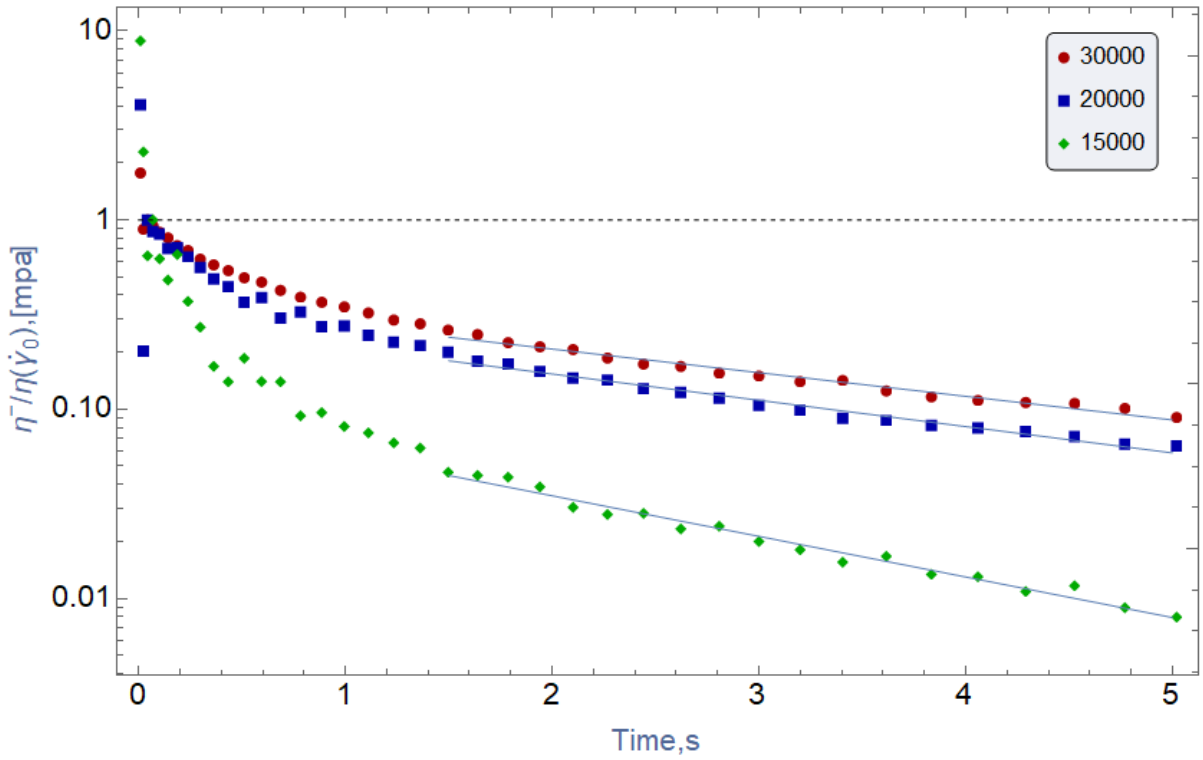


Figure 4.22. Normalized stress relaxation $\frac{\eta^-(t, \dot{\gamma}_0)}{\eta(\dot{\gamma}_0)}$ versus time (t) of different concentration regarding initial shear rate ($\dot{\gamma} = 1$)

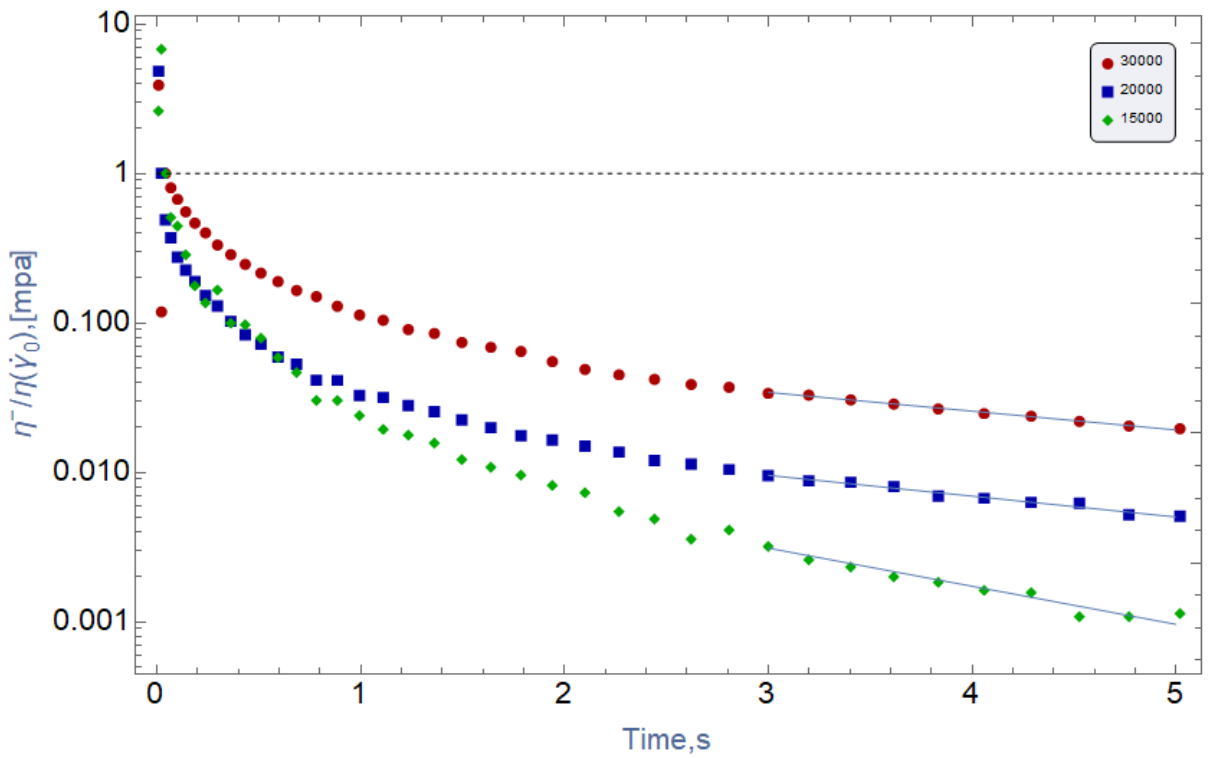


Figure 4.23. Normalized stress relaxation $\frac{\eta^-(t, \dot{\gamma}_0)}{\eta(\dot{\gamma}_0)}$ versus time (t) of different concentration regarding initial shear rate ($\dot{\gamma} = 10$)

So, it is observed that again all concentrations experience similar trends of reduction from initial steady state value in monotonous fashion (faster at non-exponential region in early time and slower in exponential region in late time).It is also seen that as the dilution increases the relaxation accelerates in non-exponential region. So again ,the non-monotonous dependency of the slope of non-exponential region decay proposed by Islam (Islam 2019) is not observed for HPAM polymer at least for three tested concentrations since in all step-rates the non-exponential decay accelerates with decrease in concentration without any abnormally.

Though, again almost parallel blue lines in figures clearly shows that the slope of reduction is independent of concentration in exponential region. This was also observed by Islam in his thesis(Islam 2019)

The below Figure 4.24 is cumulative result of Figure 4.18 to Figure 2.22 regarding the slope of exponential reduction which shows how the slope of reduction in this region is almost independent of step-rates and concentration (the small level of differences seen in diagrams is only due to some uncertainties and measurement errors)

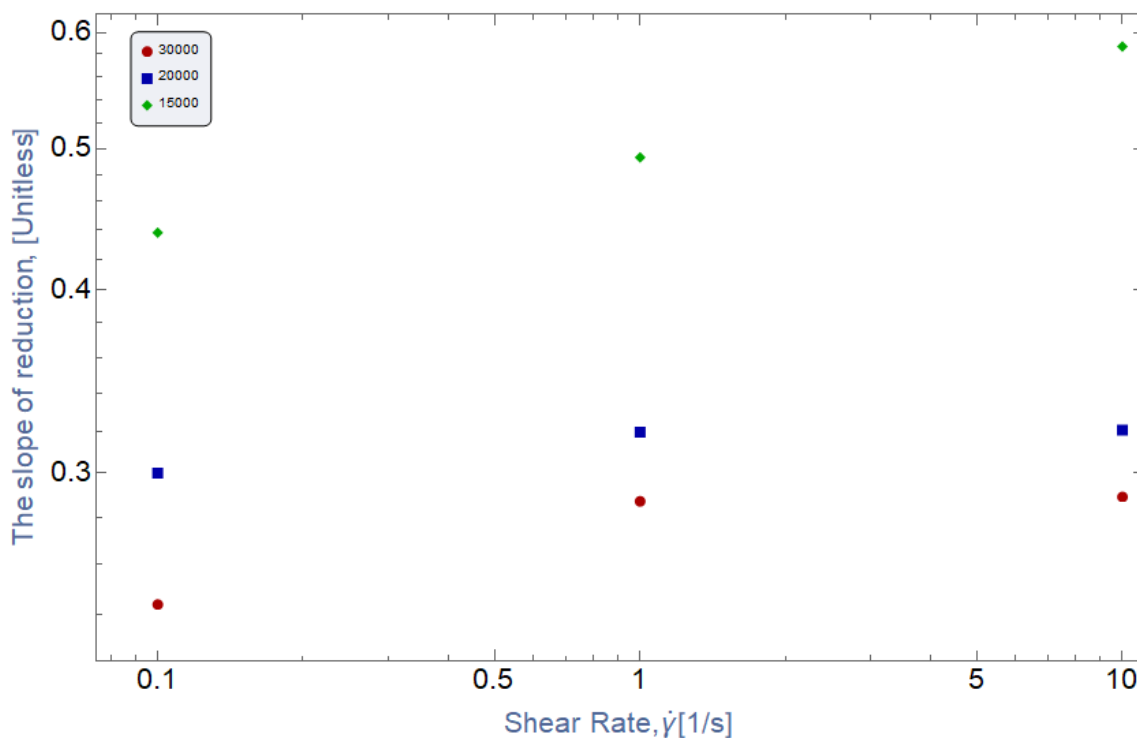


Figure 4.24. Cumulative result of slope of reduction in exponential region

4.2 Data analysis with considering physical model

At this stage of this research the data is fitted to physical models (affine LPPT, full LPPT, affine EPPT, FENE-P and C-FENE-P) to obtain best representative model for HPAM polymer. It is worth to mention that first the analytical or numerical solution of models were coded in Mathematica software and then data fitting conducted.

Data fitting approach

In following we will show the importance of the approach by which real data is fitted to model. There were two approach by which real data could fitted to model summarized below.

First approach:

First, the master curve of dimensionless viscosity versus dimensionless shear rate data ($\dot{\gamma}_D$) is fitted in shear ramping test to obtain the "appropriate" converting coefficient (C_{convert}) exactly like what was shown in Figure 2.28 and Figure 2.35. The terms "appropriate" implies the C_{convert} value by which perfect possible math is obtained between data and model. Then as it was shown in chapter 2 in equations 2.43 and 2.53 this C_{convert} equals to some products of b and λ_0 or ε and λ_e based on model. On the other hand, as it was also discussed in chapter two, according to theory, model parameter λ for affine LPPT, can be gained from the slope of exponential region that was obtained from relaxation test based on equation 2.57. Hence other model parameter (ε for affine LPPT) would automatically yields. Now one has all model parameters that is required for data fitting of both start-up and cessation of steady shear rate test in numerical and analytical solution coded in Mathematica. One should also remember that even if getting perfect math of dimensionless viscosity versus dimensionless shear rate (wi) data in shear ramping test does not necessarily mean that the model is representative, but whole picture included start-up and relaxation test result should be taken into account to recognize the best model for describing HPAM polymer in different level of concentrations $C_c=3.10^4$ ppm, $C_c=2.10^4$ ppm and $C_c=1.5.10^4$ ppm. On the contrast, by getting unfavorable result (C_{convert}) regarding data fitting of shear ramping test one can conclude on relative failure of the model for transient flow (start-up and cessation of steady shear flow).

- **Second approach:**

First the dimensionless viscosity versus dimensionless shear rate ($\dot{\gamma}_D$) curve is fitted with model to obtain converting coefficient (C_{convert}) exactly like first approach. This coefficient would establish relaxation between λ and ε , or λ_Q and b , depending on the model. So, specifying one of these parameters will automatically yield the other. The established relation is coded in Mathematica and that will give the **function (not solid number)** which relates model parameters (take λ as function of ε , as an example). Then for example model parameter ε in affine LPPT model is fitted in “dynamic ways” in Mathematica software which also changes λ accordingly such that both start-up and cessation curves are fitted **simultaneously**. Here “dynamic” implies the command in Mathematica (called manipulate) software coding which allows us to change parameters as much as it is favorable.

So, the major difference in second approach is dynamic model parameter (like ε and λ) which has been related to each other based on **function** ($\lambda(\varepsilon)$ or $\varepsilon(\lambda)$) instead of relying on solid (**constant and not changeable**) parameters (like λ) based on the slope of exponential decay of cessation of steady shear rate test in first approach. Moreover, as mentioned earlier, this would allow us to conduct best possible model fitting in start-up and relaxation simultaneously. One also should bear in mind that to reach the best possible fit, first shear ramping fitting must be precise, then the stress growth and overshoot magnitude must be as accurate as possible, and the stress relaxation is desired to be accurate at least in the start of decay.

4.2.1.1 Viscosity data fitting using full LPPT

In below dimensionless viscosity ($\frac{\eta}{\eta_0}$) versus dimensionless shear rate ($\lambda\dot{\gamma}$) data is fitted relative to full LPPT to obtain appropriate converting coefficient (C_{convert}) for HPAM polymer $C_c=3.10^4$ ppm, $C_c=2.10^4$ ppm and $C_c=1.5 \cdot 10^4$ ppm.

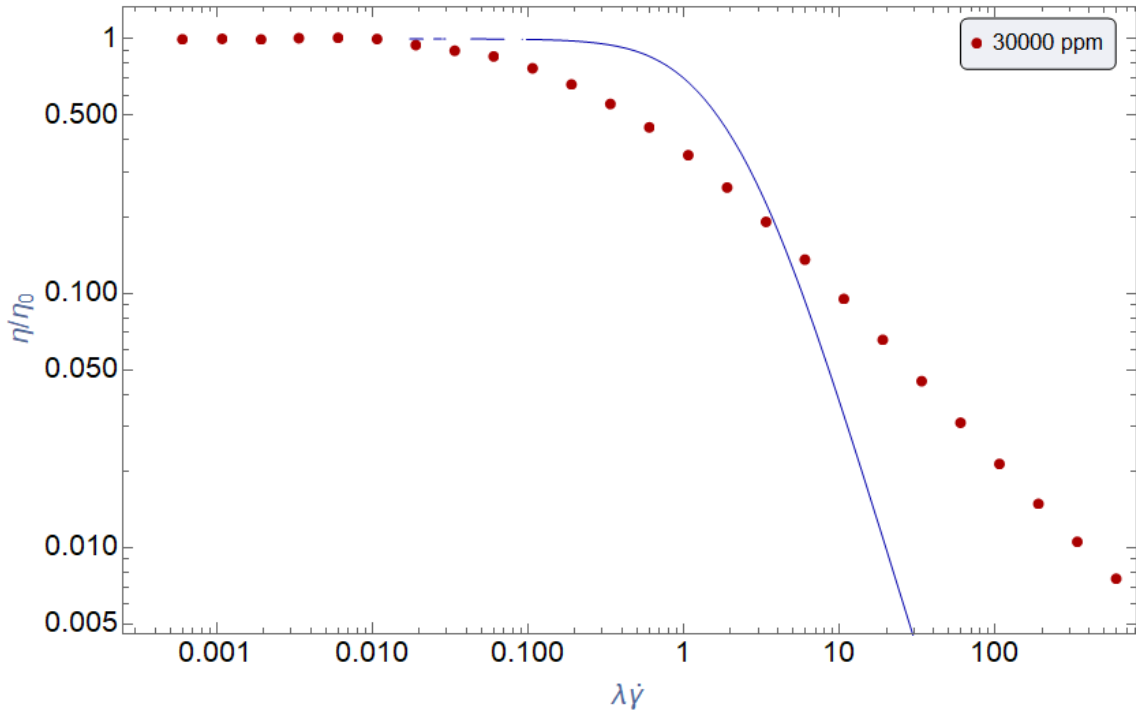


Figure 4.25. Dimensionless viscosity ($\frac{\eta}{\eta_0}$) versus dimensionless shear rate ($\lambda\dot{\gamma}$) is fitted to full LPPT model (shown with blue curve) for $Cc=3 \cdot 10^4$ ppm HPAM polymer solution

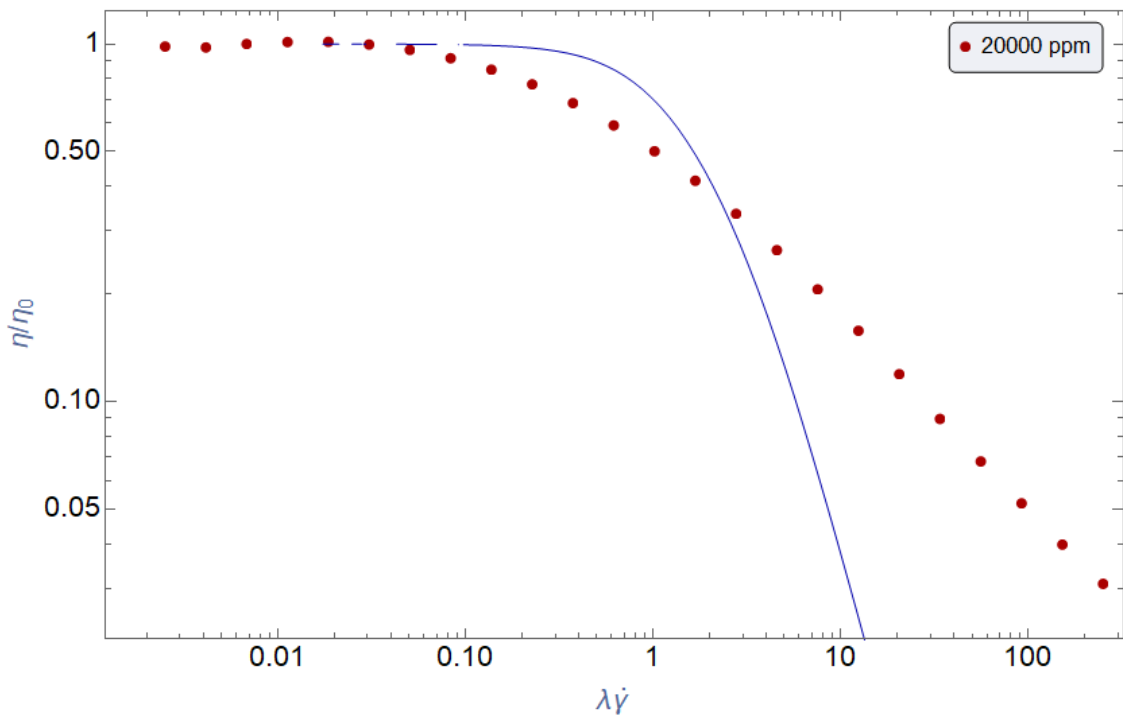


Figure 4.26. Dimensionless viscosity ($\frac{\eta}{\eta_0}$) versus dimensionless shear rate ($\lambda\dot{\gamma}$) is fitted to full LPPT model (shown with blue curve) for $Cc=2 \cdot 10^4$ ppm HPAM polymer solution

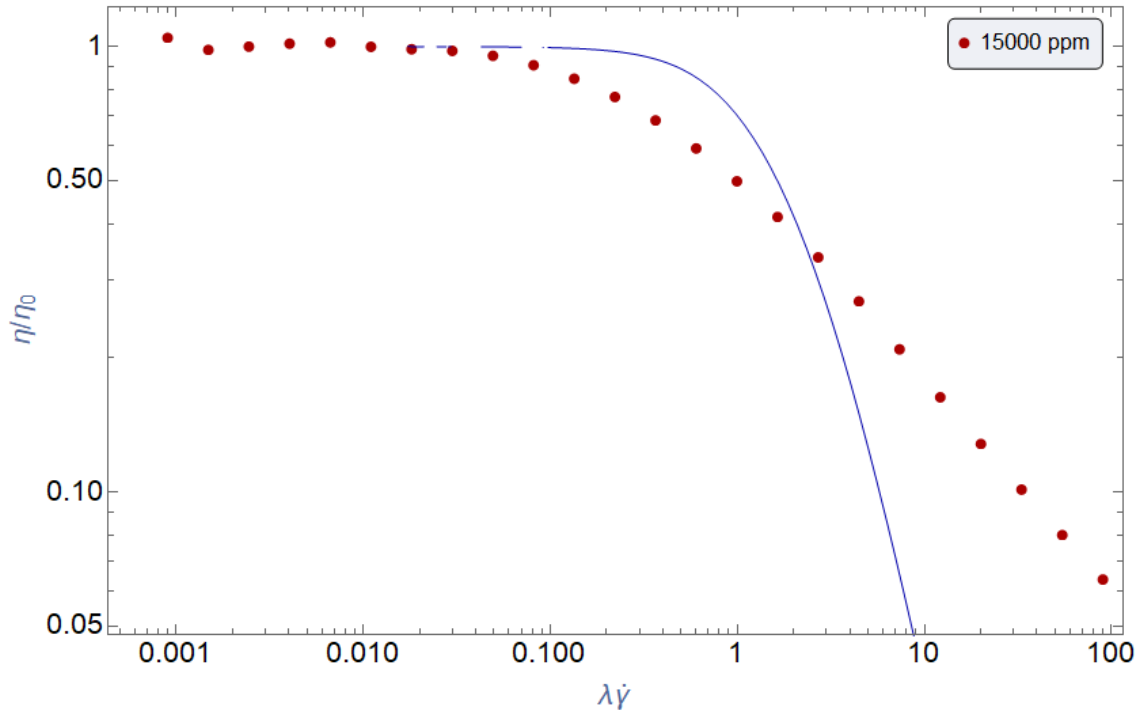


Figure 4.27. Dimensionless viscosity ($\frac{\eta}{\eta_0}$) versus dimensionless shear rate ($\lambda\dot{\gamma}$) is fitted to full LPPT model (shown with blue curve) for $Cc=1.5 \cdot 10^4$ ppm HPAM polymer solution

As it is seen from the figures the large divergence between real data and full LPPPT model is seen for all tested concentration of HPAM polymer .So even it is difficult to obtain appropriate converting coefficient (C_{convert}) that provide math between dimensionless viscosity ($\frac{\eta}{\eta_0}$) and dimensionless shear rate ($\dot{\gamma}_D = \lambda\dot{\gamma}$) for this model. Hence, this model is not recognized as representative model such that no further analysis is required to be conducted in startup and relaxation test for this model for all three tested concentrations.

4.2.1.2 Viscosity data fitting using affine LPPT

As noted in literature review chapter PPT model and FENE-P model are so similar that affine version of LPPT model data fitting is also representative for FENE-P model at least for shear ramping test. Here the figures are based on affine LPPT model parameters ,for parameter conversion one refer to equation 2.54, 2.55, 2.56 noted in part 2.6.2.5.

In below the dimensionless viscosity ($\frac{\eta}{\eta_0}$) versus dimensionless shear rate ($\dot{\gamma}_D$) is fitted relative to affine LPPT model (which is also valid for FENE-P model at least for steady flow) to obtain appropriate dimensionless converting coefficient (C_{convert}) defined by equations 2.43 and 2.53 for affine LPPT and FENE-P model respectively) for HPAM polymer $Cc=3 \cdot 10^4$ ppm, $Cc=2 \cdot 10^4$

ppm and $Cc=1.5 \cdot 10^4$ ppm. It is also worth to mention that LPPT (and also FENE-P one) model predicts dimensionless viscosity versus dimensionless shear rate based on equation 32 of Dmitry Shogin and Amundsen most recent article (Shogin 2020) and so Mathematica code for showing model was written based on it accordingly.

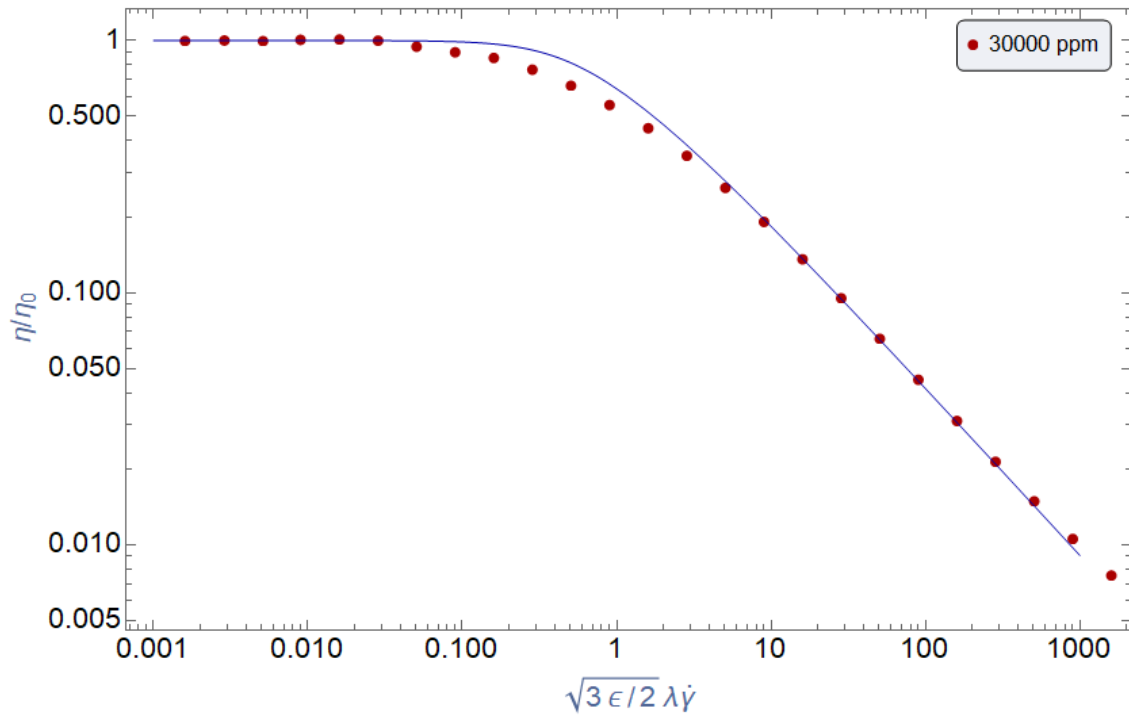


Figure 4.28. dimensionless viscosity ($\frac{\eta}{\eta_0}$) versus dimensionless shear rate ($\sqrt{\frac{3\epsilon}{2}} \lambda \dot{\gamma}$) is fitted to affine LPPT mode (shown with blue curve) for HPAM polymer $Cc=3 \cdot 10^4$ ppm

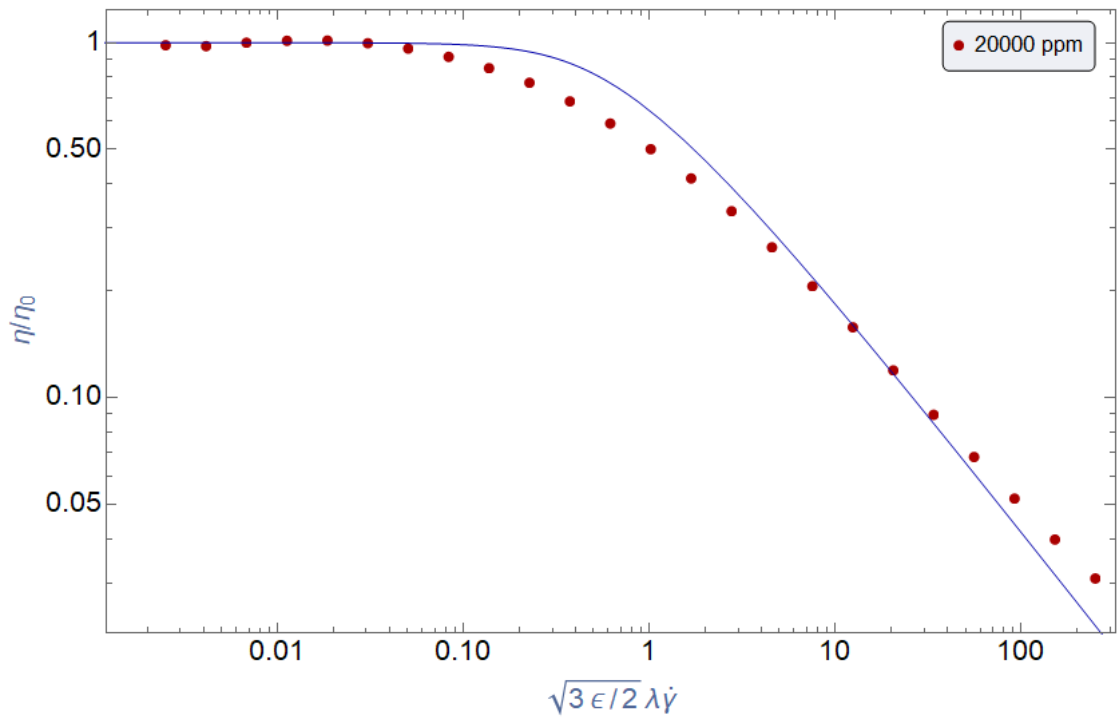


Figure 4.29. dimensionless viscosity ($\frac{\eta}{\eta_0}$) versus dimensionless shear rate ($\sqrt{\frac{3\epsilon}{2}} \lambda \dot{\gamma}$) for HPAM polymer $Cc=2.10^4$ ppm

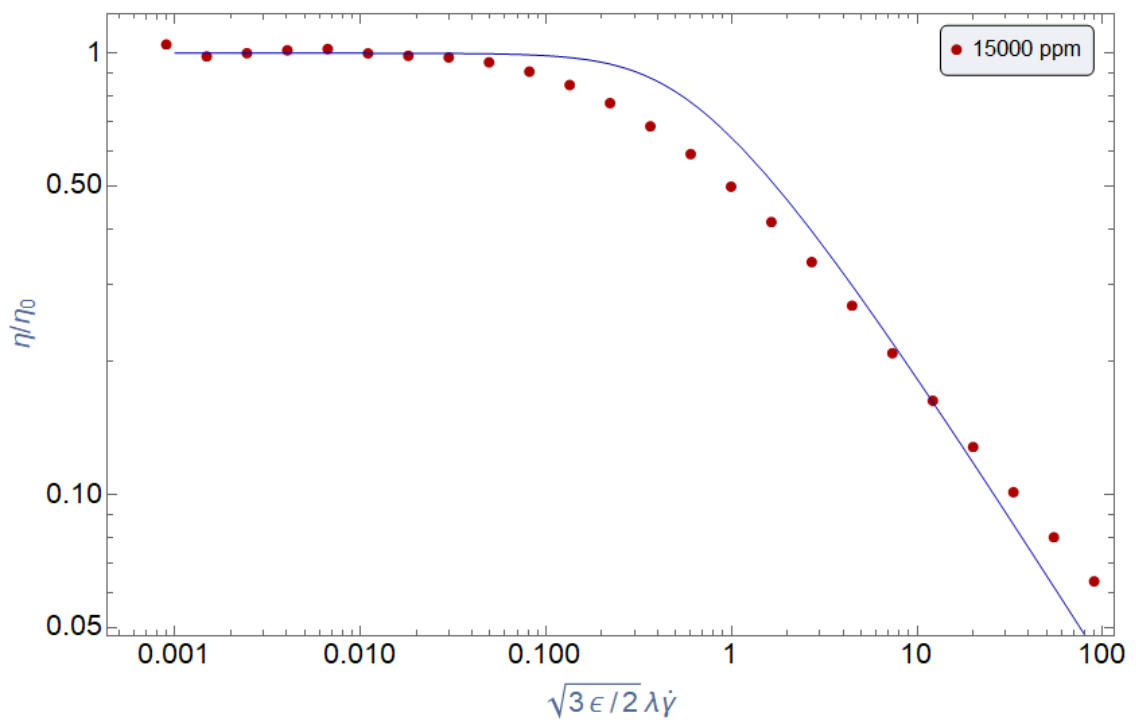


Figure 4.30. dimensionless viscosity ($\frac{\eta}{\eta_0}$) versus dimensionless shear rate ($\sqrt{\frac{3\epsilon}{2}} \lambda \dot{\gamma}$) is fitted to affine LPPT mode (shown with blue curve) for HPAM polymer $Cc=1.5.10^4$ ppm

So, the appropriate converting factor (C_{convert}) for affine LPPT model (which is also valid for FENE-P model) is determined via dynamic diagrams in Mathematica software as $C_{\text{convert}} = 1.72$, $C_{\text{convert}} = 0.25$ and $C_{\text{convert}} = 0.09$ for HPAM polymer $C_c = 3 \cdot 10^4$ ppm, $C_c = 2 \cdot 10^4$ ppm and $C_c = 1.5 \cdot 10^4$ ppm. These coefficients will be used further in start-up and relaxation test to see whether this model is representative. Moreover, as the obtained coefficient for $C_c = 2 \cdot 10^4$ ppm and $C_c = 1.5 \cdot 10^4$ ppm (0.25, 0.09 respectively) are so small both affine LPPT model and FENE-P model are not valid for further analysis of startup and relaxation of these two concentrations.

4.2.1.3 Viscosity data fitting using affine exponential PPT(EPPT)

In below dimensionless viscosity ($\frac{\eta}{\eta_0}$) versus dimensionless shear rate ($2\sqrt{\varepsilon}\lambda\dot{\gamma}$) is fitted relative to affine EPPT to obtain appropriate converting coefficient ($C_{\text{convert}} = 2\sqrt{\varepsilon}\lambda$) for HPAM polymer $C_c = 3 \cdot 10^4$ ppm, $C_c = 2 \cdot 10^4$ ppm and $C_c = 1.5 \cdot 10^4$ ppm.

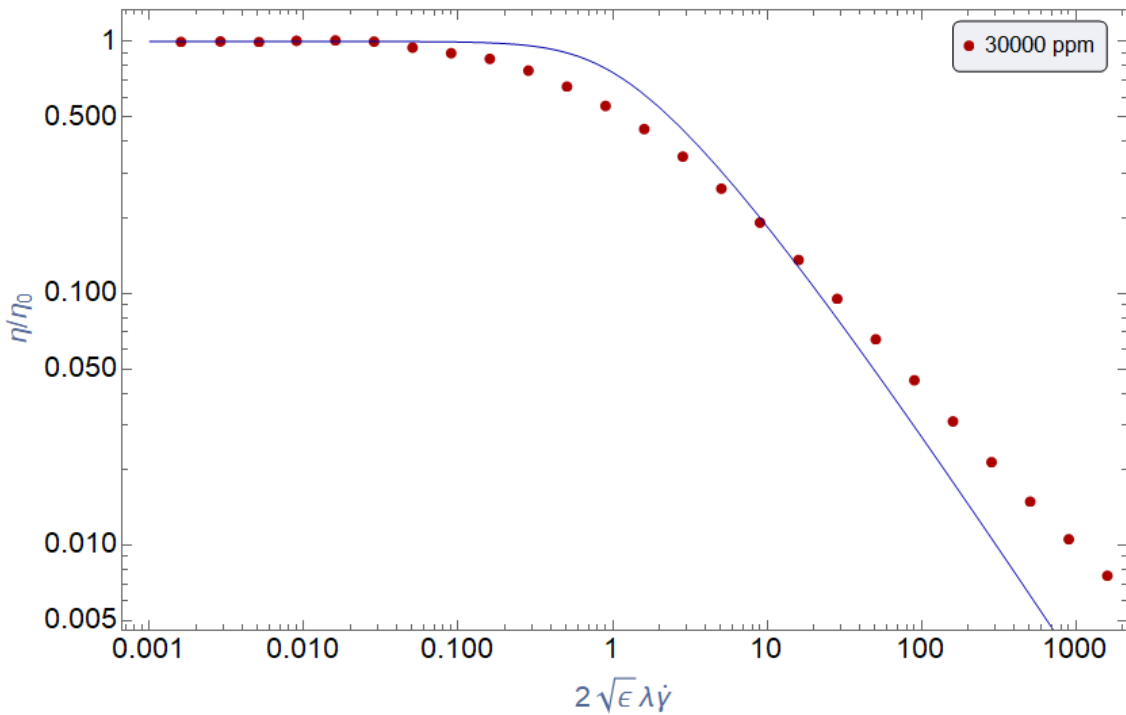


Figure 4.31. dimensionless viscosity ($\frac{\eta}{\eta_0}$) versus dimensionless shear rate ($2\sqrt{\varepsilon}\lambda\dot{\gamma}$) is fitted to affine EPPT mode (shown with blue curve) for HPAM $C_c = 3 \cdot 10^4$ ppm

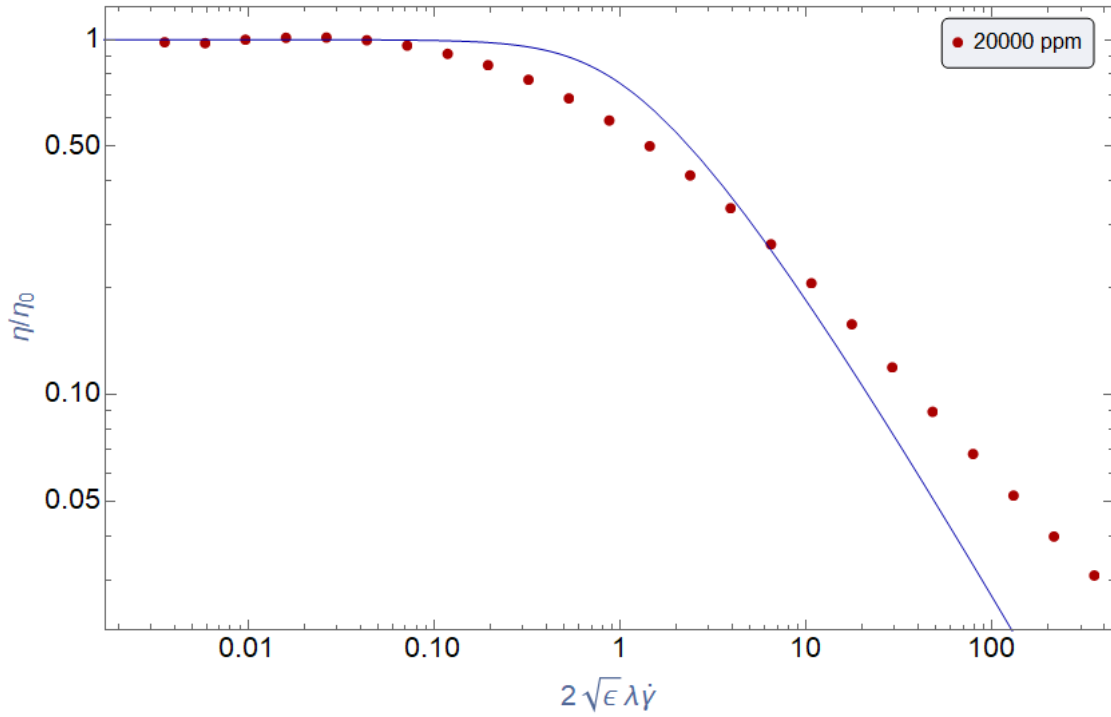


Figure 4.32. dimensionless viscosity ($\frac{\eta}{\eta_0}$) versus dimensionless shear rate ($2\sqrt{\epsilon}\lambda\dot{\gamma}$) is fitted to affine EPPT mode (shown with blue curve) for HPAM polymer $Cc=2.10^4$ ppm

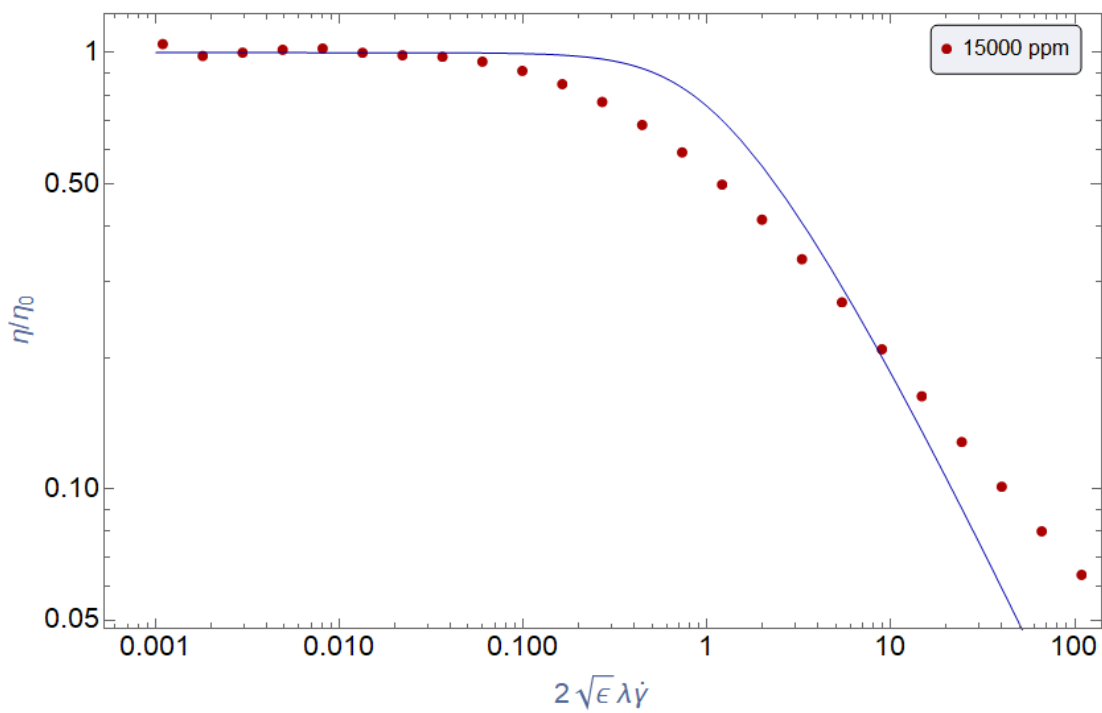


Figure 4.33. dimensionless viscosity ($\frac{\eta}{\eta_0}$) versus dimensionless shear rate ($2\sqrt{\epsilon}\lambda\dot{\gamma}$) is fitted to affine EPPT mode (shown with blue curve) for HPAM polymer $Cc=1.5.10^4$ ppm for HPAM

So, the appropriate coefficient (C_{convert}) for affine EPPT model is determined via dynamic diagrams as $C_{\text{convert}}=1.1$, $C_{\text{convert}}=0.25$ and $C_{\text{convert}}=0.09$ for HPAM polymer $C_c=3.10^4$ ppm, $C_c=2.10^4$ ppm and $C_c=1.5 \cdot 10^4$ ppm. Moreover, no further analysis was conducted for this model for transient flow due to the relatively large gap between model and data and unfavorable obtained converting factors (C_{convert}) for all level of tested concentrations. Moreover power-law slope of data is not well-described by the polylogarithmic shear-thinning of the EPTT model.

4.2.1.4 Viscosity data fitting using affine C-FENE-P model

In below dimensionless viscosity ($\frac{\eta}{\eta_0}$) versus dimensionless shear rate ($\lambda_Q \dot{\gamma}$) is fitted relative to C-FENE-P model to obtain appropriate converting factor ($C_{\text{convert}} = \lambda_Q$) for HPAM polymer $C_c=3.10^4$ ppm, $C_c=2.10^4$ ppm and $C_c=1.5 \cdot 10^4$ ppm respectively. But here our data fitting approach is somehow different from other models since there are three parameters to be adjusted (E , b , λ_Q) for C-FENE-P model. So, E and b is determined based on guess and then appropriate converting factor ($C_{\text{convert}} = \lambda_Q$) is gained based on best possible fit.

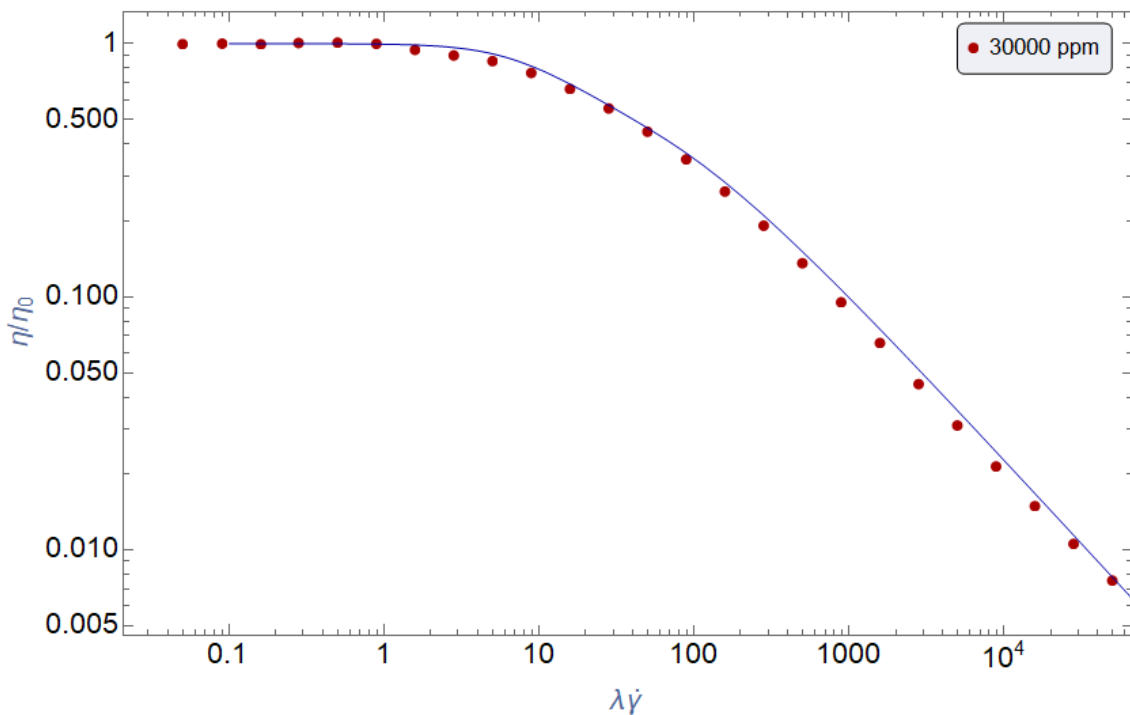


Figure 4.34. dimensionless viscosity ($\frac{\eta}{\eta_0}$) versus dimensionless shear rate ($\lambda\dot{\gamma}$) is fitted to C-FENE-P model (shown with blue curve) for HPAM polymer $C_c=3.10^4$ ppm

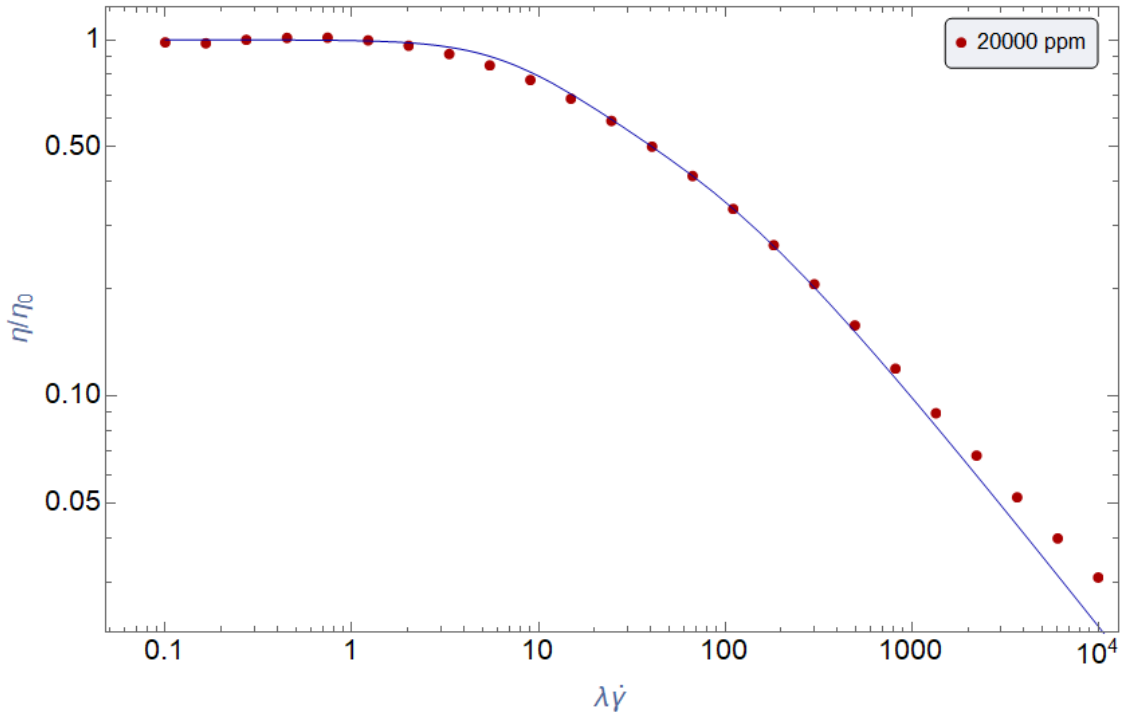


Figure 4.35. dimensionless viscosity ($\frac{\eta}{\eta_0}$) versus dimensionless shear rate ($\lambda\dot{\gamma}$) is fitted to C-FENE-P model (shown with blue curve) for HPAM polymer $Cc=2.10^4$ ppm

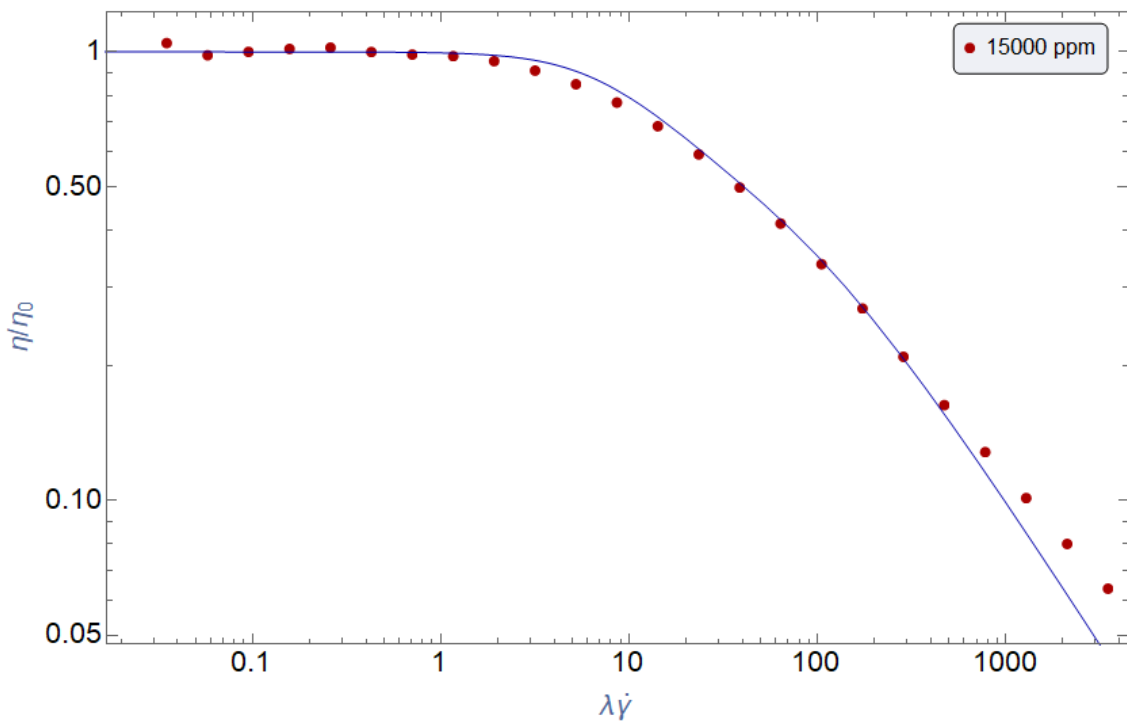


Figure 4.36. Dimensionless viscosity ($\frac{\eta}{\eta_0}$) versus dimensionless shear rate ($\lambda\dot{\gamma}$) is fitted to C-FENE-P model (shown with blue curve) for HPAM polymer $Cc=1.5.10^4$ ppm)

Hence, the appropriate converting coefficient (C_{convert}) for C-FENE-P model is determined via dynamic diagrams as $\lambda_Q=50$, $\lambda_Q=10$ and $\lambda_Q=3$ for HPAM polymer sample $C_c=3.10^4$ ppm, $C_c=2.10^4$ ppm and $C_c=1.5 \cdot 10^4$ ppm respectively, based on guessed E and b as order of $E=1$ and $b=50$. These coefficients will be used further in start-up and relaxation test to see whether this model is representative. Moreover, as it is appearing in the figures there is almost perfect match between experimental data and C-FENE-P model, though one may notice deviations at higher shear rates. In fact, it is observed that the experimental curves "bending up": this is due to a gradually developing flow instability. The shear rate becomes so high that it becomes impossible to maintain steady shear flow in the device. The experimental data from this region cannot be relied upon. Hence the deviation of experimental data from model at very high shear rate is due to measurement error rather than inaccuracy of model prediction.

4.2.2 Startup and relaxation of steady shear flow experiment

4.2.2.1 Startup and relaxation of steady shear flow data fitting with affine LPPT model

- **First approach**

As it was mentioned the model parameter λ is determined based on the slope of exponential decay in cessation of shear steady test (m_{relax}) in this approach. This slope was already known as $m_{\text{relax}} = -0.26$ from cessation of shear steady test, and consequently model parameter λ was calculated as a $\lambda = 3.84$ based on equation 2.57 in chapter 2. Then the product of λ and ε was also known from converting factor (C_{convert}) that was obtained from shear ramping test in last section ($C_{\text{convert}} = 1.72$). Hence, other model parameter (ε) is easily obtained as order of $\varepsilon = 0.13$ based on equation 2.53 in chapter 2 and Weissenberg number ($wi = \lambda \dot{\gamma}$) order of $wi = 0.384$, $wi = 3.84$ and $wi = 38.4$. In the following dimensionless shear stress growth of Startup of steady shear flow ($\frac{\eta^+(t, \dot{\gamma}_0)}{\eta(\dot{\gamma}_0)}$) versus time (t) and dimensionless shear stress relaxation of cessation of steady shear flow ($\frac{\eta^-(t, \dot{\gamma}_0)}{\eta(\dot{\gamma}_0)}$) versus time(t) is fitted with affine LPPT model, for HPAM polymer $C_c = 3.10^4$ ppm with first approach.

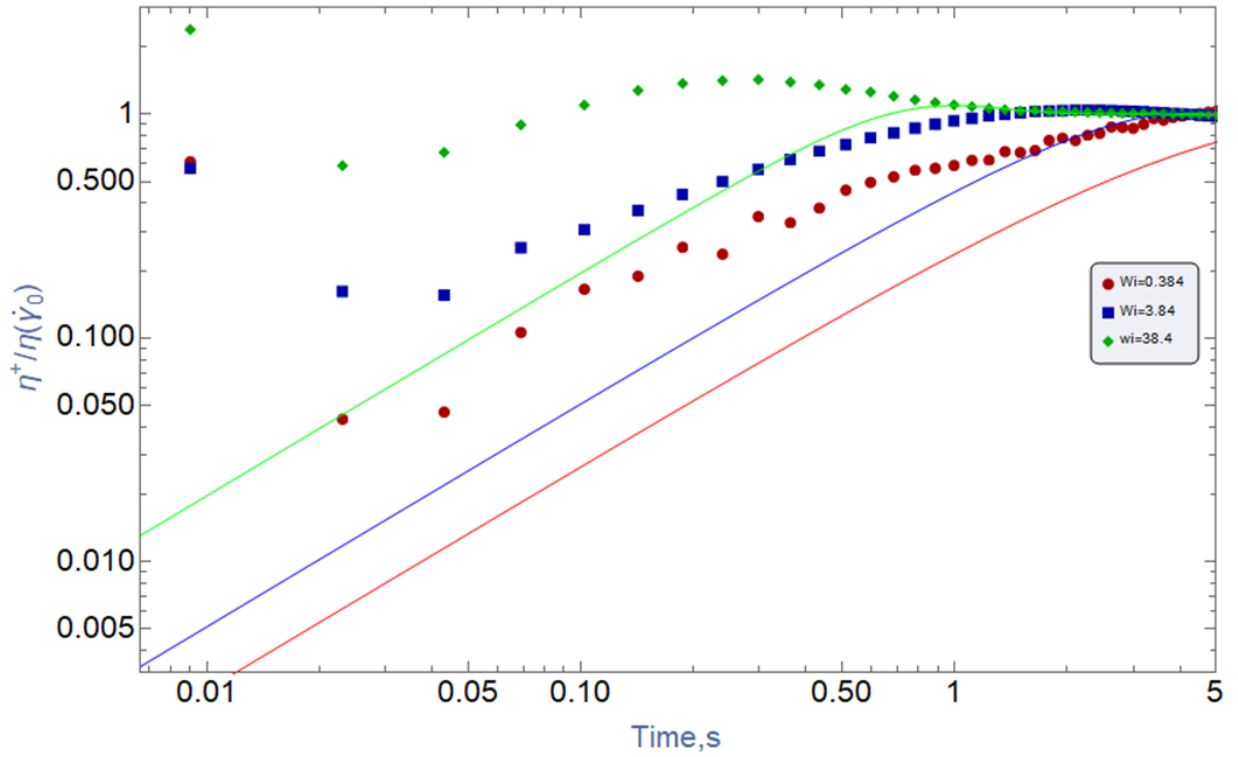


Figure 4.37. The dimensionless shear stress growth of Startup of steady shear flow ($\frac{\eta^+(t, \dot{\gamma}_0)}{\eta(\dot{\gamma}_0)}$) versus time (t) is fitted with first approach relative to affine PPT model (red, blue, green curve), for HPAM polymer $Cc = 3 \cdot 10^4$ ppm, of $wi=0.384$, $wi=3.84$ and $wi=38.4$

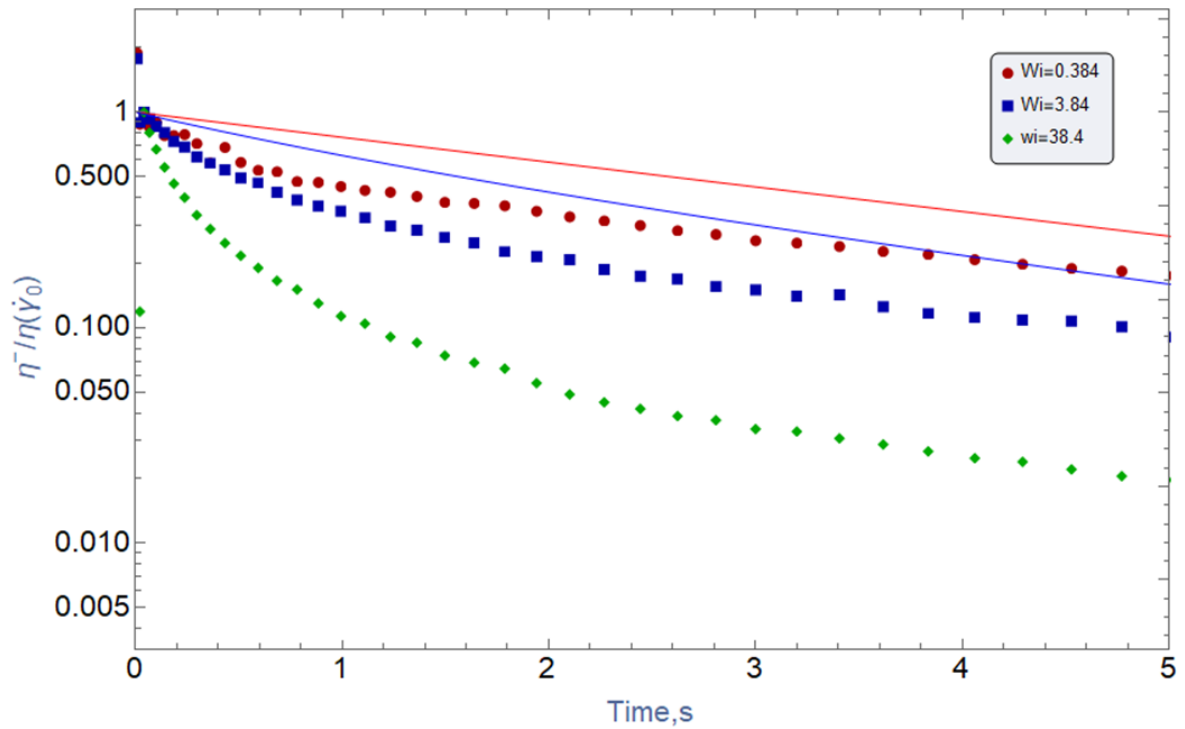


Figure 4.38. The dimensionless shear stress relaxation of cessation of steady shear flow ($\frac{\eta^-(t, \dot{\gamma}_0)}{\eta(\dot{\gamma}_0)}$) versus time (t) is fitted with first approach relative to affine PPT model (red, blue, green curve), for HPAM polymer $Cc = 3 \cdot 10^4$ ppm, with of $wi=0.384$, $wi=3.84$ and $wi=38.4$

- **Second approach**

As it was noted before, the model parameter ε and consequently λ for this approach are determined based on dynamic diagrams and the **function** $(\lambda(\varepsilon)$ or $\varepsilon(\lambda))$ that relates them to each other and they are not dependent on slope of exponential decay of cessation of steady shear rate test (m_{relax}) anymore. Furthermore, start-up and relaxation test are fitted simultaneously such that best possible fit is obtained with $\varepsilon=1.13$ and $\lambda=1.32$ and Weissenberg number ($wi = \lambda\dot{\gamma}$) as order of $wi=0.132$, $wi=1.32$ and $wi=13.2$. following diagrams summarizes data fitting with second approach.

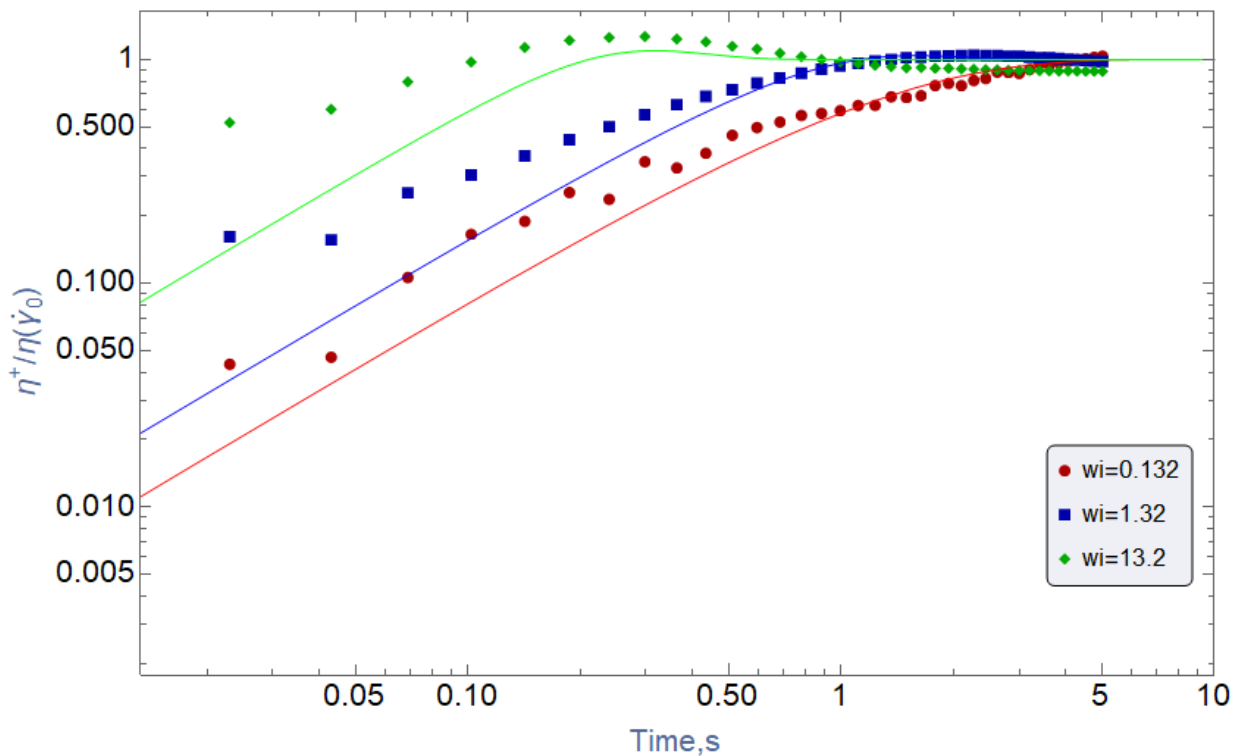


Figure 4.39. The dimensionless shear stress growth of Startup of steady shear flow $(\frac{\eta^+(t,\dot{\gamma}_0)}{\eta(\dot{\gamma}_0)})$ versus time (t) is fitted with second approach relative to affine PPT model (red, blue, green curve), for HPAM polymer $Cc = 3 \cdot 10^4$ ppm, $wi=0.132$, $wi=1.32$ and $wi=13.2$

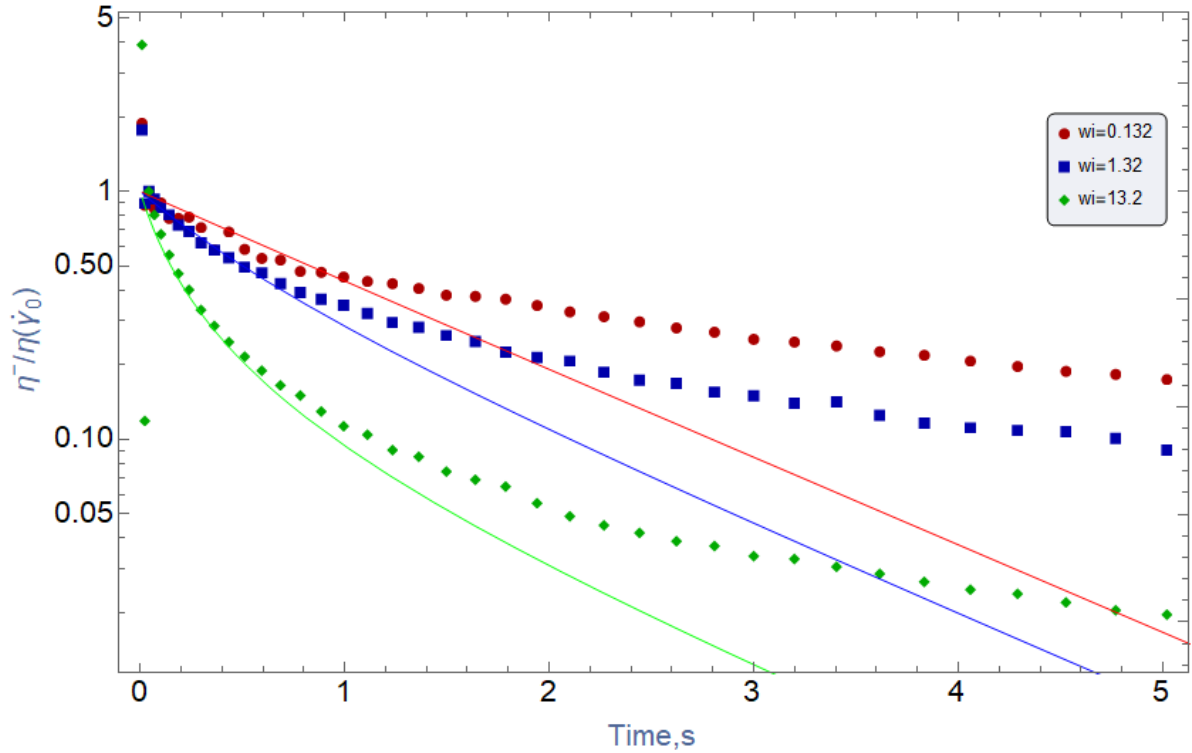


Figure 4.40. The dimensionless shear stress relaxation of cessation of steady shear flow $\frac{\eta^-(t, \dot{\gamma}_0)}{\eta(\dot{\gamma}_0)}$ versus time (t) is fitted with second approach relative to affine PPT model (red, blue, green curve), for HPAM polymer $Cc = 3 \cdot 10^4$ ppm, with $wi=0.132$, $wi=1.32$ and $wi=13.2$

- So, the importance of methodology by which the data is fitted to model is clearly seen from Above diagrams. It is seen that in case one rely on experimental result (m_{relax}) in first approach, then may end up with wrong conclusion that affine LPPT model is not representative model for describing data, though model parameter ϵ is on the typical expected range ($\epsilon=0.13$).
- On the other hand it is also observed that in case one adopted second approach of data fitting which is based on dynamic data fitting, one would gain relatively good match between data and model, though as it seen from diagram the size of overshoot is underpredicted with affine version of LPPT model even if in best possible dynamic fit. The reason for this underprediction roots up in the nature of model, where as noted in chapter 2 the maximum magnitude overshoot that affine LPPT model can predicts is of the order of $m_{overshoot} = 1.14$, while the size of overshoot for $wi = 13.2$ was already estimated as $m_{overshoot} = 1.5$, and hence the model failure regarding size of overshoot was completely predictable. Moreover, is interestingly seen that almost perfect fit was

obtained with relatively large ε in this approach ($\varepsilon=1$), while one may expect ε as order of 10⁻²-10⁻¹.

4.2.2.2 Startup of and relaxation of steady shear flow data fitting with FENE-P model

- **First approach**

Here again model parameters are gained based on experiment result. So, we had already obtain converting factor from shear ramping data fitting of affine LPPT model ($C_{convert}=1.72$) which gives product of model parameters (λ_Q and b) based on equation 2.43 ,Then model parameter b is obtained from calculated $\varepsilon=0.13$ of affine LPPT model based on equation 2.56 of chapter 2 as $b=4.5$.Hence, again other model parameters λ_Q easily yields as $\lambda_Q=9.16$.So, $b=4.5$ and $\lambda_Q=9.16$ with Weissenberg number ($wi = \gamma\dot{\lambda}_Q$) with order of $wi=0.961$, $wi=9.61$ and $wi=96.1$ is gained based on slope of exponential decay of cessation of steady shear rate test ($m_{relax}=-0.26$) and the converting factor ($C_{convert}$) of shear ramping data fitting.

The dimensionless shear stress growth of Startup of steady shear flow ($\frac{\eta^+(t,\dot{\gamma}_0)}{\eta(\dot{\gamma}_0)}$) versus time (t) and dimensionless shear stress relaxation of cessation of steady shear flow ($\frac{\eta^-(t,\dot{\gamma}_0)}{\eta(\dot{\gamma}_0)}$) versus time(t) is fitted with FENE-P model, for HPAM polymer $Cc=3.10^4$ ppm with first approach in below.

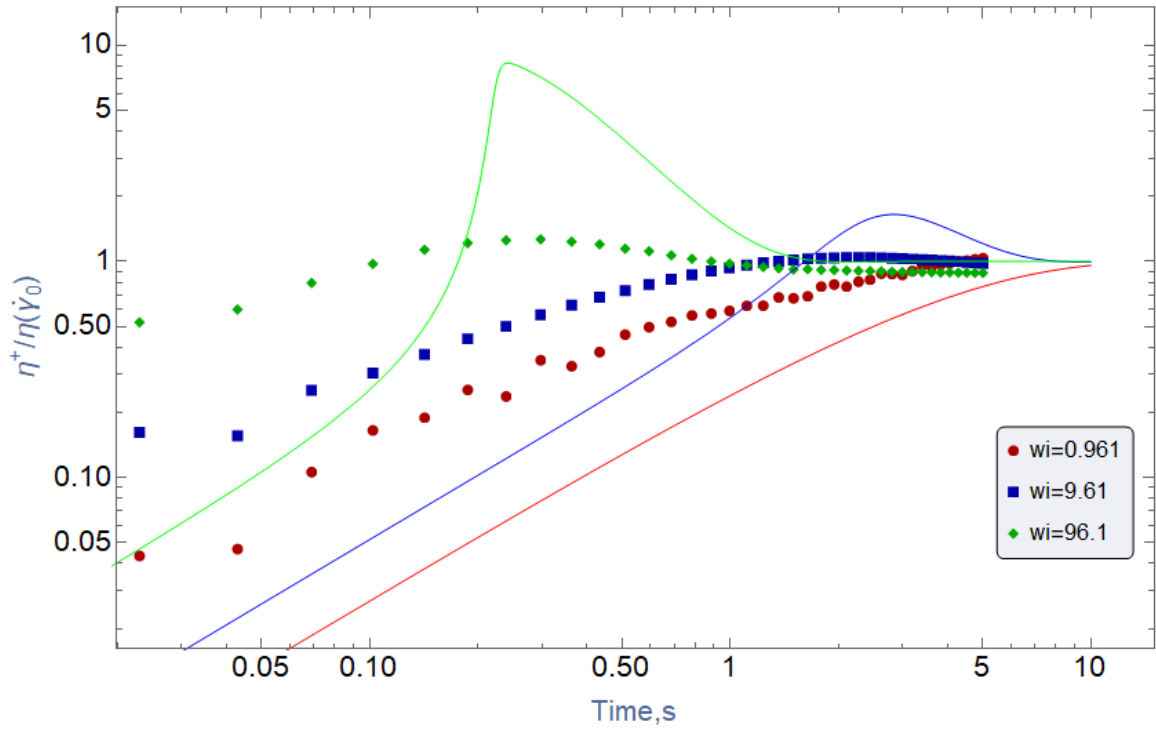


Figure 4.41. The dimensionless shear stress growth of Startup of steady shear flow ($\frac{\eta^+(t,\dot{\gamma}_0)}{\eta(\dot{\gamma}_0)}$) versus time(t) is fitted with first approach relative to FENE-P model(red, blue ,green curve), for HPAM polymer $Cc = 3 \cdot 10^4$ ppm, $wi=0.961$, $wi=9.61$ and $wi=96.1$

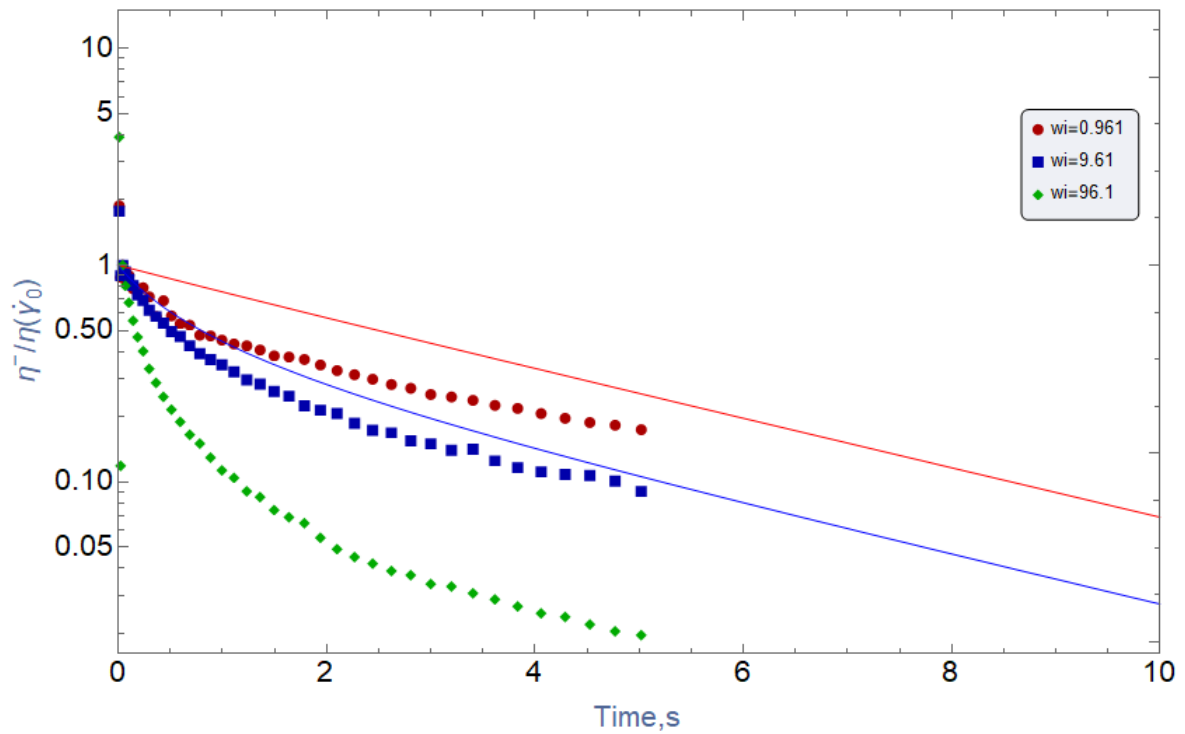


Figure 4.42. The dimensionless shear stress relaxation of cessation of steady shear flow ($\frac{\eta^-(t,\dot{\gamma}_0)}{\eta(\dot{\gamma}_0)}$) versus time(t) is fitted with first approach relative to FENE-P model(red, blue ,green curve), for HPAM polymer $Cc = 3 \cdot 10^4$ ppm, with $wi=0.961$, $wi=9.61$ and $wi=96.1$

- **Second approach**

As it was noted before, the model parameter b and consequently λ_Q for this approach are determined based on dynamic diagrams and in fact there is a **function** ($\lambda_Q(\mathbf{b})$) that relates them to each other. Hence, are not dependent on m_{relax} anymore. Furthermore, startup and cessation of shear steady test are fitted simultaneously such that best possible fit is obtained with $b=1$ and $\lambda_Q = 3.74$ and Wassenberg number as ($wi = \dot{\gamma}\lambda_Q$) as order $wi=0.374$, $wi=3.74$ and $wi=37.4$. following diagrams summarizes data fitting with second approach.

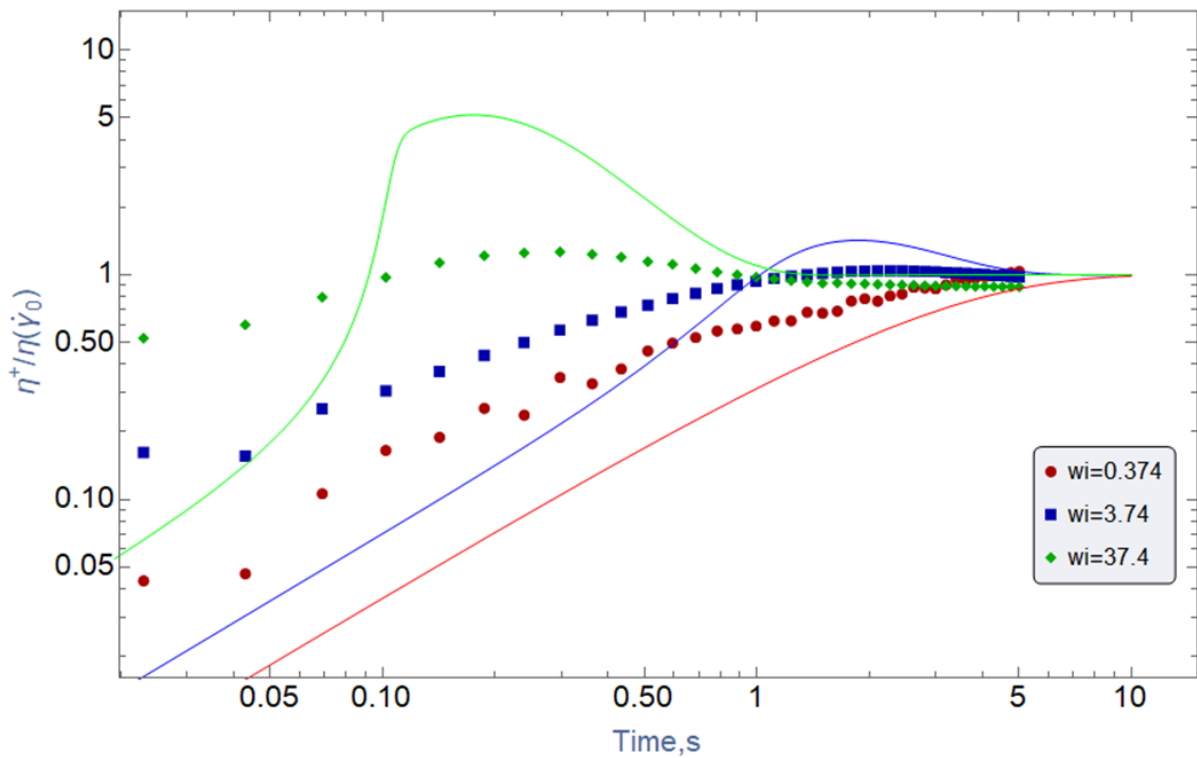


Figure 4.43. The dimensionless shear stress growth of Startup of steady shear flow ($\frac{\eta^+(t, \dot{\gamma}_0)}{\eta(\dot{\gamma}_0)}$) versus time (t) is fitted with second approach relative to FENE-P model (red, blue, green curve), for HPAM polymer $Cc = 3 \cdot 10^4$ ppm, with $wi=0.374$, $wi=3.74$ and $wi=37.4$

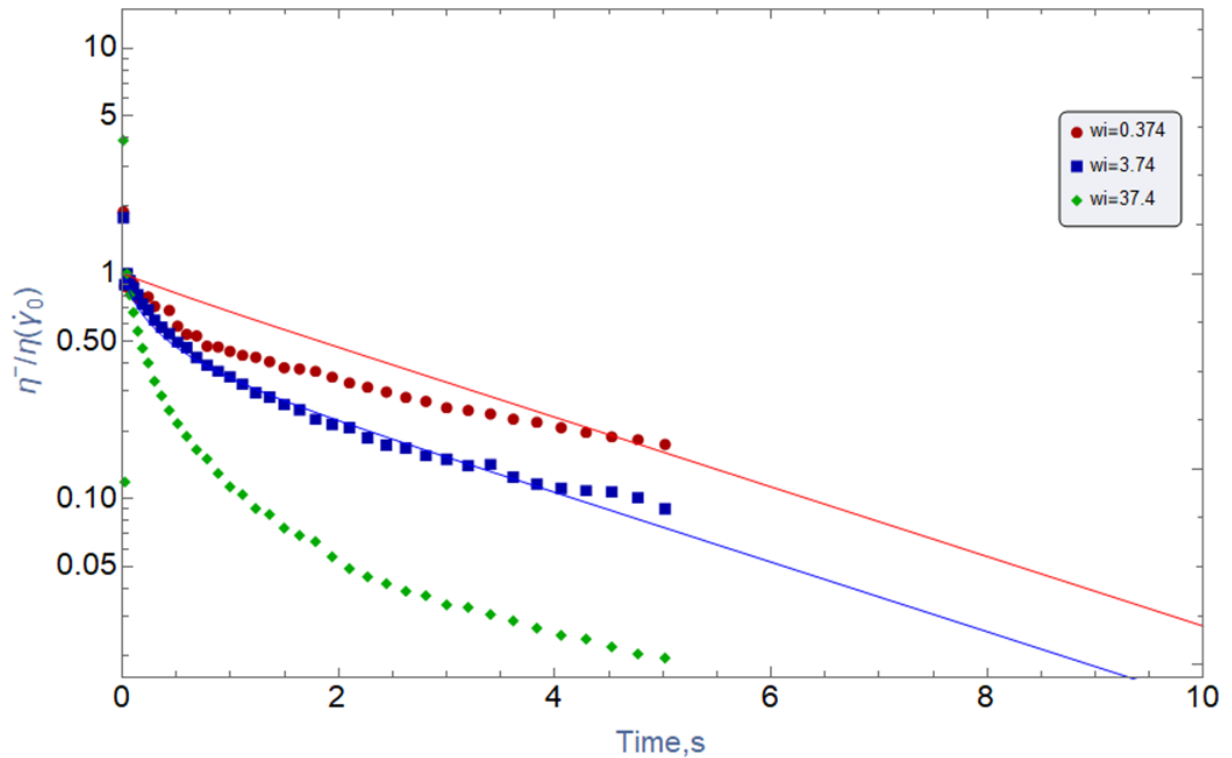


Figure 4.44 The dimensionless shear stress relaxation of cessation of steady shear flow $\frac{\eta^-(t,\dot{\gamma}_0)}{\eta(\dot{\gamma}_0)}$ versus time(t) is fitted with first second approach relative to FENE-P model(red,, blue ,green curve), for HPAM polymer $Cc = 3 \cdot 10^4$ ppm, $wi=0.374$, $wi=3.74$ and $wi=37.4$

So again, above diagrams shows clearly the importance of adopting correct approach of data fitting. With first approach (based on experiment) one could wrongly conclude on the relative failure of the model. On the other hand, when fitting is conducted based on dynamic data fitting approach (second approach), the model shows relatively favorable performance in both start-up and relaxation of steady shear ramping. Though is it seen model overpredicts the size of overshoot. The reason as it was noted in chapter 2 might be due to the fact that the model is constructed based on single-mode (relaxation time) that might react much faster or much slower relative to applied shear stress and consequently predict larger overshoot. In fact, this larger amount of overshoot can get relief by considering multiple-mode FENE-P model in which the constitutive equation and consequently size of overshoot is result of contribution from all mode. Hence even larger amount overshoot might be canceled by contribution from other mode. This is something that was addresses by Dmitry Shogin and Amundsen in their most recent article (Shogin 2020) .

Moreover, relatively good fitting was observed with low amount of $b=1$, while one should expect b to be large amount to obtain good fitting result.

4.2.2.3 Startup and cessation of steady shear flow data fitting with C-FENE-P model

The data fitting methodology here is done only based on second approach of data fitting. In fact, since all these parameters (E , b , λ_Q) are known from data fitting of shear ramping test, so we do not rely on experimental result (m_{relax}) anymore. Moreover, as we got favorable converting factor ($\lambda_Q=10$, $\lambda_Q=3$) for HPAM polymer $Cc=2.10^4$ ppm, and polymer $Cc=2.10^4$ ppm, and the model itself has constructed based on dilute solution, these two concentrations were analyzed with this model.

The dimensionless shear stress growth of Startup of steady shear flow ($\frac{\eta^+(t,\dot{\gamma}_0)}{\eta(\dot{\gamma}_0)}$) versus dimensionless time (r) and dimensionless shear stress relaxation of cessation of steady shear flow ($\frac{\eta^-(t,\dot{\gamma}_0)}{\eta(\dot{\gamma}_0)}$) versus dimensionless time(r) is fitted with C-FENE-P model, for HPAM polymer $Cc=2.10^4$ ppm with first approach in below.

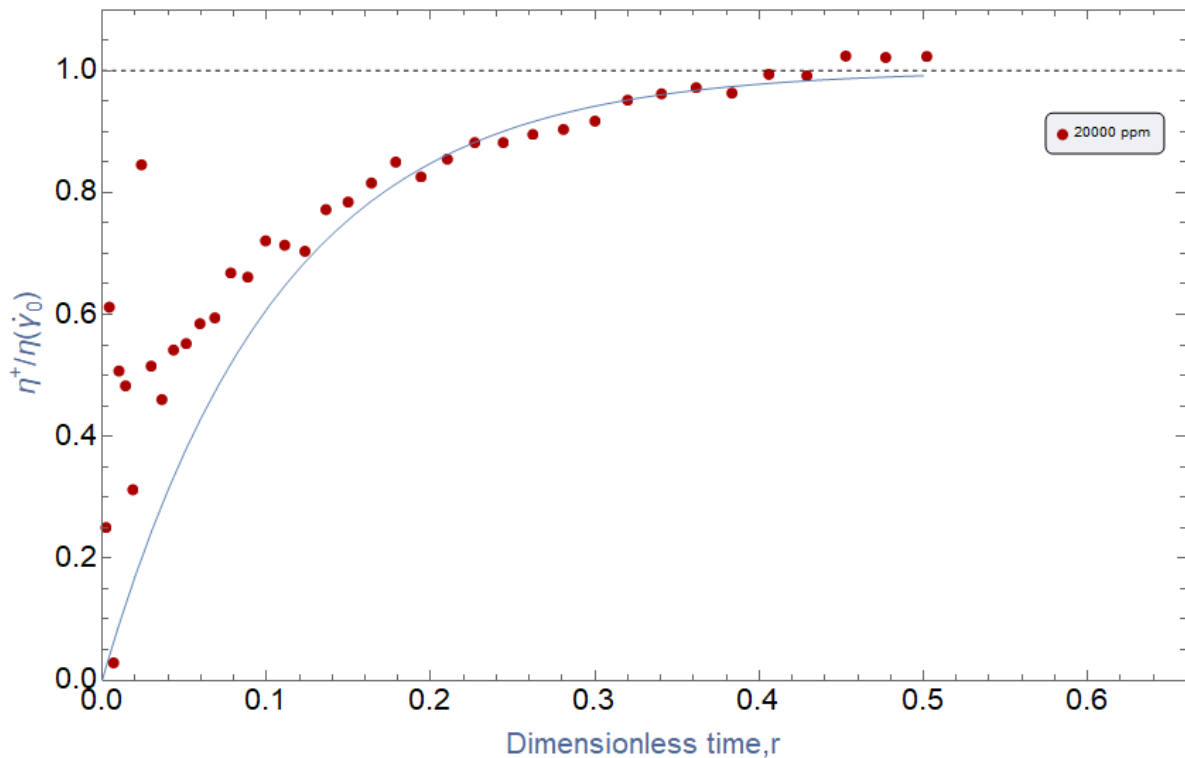


Figure 4.45. The dimensionless shear stress growth of Startup of steady shear flow ($\frac{\eta^+(t,\dot{\gamma}_0)}{\eta(\dot{\gamma}_0)}$) versus dimensionless time (r) is relative to C-FENE-P model (blue curve), for HPAM polymer $Cc = 2.10^4$ ppm, ($w_i = \gamma\lambda_Q$) $w_i = 1$

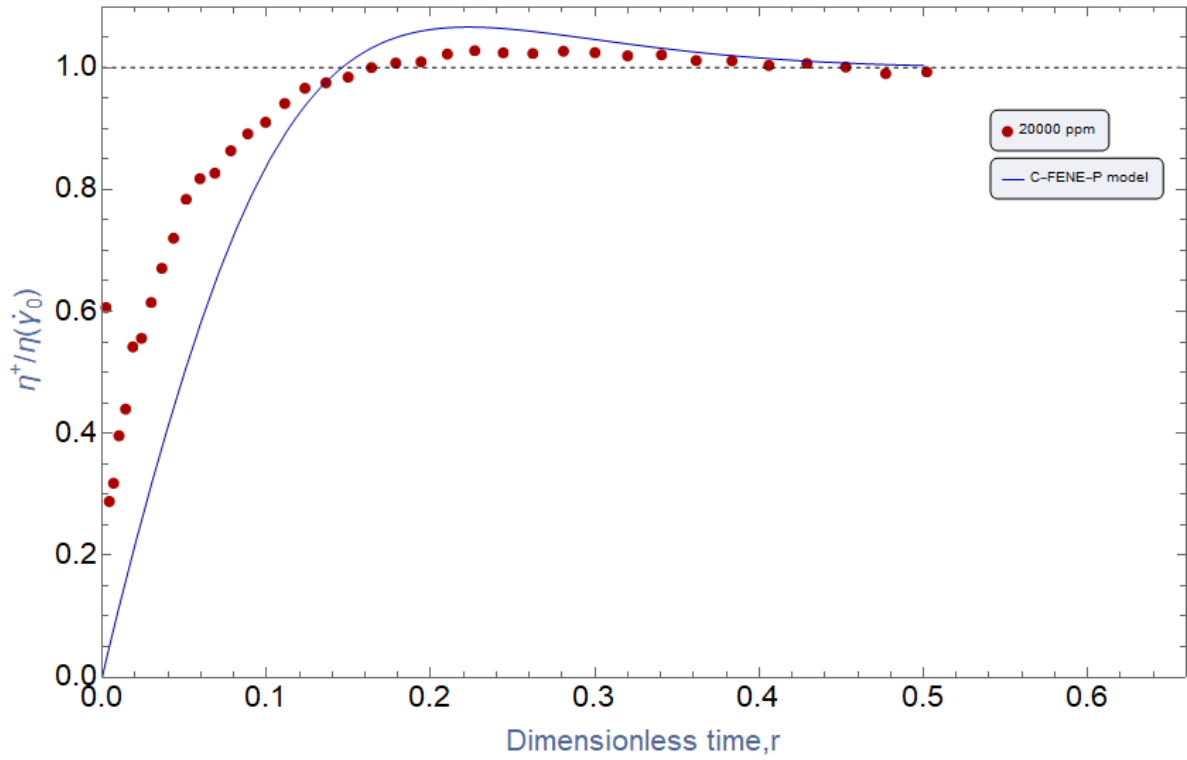


Figure 4.46. The dimensionless shear stress growth of Startup of steady shear flow ($\frac{\eta^+(t,\dot{\gamma}_0)}{\eta(\dot{\gamma}_0)}$) versus dimensionless time (r) is relative to C-FENE-P model (blue curve), for HPAM polymer $Cc = 2 \cdot 10^4$ ppm, with ($wi = \gamma\dot{\lambda}_Q$) $wi = 10$

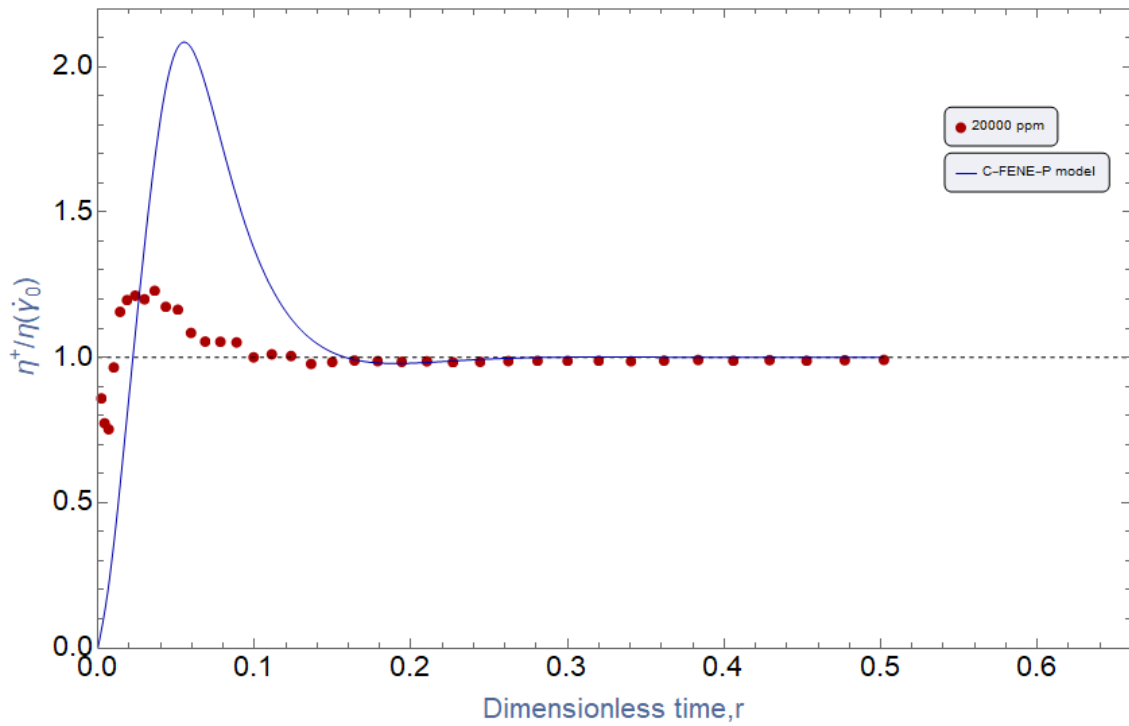


Figure 4.47. The dimensionless shear stress growth of Startup of steady shear flow ($\frac{\eta^+(t,\dot{\gamma}_0)}{\eta(\dot{\gamma}_0)}$) versus dimensionless time (r) is relative to C-FENE-P model (blue curve), for HPAM polymer $Cc = 2 \cdot 10^4$ ppm, with ($wi = \gamma\dot{\lambda}_Q$) $wi = 100$

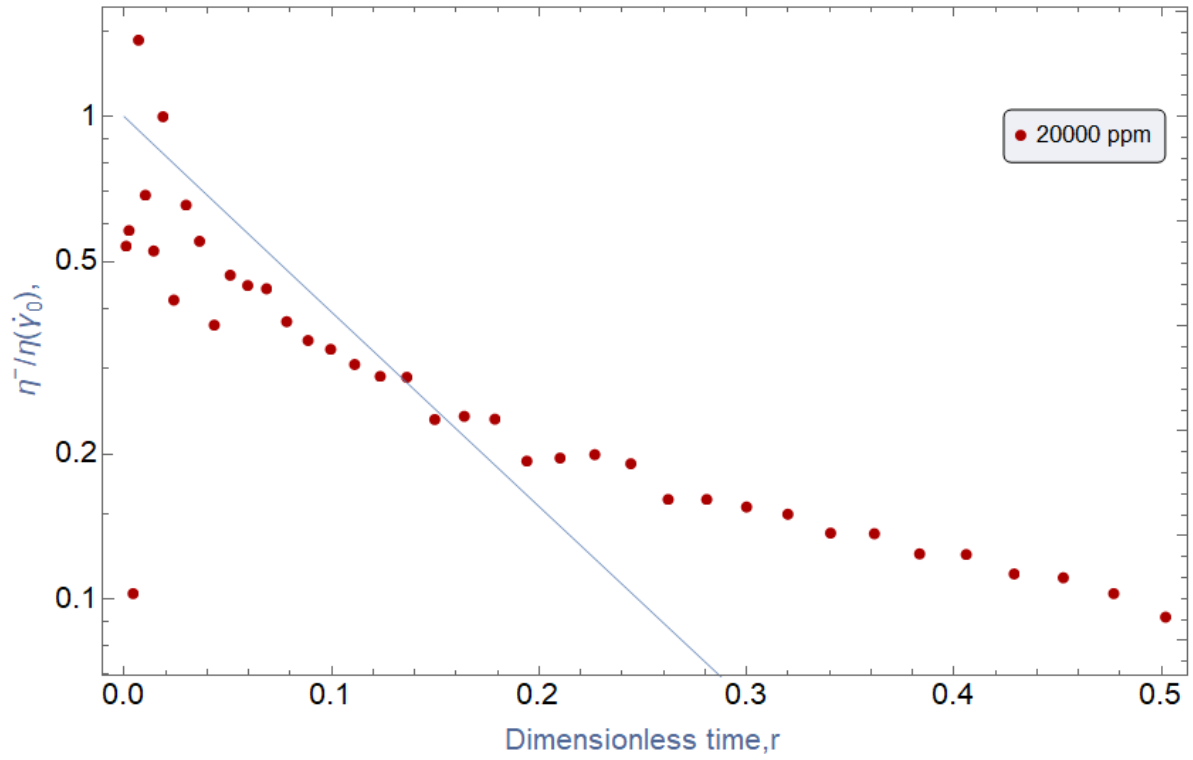


Figure 4.48. The dimensionless shear stress relaxation of cessation of steady shear flow $\frac{\eta^-(t, \dot{\gamma}_0)}{\eta(\dot{\gamma}_0)}$ versus dimensionless time(r) is fitted with relative to C-FENE-P model(blue curve), for HPAM polymer $Cc = 2 \cdot 10^4$ ppm, with $(w_i = \gamma \lambda_Q) w_i = 1$

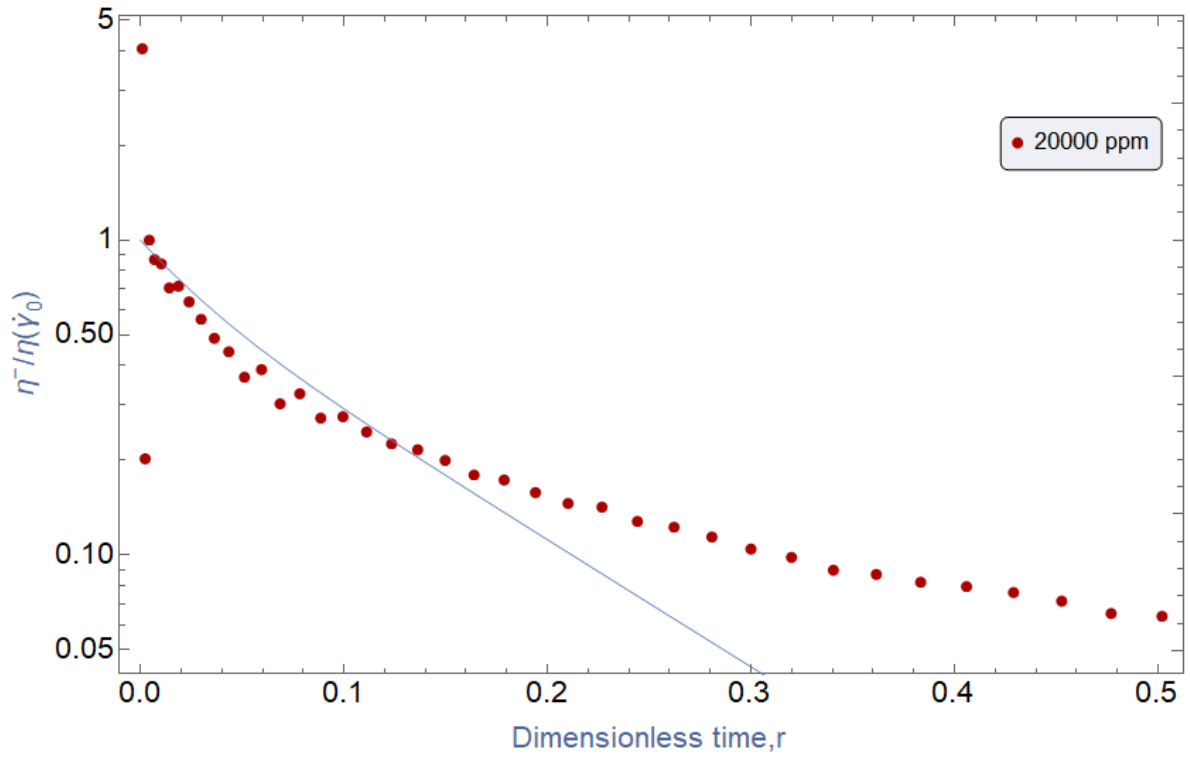


Figure 4.49. The dimensionless shear stress relaxation of cessation of steady shear flow $\frac{\eta^-(t,\dot{\gamma}_0)}{\eta(\dot{\gamma}_0)}$ versus dimensionless time(r) is fitted with relative to C -FENE-P model(blue curve), for HPAM polymer $Cc = 2 \cdot 10^4$ ppm, with ($w_i = \gamma \dot{\lambda}_Q$) $w_i = 10$

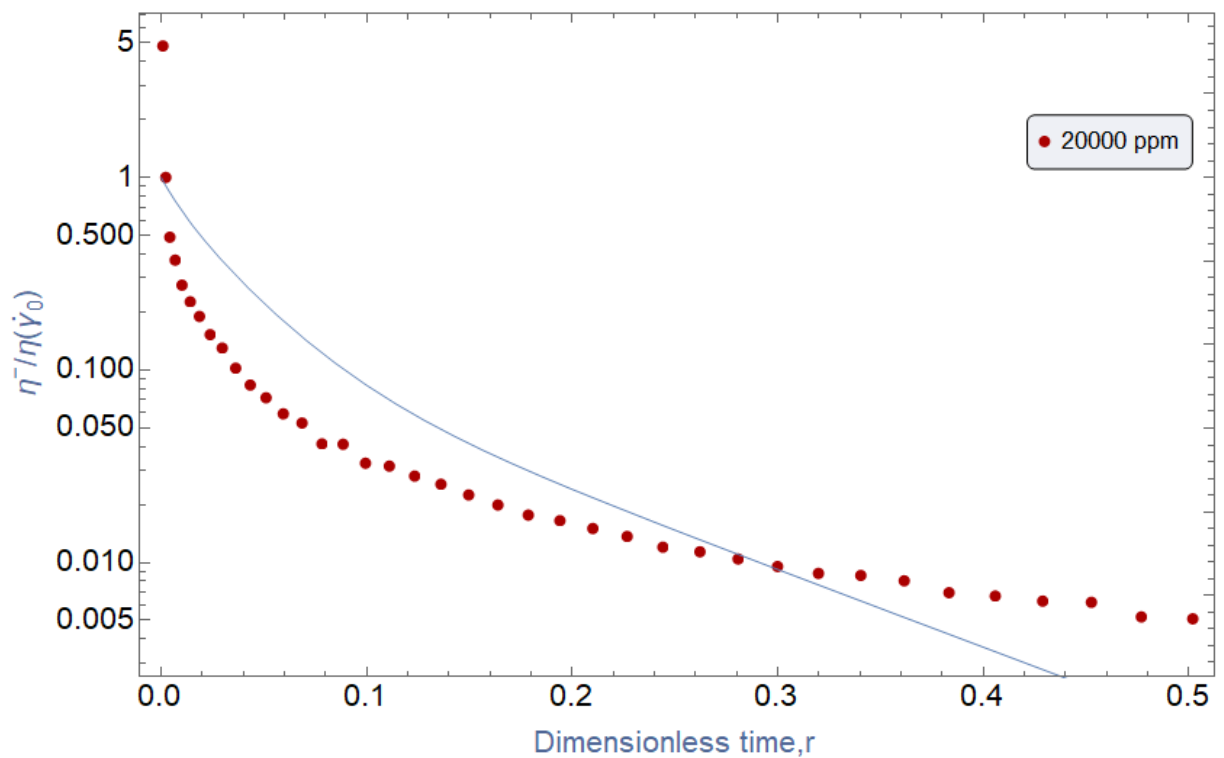


Figure 4.50. The dimensionless shear stress relaxation of cessation of steady shear flow $\frac{\eta^-(t,\dot{\gamma}_0)}{\eta(\dot{\gamma}_0)}$ versus dimensionless time(r) is fitted with relative to C -FENE-P model(blue curve), for HPAM polymer $Cc = 2 \cdot 10^4$ ppm, with ($w_i = \gamma \dot{\lambda}_Q$) $w_i = 100$

The dimensionless shear stress growth of Startup of steady shear flow ($\frac{\eta^+(t, \dot{\gamma}_0)}{\eta(\dot{\gamma}_0)}$) versus dimensionless time (r) and dimensionless shear stress relaxation of cessation of steady shear flow ($\frac{\eta^-(t, \dot{\gamma}_0)}{\eta(\dot{\gamma}_0)}$) versus dimensionless time (r) is fitted with C-FENE-P model, for HPAM polymer $Cc=1.5 \cdot 10^4$ ppm with first approach in below.

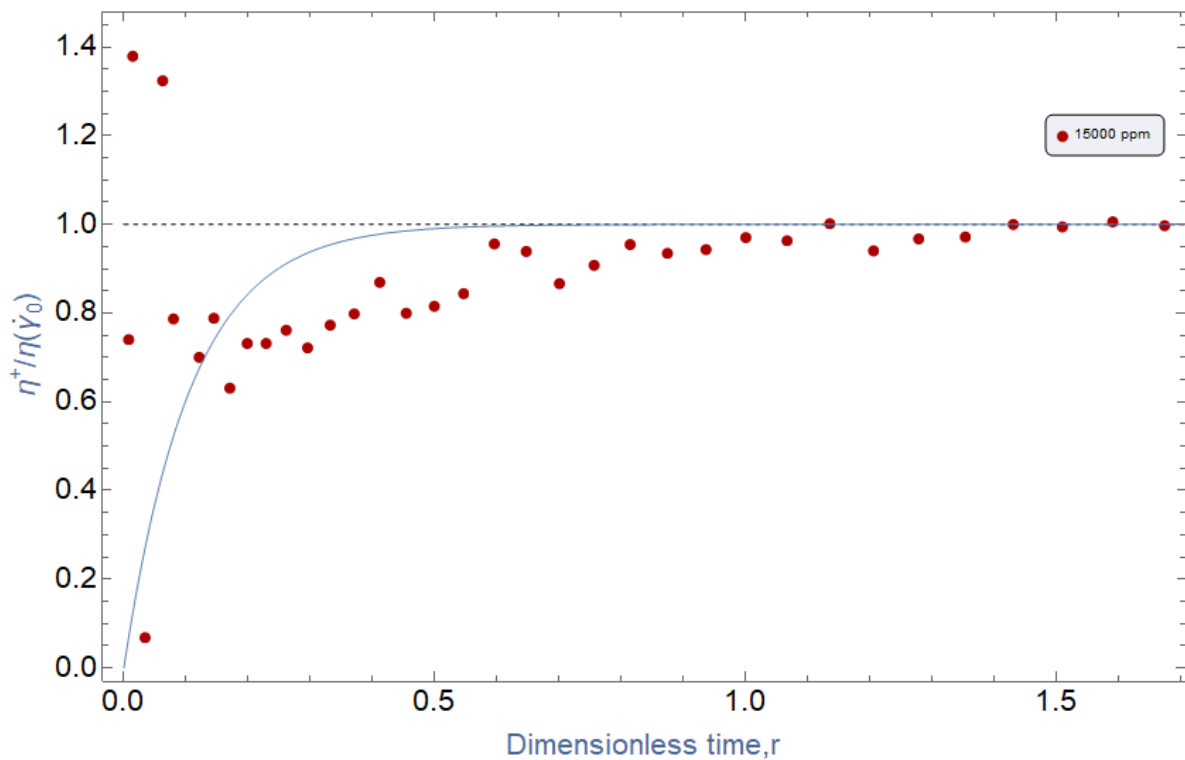


Figure 4.51 The dimensionless shear stress growth of Startup of steady shear flow ($\frac{\eta^+(t, \dot{\gamma}_0)}{\eta(\dot{\gamma}_0)}$) versus dimensionless time (r) is relative to C-FENE-P model (blue curve), for HPAM polymer $Cc = 1.5 \cdot 10^4$ ppm, with $(wi = \gamma \dot{\lambda}_Q) wi = 0.3$

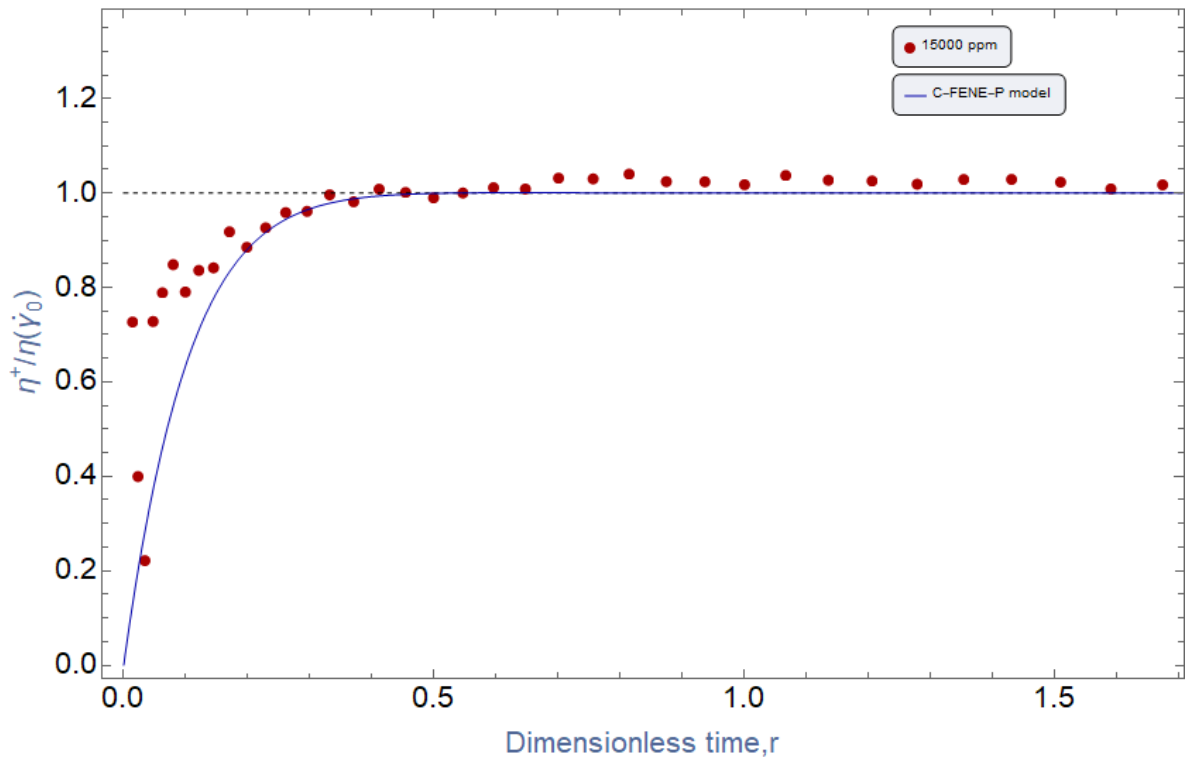


Figure 4.52. The dimensionless shear stress growth of Startup of steady shear flow ($\frac{\eta^+(t,\dot{\gamma}_0)}{\eta(\dot{\gamma}_0)}$) versus dimensionless time (r) is relative to C-FENE-P model (blue curve), for HPAM polymer $Cc = 1.5 \cdot 10^4$ ppm, with ($wi = \gamma \dot{\lambda}_Q$) $wi = 3$

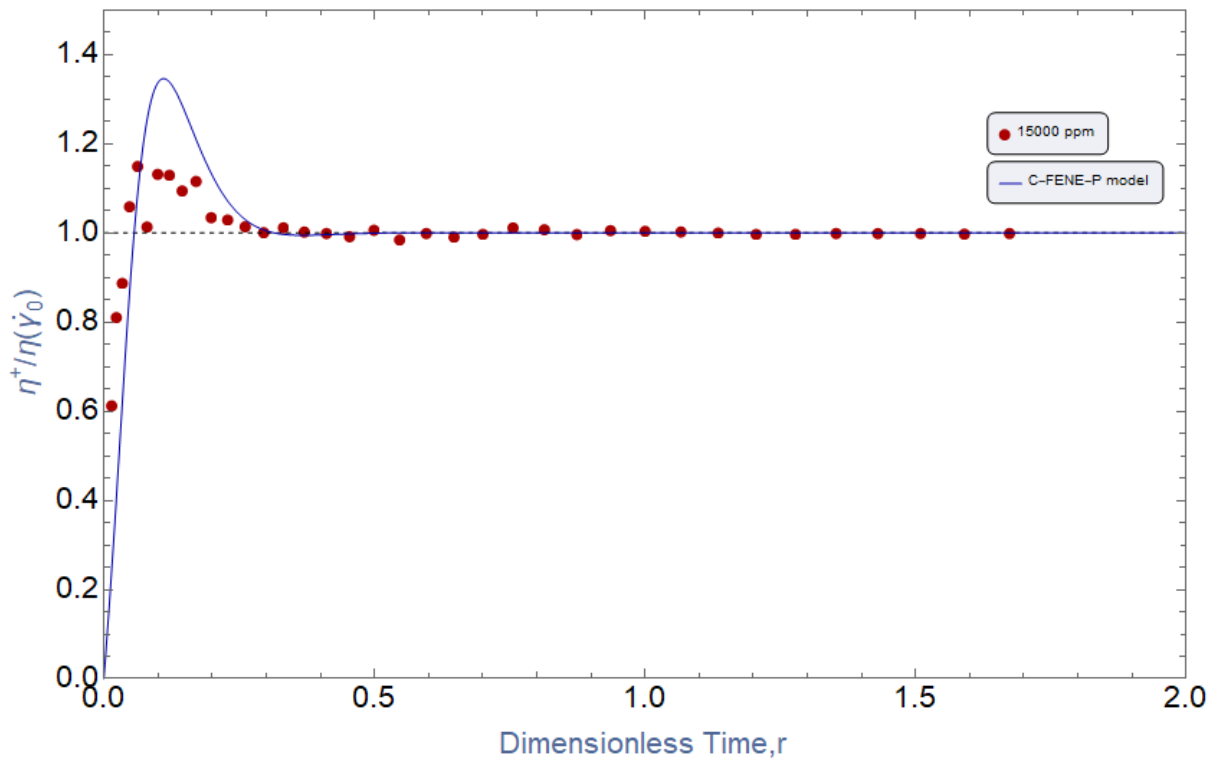


Figure 4.53. The dimensionless shear stress growth of Startup of steady shear flow ($\frac{\eta^+(t,\dot{\gamma}_0)}{\eta(\dot{\gamma}_0)}$) versus dimensionless time (r) is relative to C-FENE-P model (blue curve), for HPAM polymer $Cc = 1.5 \cdot 10^4$ ppm, with dimensionless shear rate ($wi = \gamma \dot{\lambda}_Q$) $wi = 30$

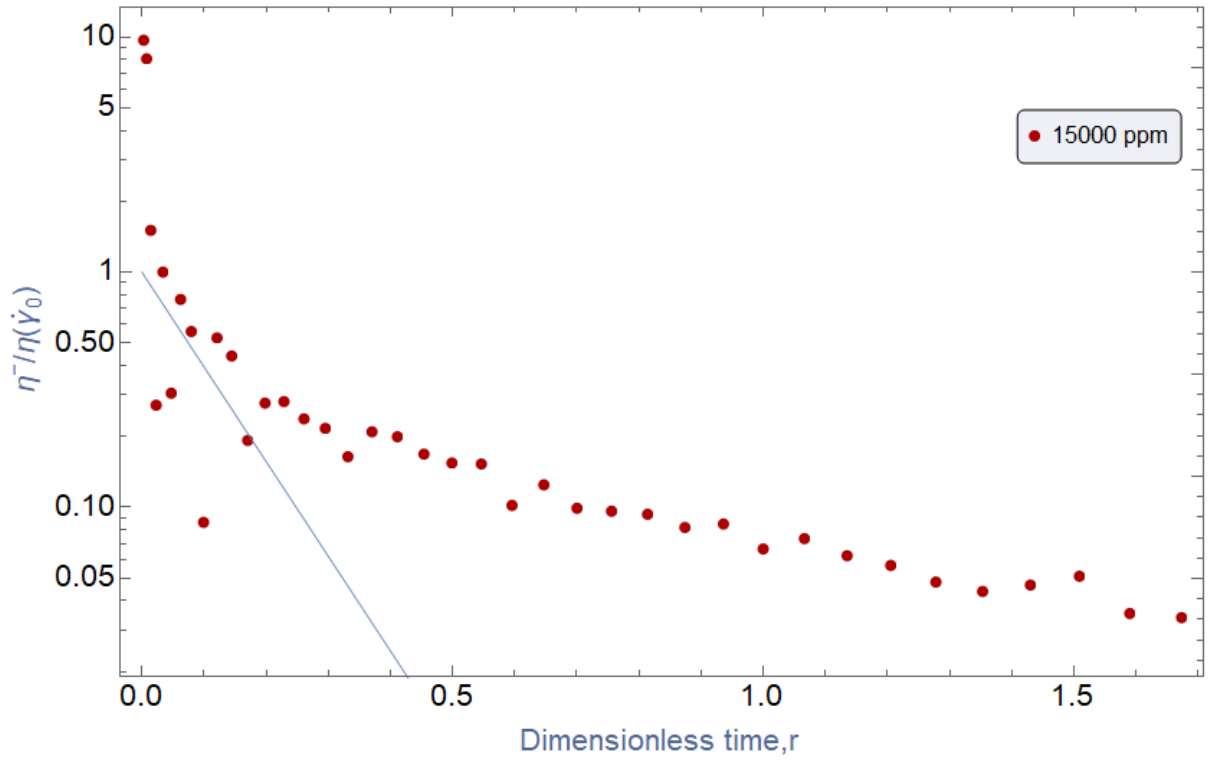


Figure 4.54. The dimensionless shear stress relaxation of cessation of steady shear flow $\frac{\eta^-(t,\dot{\gamma}_0)}{\eta(\dot{\gamma}_0)}$ versus dimensionless time(r) is fitted with relative to C -FENE-P model(blue curve), for HPAM polymer $Cc = 1.5 \cdot 10^4$ ppm, with $(wi = \gamma\lambda_Q)$ $wi = 0.3$

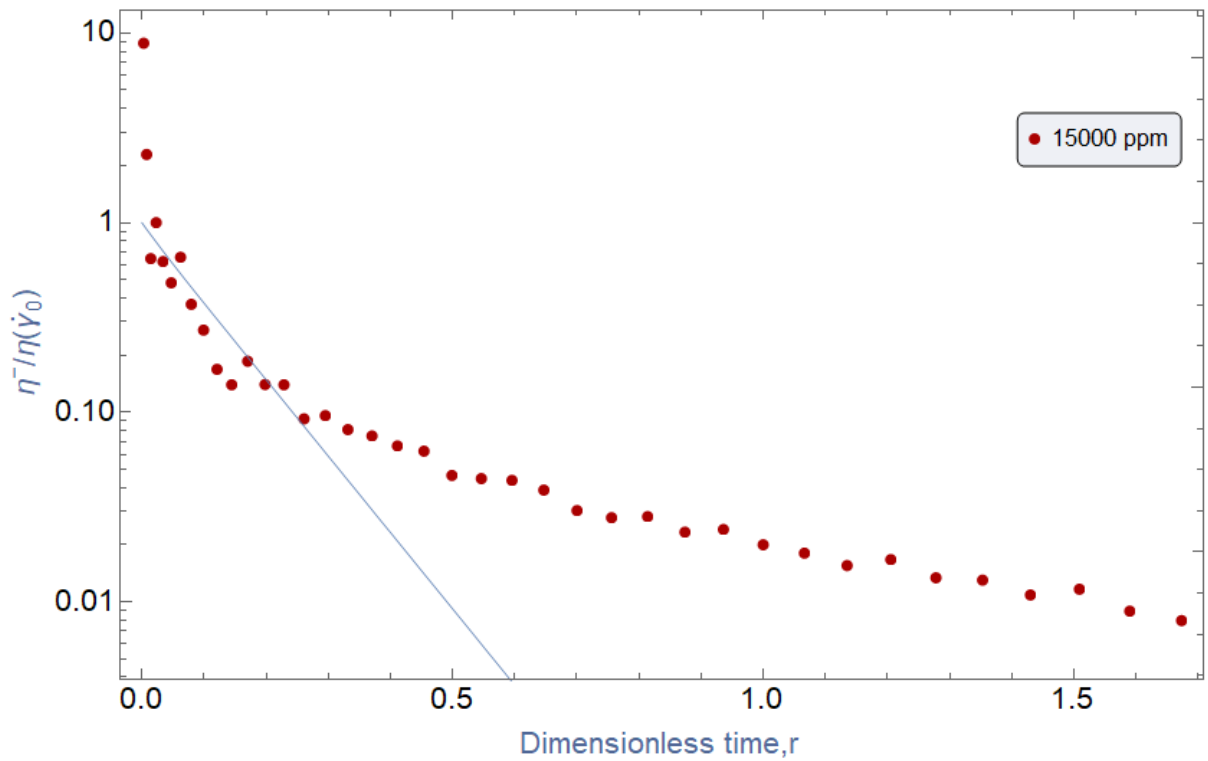


Figure 4.55. The dimensionless shear stress relaxation of cessation of steady shear flow $\frac{\eta^-(t,\dot{\gamma}_0)}{\eta(\dot{\gamma}_0)}$ versus dimensionless time(r) is fitted with relative to C -FENE-P model(blue curve), for HPAM polymer $Cc = 1.5 \cdot 10^4$ ppm, with $(wi = \gamma\lambda_Q)$ $wi = 3$

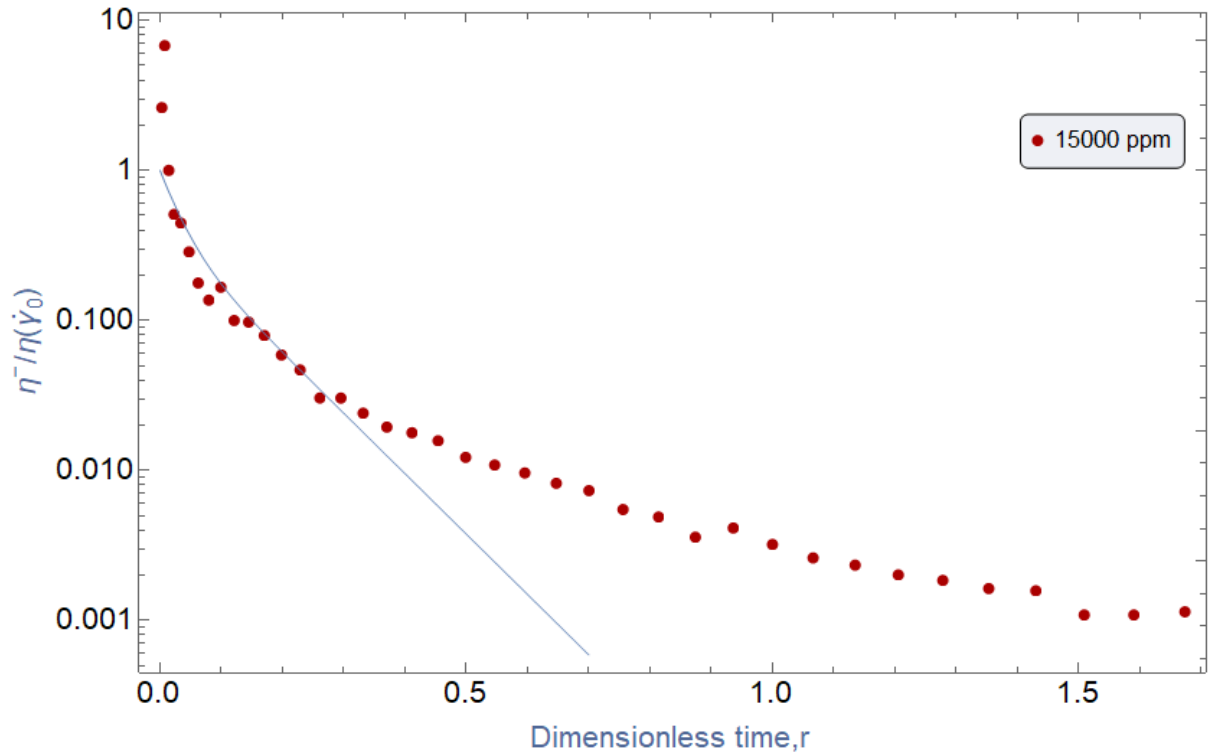


Figure 4.56. The dimensionless shear stress relaxation of cessation of steady shear flow $\frac{\eta^-(t,\dot{\gamma}_0)}{\eta(\dot{\gamma}_0)}$ versus dimensionless time(r) is fitted with relative to C-FENE-P model(blue curve), for HPAM polymer $Cc = 1.5 \cdot 10^4$ ppm, with dimensionless shear rate($wi = \gamma\dot{\lambda}_Q$) $wi = 30$

So, it can be observed from diagrams that again model overpredicts both size of overshoot and its position relative to time. Though, the level of overprediction is reduced as the concentration decrease which makes perfect sense since the model has constructed to justify dilute solution. Moreover, model predict shear stress relaxation of cessation of shear flow with relatively good accuracy at least regarding non-exponential region of decay.

5 Discussion and conclusions

5.1 Discussion and conclusion regarding data analysis without considering physical models

Following conclusions can be made in his part:

1. It was observed that the slope of power-law region of viscosity versus shear rate for HPAM polymer is dependent on the concentration.
2. Though the slope of power-law region for first normal stress differences coefficient (Ψ_1) seems to be independent of concentration. This clearly shows that first normal stress differences coefficient (Ψ_1) is viscoelastic properties of polymer which is more rely on nature properties of polymer rather than different derivatives (concentrations) of polymer.
3. The proposed theory by Islam in his thesis (Islam 2019) about the independency of both position of overshoot relative to time and the time required to arrive at steady state value, on concentration is verified by HPAM polymer at least for three concentration of $C_c=3.10^4$ ppm , $C_c=2.10^4$ ppm and $C_c= 1.5.10^4$ ppm .
4. On the other hand, the proposed hypothesis made by Islam in his thesis (Islam 2019)about non-monotonous dependency of size of overshoot , on concentration in startup of steady shear rate experiment is not observed with HPAM polymer at least in three concentrations of $C_c= 3.10^4$ ppm , $C_c= 2.10^4$ ppm and $C_c=1.5.10^4$ ppm (maybe more dilute concentration is needed to observe this phenomenon).In, fact in all these three concentrations, there is monotonous dependency between size of overshoot and concentration such that the size of overshoot increase with increase in concentration.
5. The proposed theory made by Islam in his thesis (Islam 2019) about independency of the slope of decay in non-exponential region ,on both step-rate and concentration in cessation of steady shear rate experiment is verified by HPAM polymer at least in three concentration of $C_c=3.10^4$ ppm , $C_c=2.10^4$ ppm and $C_c=1.5.10^4$ ppm.
6. On the other hand, the proposed hypothesis by Islam (Islam 2019) about non-monotonous dependency of the slope of reduction in exponential region ,on concentration in cessation of steady shear rate experiment is not observed in HPAM polymer at least in three concentration of $C_c= 3.10^4$ ppm , $C_c= 2.10^4$ ppm and $C_c=1.5.10^4$ (again maybe more dilute concentrations is required for this phenomenon

to be observed). In fact, the slope of exponential decay accelerates with decrease in concentration for HPAM polymer in monotonous fashion at least for these three concentrations.

5.2 Discussion and conclusion regarding data analysis with considering physical models

1. It was observed that both full LPPT model and affine EPPT model failed to describe both steady and transient flow for HPAM polymer in all levels of tested concentration due to the relatively high divergence between real data and proposed model.
2. The importance of methodology by which the data is fitted against model was shown throughout this work for affine-LPPT and FENE-P model. In fact, it was shown that how wrong an impression can be made about the efficiency of the model prediction when one relies on extracting model parameter (λ) from the slope of decay (m_{relax}) in the exponential part of the cessation of steady shear rate test defined by equation 2.57. It is an interesting point where theory clashes with experimental techniques;
 - In theory, the cessation of steady shear rate test is a good way to extract λ_e based on equation 2.57
 - In practice, it is not so good because of the noise related to measuring very small stresses (recall that the stresses decay even faster than exponentially so that they become very small quickly).
3. Then a relatively good model prediction (only for the most concentrated sample $C_c=3.10^4$) was observed for affine LPPT and FENE-P model both in steady and transient flow. It was done by adopting the second approach of data fitting, where one is relying on determining model parameter (like λ) based on dynamic diagrams and **pre-defined functions** instead of experimental technique (first approach) to get the best possible fit.
4. Though it was seen that even by adopting the second approach of data fitting, both affine LPPT model models and FENE-P model relatively failed in determination

of exact magnitude of overshoot. In fact, affine LPPT model underpredicts the size of overshoot, whereas the FENE-P model overpredicts this magnitude. The underprediction of affine LPPT model was predictable since as it was noted in chapter 2, the maximum magnitude of overshoot which this model can describe is of order of $m_{\text{overshoot}}=1.14$, while the maximum overshoot for real data was of order of $m_{\text{overshoot}}=1.4$. But overprediction of FENE-P may be rooted in considering single mode (relaxation time (λ)) for model. In fact, the problem with having single-mode based model is considering one relaxation time (λ) that would react faster or slower than real relaxation time relative to applied stress. Moreover, this single-based model can predict size of overshoot greater than real magnitude, while the real size of overshoot is result of contribution from all other modes and hence this relatively high overshoot can be canceled by considering other magnitude contribution from other modes. This is why it is important to consider multiple-mode based models, where constitutive equation is result of contribution from each single mode, as Dmitry Shogin has mentioned in his most recent article (Shogin 2020). In this context, considering multiple modes will not help LPPT but can help FENE-P because adding several modes will "smooth" everything out so that the overshoot will decrease.

5. Almost for the first time in literature the efficiency of most recent physical based model proposed by Shogin and Amundsen (Shogin and Amundsen 2020) called C-FENE-P was evaluated in this research. This was the only model which did not fail for description of material function of more dilute concentrations of HPAM polymer ($C_c=2.10^4$ ppm and $C_c=1.5.10^4$ ppm). On the other hand model relatively failed for description of material function of most concentrated sample ($C_c=3.10^4$ ppm) which as noted makes complete sense as model has been constructed based on kinetic theory which is only applicable for more dilute solution. But, in general C-FENE-P model was recognized as a most representative model for description of material function of HPAM polymer for both steady and transient specially for more dilute tested concentrations ($C_c=2.10^4$ ppm and $C_c=1.5.10^4$ ppm). Though like FENE-P model it overpredicts both the magnitude of overshoot and its position relative to time. But as noted, the more dilute solution, the more accurate is model prediction about magnitude of overshoot.

potentials of further works:

It would be favorable if one could conduct test even on more concentration of HPAM polymer to observe following:

1. Whether monotonous dependency of material function of HPAM polymer on concentration observed by this research for three tested concentrations can be extended for other degrees of concentration.
2. Whether C-FENE-P model is also recognized as the best model for describing material function of HPAM polymer both in steady and transient flow.
3. As only pure sample of HPAM polymer was tested in this research.it would be interesting to see whether C-FENE-P model also can justify the material function of salty version of HPAM polymer.
4. Also, it would also be interesting to give the normal stresses more attention.

References

- Alves, M. A., F. T. Pinho and P. J. J. J. o. n.-n. f. m. Oliveira (2001). "Study of steady pipe and channel flows of a single-mode Phan-Thien–Tanner fluid." **101**(1-3): 55-76.
- Andrade, L. C. F., J. A. Petronílio, C. E. d. A. Maneschy, D. O. d. A. J. J. o. t. B. S. o. M. S. Cruz and Engineering (2007). "The carreau-yasuda fluids: a skin friction equation for turbulent flow in pipes and kolmogorov dissipative scales." **29**(2): 162-167.
- Bird, R., P. Dotson and N. J. J. o. N.-N. F. M. Johnson (1980). "Polymer solution rheology based on a finitely extensible bead—spring chain model." **7**(2-3): 213-235.
- Bird, R. B., C. F. Curtiss, R. C. Armstrong and O. Hassager (1987). Dynamics of polymeric liquids, volume 2: Kinetic theory, Wiley.
- Carreau, P. J., L. Choplin, J. R. J. P. E. Clermont and Science (1985). "Exit pressure effects in capillary die data." **25**(11): 669-676.
- chegg.com. "Shear flow." from <https://www.chegg.com/homework-help/questions-and-answers/simple-shear-flow-parallel-plates-consider-flow-incompressible-newtonian-fluid-parallel-pl-q14690247>.
- D. Shogin1, a. a. P. A. A., b) (2020). "<C-FENEPMarch2020.pdf>."
- De Waele, A. J. A. J. (1923). "Oil and color Chem." **6**: 33.
- Dr. R. Giri Prasad1 (2018). "Enhanced Oil Recovery by using Polymer Flooding in Oil and Gas Industry in Tertiary Recovery Process."
- Dunstan, D. E. J. S. r. (2019). "The viscosity-radius relationship for concentrated polymer solutions." **9**(1): 1-9.
- Fleisch, D. A. (2011). A student's guide to vectors and tensors, Cambridge University Press.
- Islam, A. (2019). Experimental investigation of material functions of EOR polymer solutions, University of Stavanger, Norway.
- Islam, H. (2019). "<2019 Hedayatul Islam (1).pdf>."
- Lake, L. W. (1989). "Enhanced oil recovery."
- Lodge, A. S. (1964). Elastic liquids, Academic Press New York.
- Lodge, A. S. J. R. A. (1968). "Constitutive equations from molecular network theories for polymer solutions." **7**(4): 379-392.
- Meissner, J. J. R. A. (1971). "Elongation behavior of polyethylene melts." **10**: 230-242.
- Mezger, T. G. (2006). The rheology handbook: for users of rotational and oscillatory rheometers, Vincentz Network GmbH & Co KG.
- Morris, B. A. (2016). The science and technology of flexible packaging: multilayer films from resin and process to end use, William Andrew.
- NPD. (2018). "Enhanced Oil Recovery." from <https://www.npd.no/en/facts/publications/norwegiancontinental-shelf/norwegian-continental-shelf-no.-1—2018/a-global-focal-point-forboosting-recovery/>.

Ostwald, W. J. K. Z. (1929). "de Waele-Ostwald equation." **47**(2): 176-187.

Ostwald, W. J. O. C. C. A. J. (1923). "Kolloid-Z., 36, 99-117 (1925); A. de Waele." **6**: 33-88.

Pearce, E. J. J. o. P. S. P. L. E. (1978). "Introduction to polymer science and technology: An SPE text-book, Herman S. Kaufman and Joseph J. Falcetta, Eds., Wiley-Interscience, New York, 1977, 613 pp., \$27.50." **16**(1): 55-55.

Phan-Thien, N. J. J. o. R. (1978). "A nonlinear network viscoelastic model." **22**(3): 259-283.

Poole, R., M. Davoodi and K. J. T. B. S. o. R. Zografos, *Rheology Bulletin* (2019). "On the similarities between the simplified Phan-Thien Tanner (sPTT) and FENE-P models."

Rellegadla, S., G. Prajapat and A. Agrawal (2017). "Polymers for enhanced oil recovery: fundamentals and selection criteria." *Applied microbiology and biotechnology* **101**(11): 4387-4402.

Researchgate.com. "Shear thickening versus shear thinning." from researchgate.net/figure/The-effective-kinematic-viscosity-in-shear-thickening-green-shear-thinning-red-and_fig1_290789681.

Ribau, Â. M., L. L. Ferrás, M. L. Morgado, M. Rebelo and A. M. J. F. Afonso (2019). "Semi-Analytical Solutions for the Poiseuille–Couette Flow of a Generalised Phan-Thien–Tanner Fluid." **4**(3): 129.

Rudolph, N. and T. A. Osswald (2014). *Polymer rheology: fundamentals and applications*, Carl Hanser Verlag GmbH Co KG.

Shogin, D. (2020). " Note on Introduction on polymer flooding ".

Shogin, D. and P. J. P. o. F. Amundsen (2020). "A charged finitely extensible dumbbell model: Explaining rheology of dilute polyelectrolyte solutions." **32**(6): 063101.

Shogin, D. J. a. p. a. (2020). "Start-up and cessation of steady shear and extensional flows: Exact analytical solutions for the affine linear Phan-Thien-Tanner fluid model."

Stavland, A., H. Jonsbråten and D. Strand (2013). When will polymer viscosity be a design criterion for EOR polymer flooding. IEA-EOR 34th Annual Symposium.

Thien, N. P. and R. I. J. J. o. N.-N. F. M. Tanner (1977). "A new constitutive equation derived from network theory." **2**(4): 353-365.

Thomas, A. (2016). Polymer Flooding. Chemical Enhanced Oil Recovery (cEOR) - a Practical Overview.

Van Heel, A., M. Hulsen and B. J. J. o. n.-n. f. m. Van den Brule (1998). "On the selection of parameters in the FENE-P model." **75**(2-3): 253-271.

Warner Jr, H. R. J. I. and E. C. Fundamentals (1972). "Kinetic theory and rheology of dilute suspensions of finitely extendible dumbbells." **11**(3): 379-387.

Wedgewood, L. E., D. N. Ostrov and R. B. J. J. o. n.-n. f. m. Bird (1991). "A finitely extensible bead-spring chain model for dilute polymer solutions." **40**(1): 119-139.

Youtube.com. "extrudate swell." from https://www.youtube.com/watch?v=LWNhr2PM5_s.

Youtube.com. "Rod climbing." from <https://www.youtube.com/watch?v=P8hFf7e4sa4>.

